CONTENTS

page

Acknowledgement

I wish to express my thanks to my supervisor, Professor E.O. Tuck, for readily sharing his experience and insight in the field and for his numerous suggestions of which I was only able to follow up a few.

1. Introduction

Planing is a state of motion of a water vessel in which the draft is small compared to the length of the vessel touching the water; the vessel is effectively skimming along the surface. In this state the disturbance of the water is minimal, resulting in low inviscid drag. Planing vessels are therefore able to operate at high speeds, and this is when they tend to be most efficient. In practice most planing surfaces are relatively flat, as experience has shown that this configuration produces very low drag over large speed ranges.

Common examples of planing vessels include speedboats, windsurfers, surfboards, waterskis and skiff dinghies; many yachts are also capable of planing at sufficiently high speeds. The main factors to be considered when designing such craft are stability, manoeuvrability and minimising drag. One of the major attributes of planing vessels is that they tend to be stable even at reasonably high speeds. Therefore except in the limit of very small waterline length or very high speed, stability is not really a practical issue and as such will not be considered here. Manoeuvrability is mainly a property of the plan shape of a planing vessel and of the behaviour of appendages such as fins and rudders, and cannot really be considered in an analysis restricted to two dimensions. Therefore drag minimisation

is probably the most important objective of two-dimensional planing theory and consequently will form one of the major themes of this project.

2. Summary

The linearised two-dimensional inviscid problem is set up for a given hull shape and a relationship is found between the hull shape and the pressure distribution beneath it. This is solved numerically in the special case of a flat plate and the results used to find the wetted length, angle of attack and elevation for a given speed and weight distribution. The inviscid and viscous drag are calculated for a given speed in terms of the weight distribution, as well as the minimum total drag for a given speed.

The possibility of eliminating the leading edge splash is then addressed by considering two other shapes: a flat plate that is parabolic at the leading edge, and the vertex up parabola. Conditions are found under which these shapes will have no leading edge splash, and their corresponding drag is compared to that of the flat plate.

3. Problem Formulation

3.1 Assumptions

In order to find the pressure distribution beneath a planing hull of given shape, we assume that viscous effects are confined to a boundary layer of negligible thickness in which no separation occurs, and consider the inviscid problem outside this boundary layer. We can then use the result of boundary layer theory that the pressure obtained by solving the outer inviscid problem will approximately equal the pressure on the body.

We also consider here only two-dimensional hulls. That is to say, the hull has finite extent in the direction of motion but extends to infinity in the direction parallel to the surface of the water and perpendicular to the direction of motion. Therefore we can assume in the absence of turbulence that the flow will have no component of velocity in this direction and be two-dimensional. In practice of course no planing vessel has infinite breadth; in most cases the wetted breadth is of similar magnitude to the wetted length. However in the case of hulls that are straight in the sideways direction (i.e. have a constant cross-section taken in the direction of motion), the flow beneath the hull will be predominantly in the direction of motion except near the edges. Hence in this case the two-dimensional flow calculated should closely

approximate the actual three-dimensional flow except near the edges.

The undisturbed water surface is considered to be flat; the only waves that exist are those that result from the presence of the hull. The vessel is also assumed to be moving at constant velocity, so that the flow is steady with respect to an inertial frame moving with the body. It is this frame which will be used in the formulation of the problem.

For a planing vessel, the assumption of small draft permits a major simplification in the equations of motion - that of linearisation. We assume the flow to be a small perturbation of a uniform stream, such that vertical velocities, deviations in horizontal velocity, surface elevations and pressure variations are everywhere small. This will be for the most part true for any vessel with a relatively flat plan shape. However most planing vessels, including the flat plate we will be considering, have a point at the leading edge near which this assumption breaks down. We will see how the violation of this assumption becomes evident in the solution of the linearised problem.

For the purposes of this project, we will be considering the practical problem of a planing vessel with a given weight distribution upon it. It is a matter of observation that the wetted

length of such a vessel is not known in advance; it changes markedly as the speed and weight distribution of the vessel change. Therefore in the general case neither the forward or rear attachment points are known. However in the case of flat or concave hulls (those with negative second derivative) with a sharp trailing edge, or "transom", we can assume that the flow leaves the hull at this point. This is generally the case in practice even with slightly convex hulls. Hence the trailing edge position will be assumed to correspond to the rear detachment point, but the wetted length and hence the leading edge position will depend on the speed and weight distribution of the vessel.

One assumption that we must make about the trailing edge is that of smooth detachment; that is, there is no pressure discontinuity between the hull and the free surface, so the flow breaks away cleanly from the trailing edge. This is not always the case in practice; at low speeds the flow tends to rise almost vertically from the trailing edge instead of breaking away almost horizontally. However we will assume throughout that the pressure at the trailing edge of the hull matches the pressure of the free surface. This is known as the Kutta Condition.

3.2 The Linearised Geometry

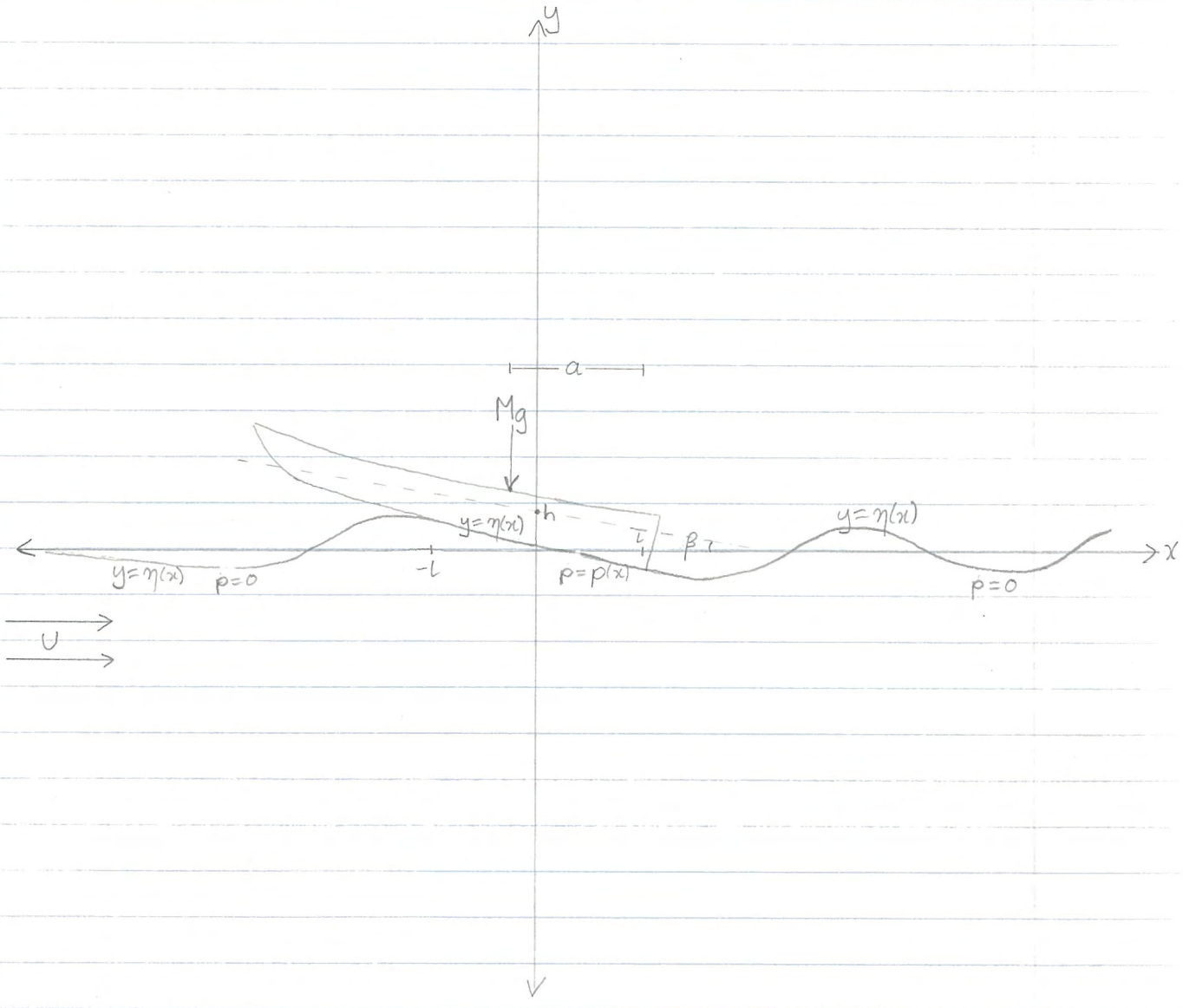

Fig. 1 The Linearised Problem

As mentioned previously, we take the origin of coordinates to be at rest relative to the body. We take the y direction to be vertical, and the x direction to be in the direction that the uniform stream is travelling. $y=0$ corresponds to the undisturbed free surface elevation, and $x=0$ is taken to be midway between the leading and trailing edges. $y=\eta(x)$ is the equation of the disturbed water surface. On $(-\infty, -L]$ and $[L, \infty)$ this is the height of the free surface, and on $[-L, L]$ it is the actual vertical displacement of the body. We note therefore that $\eta(x)$ is known to within a few parameters on $[-L, L]$.

For the free-body problem that we are dealing with, we must give the planing surface two degrees of freedom. These are the angle through which the body is rotated and the vertical displacement of the body, neither of which are known in advance.

For the linearisation to hold, we can write an expression for the shape of the body when unrotated as

$$y = \varepsilon f(x) \qquad (3.1)$$

in linearised form, where ε is a dimensionless small parameter and $f(x)$ is independent of ε with $f(0)=0$. $f(x)$ must therefore have the dimensions of length; an alternative way to write this would

be $f(x) = \ell\, g(x/\ell)$. When this shape is rotated clockwise through an angle β, its equation becomes

$$y\cos\beta + x\sin\beta = \varepsilon f(x\cos\beta - y\sin\beta) \qquad (3.2)$$

In order to linearise this, we note that the linearisation requires that the displacement of the rotated shape be also of order ε; therefore since the rotation changes the displacement by an amount which is of order β, this implies

$$\beta = O\{\varepsilon\}$$

We can hence linearise (3.2) as follows. Write

$$y + x\beta + O\{(\beta)^2\} = \varepsilon F(x, y, \beta)$$

$$= \varepsilon f(u) \quad \text{with} \quad u = x\cos\beta - y\sin\beta$$

$$= \varepsilon\left[F(x,y,0) + \left.\frac{\partial F}{\partial \beta}\right|_{\beta=0} \cdot \beta + O\{\beta^2\} \right]$$

from Taylor's theorem

$$= \varepsilon F(x,y,0) + O\{\varepsilon\beta\}$$

$$= \varepsilon f(x) + O\{\varepsilon\beta\}$$

$$\therefore \quad y = \varepsilon f(x) - \beta x + O\{\varepsilon\beta, \beta^2\}$$

or in linearised form

$$y = \varepsilon f(x) - \beta x \qquad (3.3)$$

We also allow the body to be displaced vertically by an amount h which must be of order ε for the linearisation to hold. Therefore we have in total on $[-L,L]$

$$\eta(x) = \varepsilon f(x) - \beta x + h \qquad (3.4)$$

where ε and $f(x)$ are given and β and h are to be determined later.

We take p to be the excess over atmospheric pressure, so that $p=0$ on the free surface $(-\infty,-L]$ and $[L,\infty)$, and $p=p(x)$ is to be solved for on $[-L,L]$. The constant free stream velocity is denoted by 'U', the total mass of the planing vessel per unit breadth is 'M', and the centre of mass is situated a distance 'a' from the trailing edge. 'ρ' is the water density and 'g' is the acceleration due to gravity. When the body is rotated, the wetted length of the body is actually $2L/\cos\beta$, but in linearised form this remains $2L$. Similarly the x coordinate of the centre of mass is $L-a\cos\beta$ which in linearised form remains $L-a$.

We shall also be using a dimensionless quantity known as the Froude number. This is often used with regard to displacement vessels and has the value $U/\sqrt{gL}$, where L is the length of the ship. We shall define two Froude numbers as follows:

$$F_a \equiv \frac{U}{\sqrt{ga}} \qquad (3.5a)$$

$$F_L \equiv \frac{U}{\sqrt{gL}} = \frac{U}{\sqrt{2gl}} \qquad (3.5b)$$

For computational convenience we shall also define the quantity

$$f \equiv \frac{U^2}{gl} \qquad (3.6a)$$

$$\text{so that} \quad F_L = \sqrt{\frac{f}{2}} \qquad (3.6b)$$

It is important to note that for a general planing vessel, F_L is not a known quantity because L is not known in advance. The only independent length scale is 'a', so that F_a is the true independent quantity describing the flow.

3.3 The Linearised Equations of Motion

The inviscid problem involves solving Laplace's equation for the velocity potential Φ, subject to certain boundary conditions. The two boundary conditions on the surface are Bernoulli's equation and the kinematic boundary condition. Normally these must be applied on the unknown surface $y = \eta(x)$, but linearisation allows us to avoid this difficulty. We note that for any differentiable function $F(x,y)$, Taylor's theorem states

$$F(x,\eta(x)) = F(x,0) + \left.\frac{\partial F(x,y)}{\partial y}\right|_{y=0} \cdot \eta(x) + O\{(\eta(x))^2\} \qquad (3.7)$$

Now $\eta(x) = O\{\varepsilon\}$ on $[-L,L]$ from (3.4), and since the trailing wave amplitude is of the same order as the trailing edge height, we have $\eta(x) = O\{\varepsilon\}$ everywhere. Therefore (3.7) becomes

$$F(x,\eta(x)) = F(x,0) + O\{\varepsilon\}$$

so that to first order,

$$F(x,\eta(x)) = F(x,0)$$

Therefore one effect of linearisation is that all surface boundary conditions can be applied on $y=0$ instead of on the unknown surface $y=\eta(x)$.

Bernoulli's equation applied on the free surface gives

$$\frac{p}{\rho} + g\eta + \frac{1}{2}q^2 = \frac{1}{2}U^2 \quad \text{on} \quad y=0 \qquad (3.8)$$

where $\underline{q} = \nabla\Phi$ and $q^2 \equiv \underline{q}.\underline{q}$
This immediately implies that $p(x)$ and $(q^2 - U^2)$ are also of order ε.

Writing $\Phi = Ux + \phi$, where ϕ is the perturbation of the free stream velocity potential, gives

$$\underline{q} = \left(U + \frac{\partial\phi}{\partial x}\right)\underline{i} + \frac{\partial\phi}{\partial y}\underline{j}$$

so $$q^2 = U^2 + 2U\frac{\partial\phi}{\partial x} + \left(\frac{\partial\phi}{\partial x}\right)^2 + \left(\frac{\partial\phi}{\partial y}\right)^2$$

where $\frac{\partial\phi}{\partial x}$ and $\frac{\partial\phi}{\partial y}$ are of order ε;
hence ϕ is also of order ε.

In linearised form this becomes

$$q^2 = U^2 + 2U\left.\frac{\partial\phi}{\partial x}\right|_{y=0}$$

so (3.8) becomes

$$\frac{p}{\rho} + g\eta + U\frac{\partial\phi}{\partial x} = 0 \quad \text{on} \quad y=0 \qquad (3.9)$$

The kinematic boundary condition, that a particle on the surface moves upwards

with the surface, gives

$$\left.\frac{\partial \Phi}{\partial y}\right|_{y=\eta} = \frac{D\eta}{Dt}$$

i.e. $$\left.\frac{\partial \phi}{\partial y}\right|_{y=\eta} = \left(U + \left.\frac{\partial \phi}{\partial x}\right|_{y=\eta}\right)\frac{d\eta}{dx}$$

so that in linearised form

$$\left.\frac{\partial \phi}{\partial y}\right|_{y=0} = U\frac{d\eta}{dx} \qquad (3.10)$$

The boundary condition at infinity states that the flow must tend to that of the free stream as $y \to -\infty$, and this implies

$$\nabla\phi \to \underline{0} \quad \text{as} \quad y \to -\infty$$

We can satisfy this by requiring that

$$\phi \to 0 \quad \text{as} \quad y \to -\infty \qquad (3.11)$$

The other boundary condition that we need is the radiation condition (see e.g. Newman (1977) pp. 288-289). Our assumptions of steady flow and no waves other than those caused by the body imply that there should be no waves upstream, i.e.

$$\eta(x) \to 0 \quad \text{as} \quad x \to -\infty \qquad (3.12)$$

In terms of ϕ, Laplace's equation becomes

$$\nabla^2(Ux+\phi)=0$$

$$\therefore \quad \nabla^2\phi=0$$

Therefore the full problem to be solved is

$$\nabla^2\phi=0 \quad \text{on} \quad y\leq 0 \tag{3.13a}$$

subject to

$$\frac{p}{\rho}+g\eta+U\frac{\partial\phi}{\partial x}=0 \quad \text{on} \quad y=0 \tag{3.13b}$$

$$\left.\frac{\partial\phi}{\partial y}\right|_{y=0}=U\frac{d\eta}{dx} \tag{3.13c}$$

$$\phi\to 0 \quad \text{as} \quad y\to-\infty \tag{3.13d}$$

$$\eta(x)\to 0 \quad \text{as} \quad x\to-\infty \tag{3.13e}$$

$$p=0 \quad \text{on} \quad (-\infty,-L] \text{ and } [L,\infty) \tag{3.13f}$$

$$\eta(x)=\varepsilon f(x)-\beta x+h \quad \text{on} \quad [-L,L] \tag{3.13g}$$

where the unknowns are $\phi(x,y)$ on $y\leq 0$, $\eta(x)$ on $(-\infty,-L]$ and $[L,\infty)$, and $p(x)$ on $[-L,L]$.

4. Historical Summary

Early formulations of the planing problem involved neglecting gravity in the Bernoulli surface boundary condition, which corresponds to the limit as $F_L \to \infty$. Wagner (1932) solved the nonlinear problem for the zero-gravity case in infinite water depth, and showed that for a flat plate at a prescribed angle of attack and wetted length, the trailing edge height above the undisturbed water surface is infinite. One way of avoiding this paradox was found by Green (1936) who solved the same problem but in finite water depth, and obtained a finite trailing edge height for the flat plate. Both of these authors incorporated a leading edge splash into their modelling of the problem.

The first successful attempt at linearised planing theory was by Maruo (1951). He linearised the free surface boundary conditions as used here, and gave an expression relating $p(x)$ and dy/dx. Because using dy/dx eliminated the constant h, the vertical displacement of the hull was not discussed. He used a fixed wetted length and angle of attack, and assumed the pressure to be continuous at the trailing edge. Maruo noted that in the linearised case the pressure at the leading edge must be infinite due to the presence of the splash. He therefore assumed a pressure distribution of the form

$$\frac{p}{\rho U^2} = a_0 \left(\frac{1-\cos\theta}{\sin\theta} \right) + \sum_{n=1}^{\infty} a_n \frac{\sin n\theta}{n}$$

(with $x = -l\cos\theta$, $0 \le \theta \le \pi$ and the flow in the negative x direction), and solved for the first few coefficients a_n.

Squire (1957), without prior knowledge of Maruo's work, developed a remarkably similar linearised theory in which he derived the same planing equation, and for the flat plate example assumed the same form for $p(x)$. He improved on Maruo's work however by noting that the wetted length is not an input quantity in the general case, and showed that for a given angle of attack it could be determined in terms of the net lift, which he recognised as an input quantity. Squire showed that Wagner's trailing edge paradox (which still existed in the infinite Froude number limit of Maruo's theory although he did not compute it in his paper) could be resolved by allowing the wetted length to vary so as to give a constant net lift. He also questioned the validity of the Kutta condition and derived a minimum velocity requirement for it to hold.

A high Froude number approximation to the linearised theory was given by Cumberbatch (1958) who used an expansion in powers of $\kappa \equiv gl/U^2$ for $p(x)$. He used a fixed wetted length and angle of attack, as did Maruo. Cumberbatch also considered the case of the vertex-up parabola at high Froude number

and showed how the pressure singularity could be removed to first order in x by choosing the parabola curvature and angle of attack appropriately.

It was not until much later that Oertel (1975) incorporated into a theory for planing the fact that for the free-body problem neither the angle of attack nor the wetted length is an input quantity, but rather the net lift and moment, which are predetermined by the weight distribution of the body if it is to be in equilibrium. As well as the flat plate, Oertel also considered the vertex-down parabola where the position of both the leading and trailing edges must be found.

Most recent work on planing has extended from the two-dimensional linear problem into either the three-dimensional linear problem (see e.g. Oertel (1975), Wang and Rispin (1971)), or the two-dimensional nonlinear problem at the leading edge and its matching to the linear solution away from the leading edge (e.g. Bessho (1994)).

5. The Planing Equation

In the following an equation relating $p(x)$ and $\eta(x)$ is obtained by solving the system (3.13). It is shown how this system leads to a singularity and then how this singularity can be avoided by introducing an artificial viscosity.

5.1 Standard Approach

Combining (3.9) and (3.10) to eliminate η we obtain

$$\frac{\partial^2\phi}{\partial x^2} + \frac{g}{U^2}\frac{\partial\phi}{\partial y} = \frac{-1}{\rho U}\frac{dp}{dx} \quad \text{on } y=0$$

as our surface boundary condition. Letting $K \equiv g/U^2$ this gives

$$\frac{\partial^2\phi}{\partial x^2} + K\frac{\partial\phi}{\partial y} = \frac{-1}{\rho U}\frac{dp}{dx} \quad \text{on } y=0 \qquad (5.1)$$

We now solve Laplace's equation by taking Fourier transforms with respect to x. Since we might expect there to be waves downstream of the body and there is no viscosity to damp them out, it is evident that in the steady state ϕ will oscillate indefinitely as $x \to \infty$. Hence the Dirichlet condition, i.e. that $\int_{-\infty}^{\infty} \phi(x,y)\,dx$ exists, is not satisfied.

Although this is not a necessary condition for the existence of the Fourier transform, those functions for which the

$$\int |\quad| dx < \infty$$

necessary condition ($\int_{-\infty}^{\infty} \phi(x,y)\,dx$ is bounded) is satisfied, but the Dirichlet condition is not, generally result in singularities. We may therefore anticipate having trouble with the inversion formula.

Letting

$$F(k,y) \equiv \mathcal{F}\{\phi(x,y)\} = \frac{1}{\sqrt{2\pi}} \int_{-\infty}^{\infty} \phi(x,y)\, e^{ikx}\, dx,$$

taking the Fourier transform of

$$\frac{\partial^2 \phi}{\partial x^2} + \frac{\partial^2 \phi}{\partial y^2} = 0$$

gives

$$-k^2 F(k,y) + \frac{\partial^2 F(k,y)}{\partial y^2} = 0$$

which has the solution

$$F(k,y) = A(k)\, e^{ky} + B(k)\, e^{-ky}$$

For $\lim_{y\to-\infty} \phi(x,y) = 0$, we need $\lim_{y\to-\infty} F(k,y) = 0$.

Therefore

$$A(k) = 0 \quad \text{for} \quad k<0$$
$$B(k) = 0 \quad \text{for} \quad k>0$$

$$\Rightarrow F(k,y) = \begin{cases} A(k)\, e^{|k|y} & k>0 \\ B(k)\, e^{|k|y} & k<0 \end{cases}$$

These can be combined to form the general expression

$$F(k,y) = C(k)\, e^{|k|y} \qquad (5.2)$$

Taking the Fourier transform of (5.1) gives

$$-k^2 F(k,0) + K \frac{\partial F}{\partial y}(k,0) = \frac{ik}{\rho U} P(k) \qquad (5.3)$$

where $P(k) = \frac{1}{\sqrt{2\pi}} \int_{-\infty}^{\infty} p(x)\, e^{ikx}\, dx$

From (5.2)

$$F(k,0) = C(k)$$
$$\frac{\partial F}{\partial y}(k,0) = C(k) \cdot |k|$$

Substituting these into (5.3) gives

$$-k^2 C(k) + K|k| C(k) = \frac{ik}{\rho U} P(k)$$

$$\therefore C(k) = \frac{-ik P(k)}{\rho U (k^2 - K|k|)}$$
$$= \frac{-i P(k)}{\rho U (k - K \operatorname{sgn} k)} \qquad (5.4)$$

Hence (5.2) becomes

$$F(k,y) = \frac{-i P(k)\, e^{|k|y}}{\rho U (k - K \operatorname{sgn} k)}$$

The inversion formula then gives

$$\phi(x,y) = \frac{1}{\sqrt{2\pi}} \int_{-\infty}^{\infty} \frac{-i P(k)\, e^{|k|y}}{\rho U (k - K \operatorname{sgn} k)} \cdot e^{-ikx}\, dk$$

$$= \frac{-i}{\sqrt{2\pi}\rho U} \int_{-\infty}^{\infty} \left(\frac{1}{\sqrt{2\pi}} \int_{-\infty}^{\infty} p(u) e^{iku}\, du \right) \frac{e^{|k|y} e^{-ikx}}{k - K \operatorname{sgn} k}\, dk$$

$$= \frac{-i}{2\pi\rho U} \int_{-\infty}^{\infty} p(u) \left(\int_{-\infty}^{0} \frac{e^{-ky} e^{-ik(x-u)}}{k+K}\, dk + \int_{0}^{\infty} \frac{e^{ky} e^{-ik(x-u)}}{k-K}\, dk \right) du$$

?? (interchanging the order of integration)

$$= \frac{-i}{2\pi\rho U} \int_{-\infty}^{\infty} p(u) \left(-\int_{0}^{\infty} \frac{e^{\nu y} e^{i\nu(x-u)}}{\nu - K}\, d\nu + \int_{0}^{\infty} \frac{e^{\nu y} e^{-i\nu(x-u)}}{\nu - K}\, d\nu \right) du$$

(letting $\nu = |k|$)

so

$$\phi(x,y) = \frac{-1}{\rho U \pi} \int_{-\infty}^{\infty} p(u) \int_{0}^{\infty} \frac{e^{\nu y} \sin \nu(x-u)}{\nu - K}\, d\nu\, du \qquad (5.5)$$

We note already that the integrand has a singularity at $\nu = K$. Using (3.10) now to change this into an expression for $\eta(x)$:

$$\frac{d\eta}{dx} = \frac{-1}{\rho U^2 \pi} \lim_{y \to 0^-} \int_{-\infty}^{\infty} p(u) \int_{0}^{\infty} \frac{\nu e^{\nu y}}{\nu - K} \sin \nu(x-u)\, d\nu\, du$$

assuming it is justified to differentiate under the integral.

Therefore

$$\eta(x) = \frac{1}{\rho U^2 \pi} \lim_{y \to 0^-} \int_{-\infty}^{\infty} p(u) \int_{0}^{\infty} \frac{e^{\nu y}}{\nu - K} \cos \nu(x-u)\, d\nu\, du + c$$

$$= \frac{1}{\rho U^2 \pi} \lim_{y \to 0^-} \int_{-l}^{l} p(u) \int_{0}^{\infty} \frac{e^{\nu y}}{\nu - K} \cos \nu(x-u)\, d\nu\, du + c$$

since $p(x)$ is zero everywhere except on $[-l, l]$.

This can be written in the form

$$\eta(x) = \frac{1}{\rho U^2 \Pi} \int_{-L}^{L} p(u)\, I(x-u)\, du + c \qquad (5.6)$$

where the so-called "kernel" is defined by

$$I(m) = \lim_{y \to 0^-} \int_0^\infty \frac{e^{\nu y} \cos m\nu}{\nu - K}\, d\nu$$

$$\therefore \quad I(m) = \int_0^\infty \frac{\cos m\nu}{\nu - K}\, d\nu$$

In order to determine the constant 'c' in (5.6) we use the other surface boundary condition for $\eta(x)$. Using (5.5) and the surface boundary condition (3.9) we obtain

$$\eta(x) = \frac{1}{\rho g \Pi} \lim_{y \to 0^-} \int_{-L}^{L} p(u) \int_0^\infty \frac{\nu e^{\nu y}}{\nu - K} \cos \nu(x-u)\, d\nu\, du - \frac{p(x)}{\rho g}$$

$$= \frac{1}{\rho g \Pi} \lim_{y \to 0^-} \int_{-L}^{L} p(u) \int_0^\infty e^{\nu y} \cos \nu(x-u)\, d\nu\, du$$

$$+ \frac{K}{\rho g \Pi} \lim_{y \to 0^-} \int_{-L}^{L} p(u) \int_0^\infty \frac{e^{\nu y}}{\nu - K} \cos \nu(x-u)\, d\nu\, du - \frac{p(x)}{\rho g} \qquad (5.7)$$

We note that

$$\int_0^\infty e^{\nu y} \cos m\nu\, d\nu$$

$$= \frac{1}{2} \int_0^\infty e^{(y+im)\nu} + e^{(y-im)\nu}\, d\nu$$

$$= \frac{-y}{m^2 + y^2},$$

so

$$\frac{1}{\rho g \Pi} \lim_{y \to 0^-} \int_{-L}^{L} p(u) \int_0^\infty e^{vy} \cos v(x-u)\, dv\, du$$

$$= \frac{1}{\rho g \Pi} \lim_{y \to 0^-} \int_{-L}^{L} p(u) \cdot \frac{-y}{(x-u)^2 + y^2}\, du$$

$$= \frac{1}{\rho g} \lim_{z \to 0^+} \int_{-L}^{L} p(u) \cdot \frac{1}{\Pi} \frac{z}{(u-x)^2 + z^2}\, du$$

and $\lim_{z \to 0^+} \frac{1}{\Pi} \frac{z}{(u-x)^2 + z^2}$ is a Dirac delta function since it is zero everywhere except at $u - x = 0$ where it is infinite, and

$$\lim_{z \to 0^+} \int_{-\infty}^{\infty} \frac{1}{\Pi} \frac{z}{(u-x)^2 + z^2}\, du$$

$$= \lim_{z \to 0^+} \left[\frac{1}{\Pi} \operatorname{Tan}^{-1}\left(\frac{u-x}{z}\right) \right]_{-\infty}^{\infty} = 1$$

Therefore (5.7) becomes

$$\eta(x) = \frac{1}{\rho g} \int_{-L}^{L} p(u)\, \delta(u-x)\, du + \frac{1}{\rho v^2 \Pi} \int_{-L}^{L} p(u) \int_0^\infty \frac{\cos v(x-u)}{v - K}\, dv\, du - \frac{p(x)}{\rho g}$$

$$= \frac{1}{\rho v^2 \Pi} \int_{-L}^{L} p(u)\, I(x-u)\, du \qquad (5.8)$$

as in (5.6), so that the constant 'c' in (5.6) is zero.

$I(m)$ still has a singularity at $v=K$. However if we take the integral to be the Cauchy principal value, $I(m)$ may still exist. In this case we can evaluate $I(m)$ by considering $\int_c \frac{e^{imv}}{v-K}\,dv$ around the circuits shown:

case i) : $m>0$

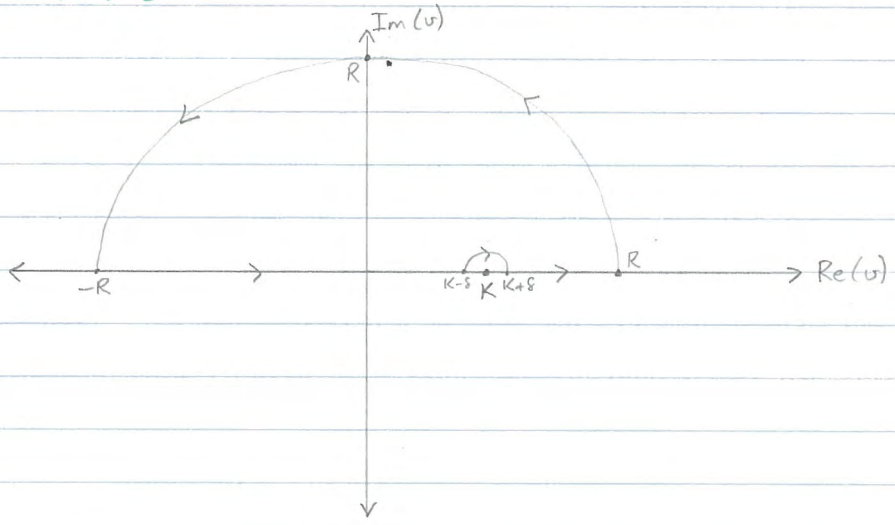

As $R\to\infty$ and $\delta\to 0$ we have

$$\int_{-\infty}^{\infty} \frac{e^{imv}}{v-K}\,dv - \pi i\, e^{imK} = 0$$

from Jordan's lemma and the residue theorem

$$\Rightarrow \int_{-\infty}^{\infty} \frac{\cos mv}{v-K}\,dv + I(m) + i\int_{-\infty}^{\infty} \frac{\sin mv}{v-K}\,dv - \pi i \cos mK + \pi \sin mK = 0$$

equating real parts,

$$I(m) = -\pi \sin Km - \int_{-\infty}^{\infty} \frac{\cos mv}{v-K}\,dv$$

case ii) : $m < 0$

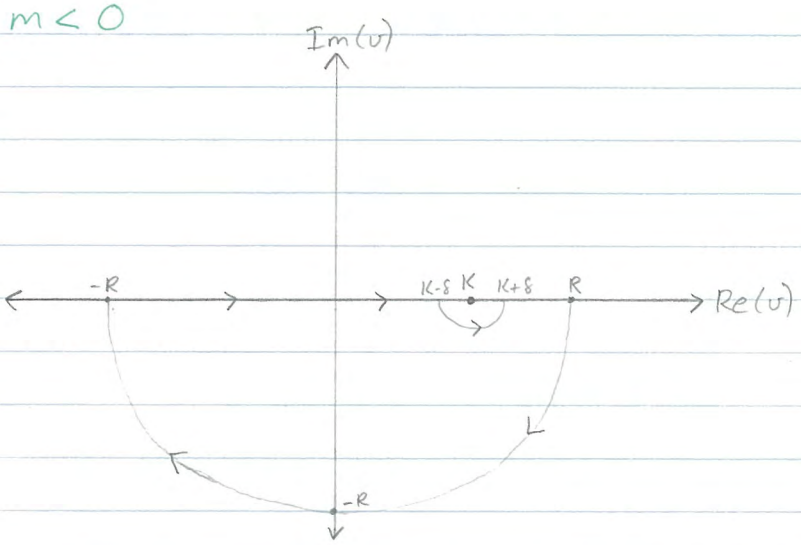

Here similarly we have

$$\int_{-\infty}^{\infty} \frac{e^{im\upsilon}}{\upsilon - K}\, d\upsilon + \pi i\, e^{imK} = 0$$

which gives

$$I(m) = \pi \sin Km - \int_{-\infty}^{0} \frac{\cos m\upsilon}{\upsilon - K}\, d\upsilon$$

Therefore the combined solution is

$$I(m) = \pi \sin |Km| - \int_{-\infty}^{0} \frac{\cos m\upsilon}{\upsilon - K}\, d\upsilon$$

$$= \pi \sin |Km| + \int_{0}^{\infty} \frac{\cos mw}{w + K}\, dw \qquad (5.9)$$

We now check to see whether this solution satisfies the radiation condition (3.12). Looking at (5.8) we see that for this to be satisfied for any $p(x)$ we need

$$I(x-u) \to 0 \quad \text{as} \quad x \to -\infty$$

i.e. $$I(m) \to 0 \quad \text{as} \quad m \to -\infty$$

From (5.9) we see that

$$I(m) \to \pi \sin |Km| \quad \text{as} \quad m \to -\infty$$

since $$\int_0^\infty \frac{\cos mw}{w+K}\, dw \to 0 \quad \text{as} \quad m \to -\infty$$

by the Riemann-Lebesgue lemma. Therefore $I(m)$ oscillates sinusoidally as $m \to -\infty$ instead of tending to zero so the radiation condition is violated.

We note also that the integral of $\frac{\cos mv}{v-K}$ around the semicircular arc around $v=K$ is purely imaginary, so that we cannot take the integral for $I(m)$ to pass around the singularity in the complex plane either, because then $\eta(x)$ would have an imaginary part. It turns out that we get an acceptable result if we take

$$I(m) = \text{Re} \int_c \frac{e^{imv}}{v-K}\, dv$$

where c is the contour below,

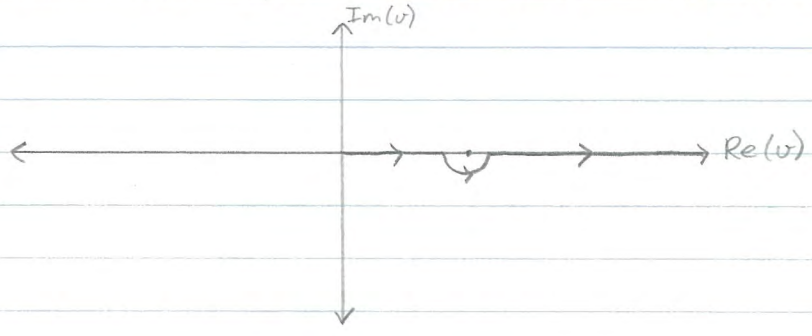

but we cannot arrive at this through the above derivation so we must try an alternative derivation.

5.2 Artificial Viscosity

The approach used in the previous section results in the function $I(m)$ oscillating sinusoidally as $m \to -\infty$. We can overcome this by introducing an artificial viscosity (see Lamb (1932) p. 399) into the surface boundary condition (5.1) so that it becomes

$$\frac{\partial^2 \phi}{\partial x^2} + \alpha \frac{\partial \phi}{\partial x} + K \frac{\partial \phi}{\partial y} = \frac{-1}{\rho U} \frac{dp}{dx} \quad \text{on } y=0, \qquad (5.10)$$

and subsequently letting $\alpha \to 0$ through positive values. We will see that choosing α to be positive results in the radiation condition being satisfied.

Taking the Fourier transform of (5.10) gives

$$-k^2 F(k,0) - \alpha i k F(k,0) + K \frac{\partial F}{\partial y}(k,0) = \frac{ik}{\rho U} P(k)$$

With $F(k,y) = C(k) e^{|k|y}$ as in (5.2) this gives

$$C(k) = \frac{ik P(k)}{\rho U(-k^2 - \alpha i k + K|k|)}$$

so

$$F(k,y) = \frac{i P(k) e^{|k|y}}{\rho U(-k - \alpha i + K \operatorname{sgn} k)}$$

Thus

$$\phi(x,y) = \frac{i}{\sqrt{2\pi}\rho U}\int_{-\infty}^{\infty} \frac{P(k)\, e^{|k|y}\, e^{-ikx}}{-k-\alpha i + K\,\mathrm{sgn}\,k}\, dk$$

$$= \frac{i}{2\pi\rho U}\int_{-l}^{l} p(u)\int_{-\infty}^{\infty} \frac{e^{|k|y}\, e^{-ik(x-u)}}{-k-\alpha i + K\,\mathrm{sgn}\,k}\, dk\, du$$

$$= \frac{i}{2\pi\rho U}\int_{-l}^{l} p(u)\left[\int_{-\infty}^{0} \frac{e^{-ky}\, e^{-ik(x-u)}}{-k-\alpha i - K}\, dk + \int_{0}^{\infty} \frac{e^{ky}\, e^{-ik(x-u)}}{-k-\alpha i + K}\, dk\right] du$$

$$= \frac{i}{2\pi\rho U}\int_{-l}^{l} p(u)\left[\int_{0}^{\infty} \frac{e^{vy}\, e^{iv(x-u)}}{v-\alpha i - K}\, dv - \int_{0}^{\infty} \frac{e^{vy}\, e^{-iv(x-u)}}{v+\alpha i - K}\, dv\right] du$$

so

$$\left.\frac{\partial\phi}{\partial y}\right|_{y=0} = \frac{i}{2\pi\rho U}\int_{-l}^{l} p(u)\left[\int_{0}^{\infty} \frac{v e^{iv(x-u)}}{v-\alpha i-K}\, dv - \int_{0}^{\infty} \frac{v e^{-iv(x-u)}}{v+\alpha i-K}\, dv\right] du$$

and from (3.10)

$$\eta(x) = \frac{1}{2\pi\rho U^2}\int_{-l}^{l} p(u)\left[\int_{0}^{\infty} \frac{e^{iv(x-u)}}{v-\alpha i-K}\, dv + \int_{0}^{\infty} \frac{e^{-iv(x-u)}}{v+\alpha i-K}\, dv\right] du + c \qquad (5.11)$$

Let

$$I_1(m) = \int_0^{\infty} \frac{e^{imv}}{v-(K+\alpha i)}\, dv$$

$$I_2(m) = \int_0^{\infty} \frac{e^{-imv}}{v-(K-\alpha i)}\, dv$$

These can be solved by considering

$$\int_{C_1} \frac{e^{imv}}{v-(K+\alpha i)}\, dv$$

and

$$\int_{C_2} \frac{e^{-imv}}{v-(K-\alpha i)}\, dv$$

case 1) : $m > 0$

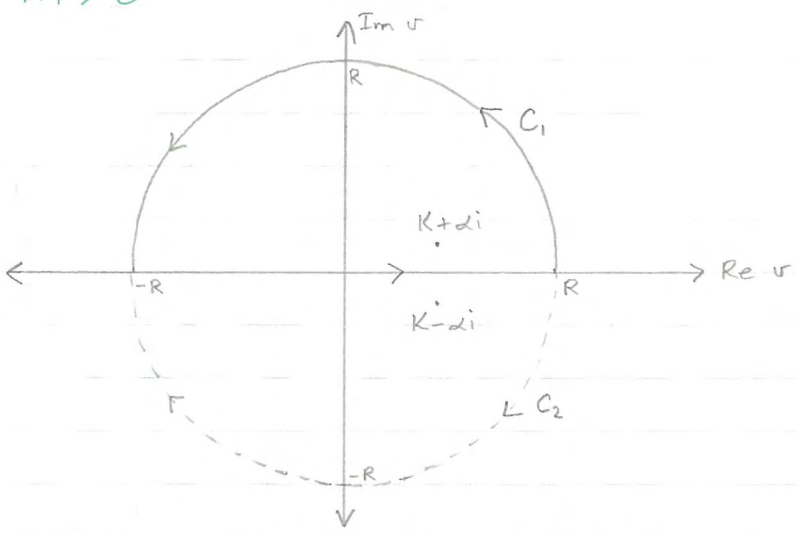

$$\int_{-\infty}^{0} \frac{e^{imv}}{v-(K+\alpha i)}\,dv + I_1(m) = 2\pi i\, e^{im(K+\alpha i)}$$

$$\int_{-\infty}^{0} \frac{e^{-imv}}{v-(K-\alpha i)}\,dv + I_2(m) = -2\pi i\, e^{-im(K-\alpha i)}$$

case 11) : $m < 0$

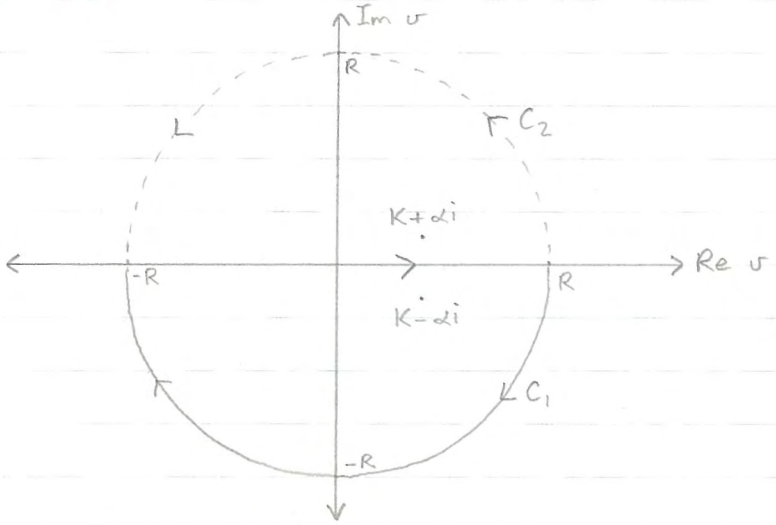

$$\int_{-\infty}^{0} \frac{e^{imv}}{v-(K+\alpha i)}\,dv + I_1(m) = 0$$

$$\int_{-\infty}^{0} \frac{e^{-imv}}{v-(K-\alpha i)}\,dv + I_2(m) = 0$$

Combining these we get

$$I_1(m) = -\int_{-\infty}^{0} \frac{e^{imv}}{v-(K+\alpha i)}\,dv + 2\pi i\, H(m)\, e^{-m\alpha} e^{iKm}$$

$$I_2(m) = -\int_{-\infty}^{0} \frac{e^{-imv}}{v-(K-\alpha i)}\,dv - 2\pi i\, H(m)\, e^{-m\alpha} e^{-iKm}$$

where $H(m)$ is the Heaviside unit step function. Hence (5.11) becomes

$$\eta(x) = \frac{1}{2\pi\rho U^2}\int_{-l}^{l} p(u)\left[I_1(x-u) + I_2(x-u)\right]du + c$$

$$= \frac{1}{\rho U^2 \pi}\int_{-l}^{l} p(u)\, I(x-u)\,du + c$$

where

$$I(m) = -\frac{1}{2}\int_{-\infty}^{0} \frac{e^{imv}}{v-(K+\alpha i)} + \frac{e^{-imv}}{v-(K-\alpha i)}\,dv - 2\pi H(m) e^{-m\alpha}\sin Km \qquad (5.12)$$

We now note that, for $\alpha > 0$, as $x \to -\infty$ $(m \to -\infty)$ and as $x \to \infty$ $(m \to \infty)$, $I(m) \to 0$ by the Riemann-Lebesgue lemma. Instead of using the other boundary condition to find the constant 'c' as in the previous section, we will simply apply the physical argument that the mean water level must be at $y=0$, implying $c=0$. Therefore for any $\alpha > 0$, $\eta(x) \to 0$ as $x \to -\infty$ so the radiation condition is satisfied.

We now take the limit of (5.12) as $\alpha \to 0^+$ in such a way that

$m\alpha \to 0 \quad \forall\ m \in \mathbb{R}$. This gives

$$I(m) = -\int_{-\infty}^{0} \frac{\cos mv}{v-K}\, dv - 2\pi H(m) \sin Km$$

$$= \int_{|Km|}^{\infty} \frac{\cos(t-|Km|)}{t}\, dt - 2\pi H(m) \sin Km$$

on letting $t = -|m|.(v-K)$

$$= \cos Km \int_{|Km|}^{\infty} \frac{\cos t}{t}\, dt + \sin|Km| \int_{|Km|}^{\infty} \frac{\sin t}{t}\, dt - 2\pi H(m) \sin Km$$

$$\therefore\ I(m) = g(Km) - 2\pi H(m) \sin Km \qquad (5.13)$$

where

$$g(\xi) \equiv \cos\xi \int_{|\xi|}^{\infty} \frac{\cos t}{t}\, dt + \sin|\xi| \int_{|\xi|}^{\infty} \frac{\sin t}{t}\, dt \qquad (5.14)$$

We still have $I(m) \to 0$ as $x \to -\infty$, but now the downstream waves extend to infinity without being damped out. Hence our final equation relating $\eta(x)$ and $p(x)$ is

$$\eta(x) = \frac{1}{\rho U^2 \pi} \int_{-L}^{L} p(u)\, I(x-u)\, du \qquad (5.15)$$

where $I(m)$ is given by (5.13) and (5.14)

5.3 Properties of the Planing Equation

Equation (5.15) is an integral equation for the unknown pressure distribution $p(x)$, which must be solved for in terms of $\eta(x)$ which is assumed known. The kernel function $I(x-u)$ is expressed in terms of the so-called cosine and sine integrals defined as follows:

$$ci(\xi) = -\int_{\xi}^{\infty} \frac{\cos t}{t}\, dt$$

$$si(\xi) = -\int_{\xi}^{\infty} \frac{\sin t}{t}\, dt$$

so that from (5.14),

$$g(\xi) = -\cos\xi \,.\, ci(|\xi|) - \sin|\xi| \,.\, si(|\xi|) \qquad (5.16)$$

The cosine integral is seen to tend to negative infinity as $\xi \to 0^+$, so that $I(x-u)$ is singular at $u=x$. Thus the planing equation is a singular integral equation. In the general case no closed form solution exists for $p(x)$; however in the limit as $K \to 0$ the planing equation becomes the airfoil equation, which does have an exact solution.

To find the behaviour of $g(\xi)$ as $|\xi| \to 0$ we must look at the behaviour of $ci(\xi)$ and $si(\xi)$ as $\xi \to 0^+$.

If we consider $\int_C \frac{e^{iz}}{z}$ around the contour shown:

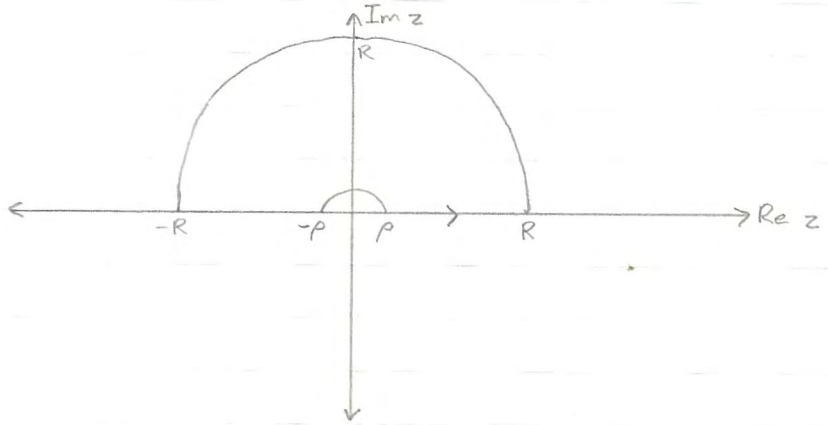

this gives

$$2\int_\rho^R \frac{i\sin z}{z} - i\pi = 0 \qquad \text{as } R\to\infty,\ \rho\to 0$$

since $\frac{\sin z}{z}$ is even and $\frac{\cos z}{z}$ is odd,

so

$$\lim_{\xi\to 0^+} si(\xi) = -\frac{\pi}{2}$$

If we now assume that $ci(\xi)$ is finite for $\xi > 0$, we can say

$$\int \frac{\cos t}{t}\,dt = F(t) + c$$

where $F(\infty)$ is finite. We can also say

$$\int \frac{\cos t}{t}\,dt = \int \frac{1}{t} + O\{t\}\,dt$$
$$= \log_e t + O\{t^2\}$$

Therefore

$$F(t) + c = \log_e t + O\{t^2\} \quad \text{as } t\to 0$$

so

$$\int_\zeta^\infty \frac{\cos t}{t}\,dt = [F(\infty)+c] - [\log_e \zeta + O\{\zeta^2\}] \quad \text{as } \zeta \to 0^+$$

$$= \text{constant} - \log_e \zeta + O\{\zeta^2\} \quad \text{as } \zeta \to 0^+$$

As $\zeta \to 0$ (5.16) can be written

$$g(\zeta) = (1 + O\{\zeta^2\})(\text{constant} - \log_e|\zeta| + O\{\zeta^2\})$$

$$-(|\zeta| + O\{\zeta^3\})\left(-\frac{\pi}{2} + O\{\zeta^a\}\right) \quad \text{with } a>0$$

which becomes, using the fact that $\zeta^2 \log_e|\zeta| = o(\zeta)$ as $\zeta \to 0$,

$$g(\zeta) = \text{constant} - \log_e|\zeta| + O\{\zeta\} \quad \text{as } \zeta \to 0 \quad (5.17)$$

(5.13) now gives

$$I(m) = \text{constant} - \log_e|Km| + O\{m\} \quad \text{as } m \to 0 \quad (5.18)$$

If we take the planing equation in derivative form by differentiating both sides with respect to x it becomes

$$\frac{d\eta}{dx} = \frac{1}{\rho V^2 \pi}\int_{-L}^{L} p(u)\,\frac{d}{dx}\left(I(x-u)\right)\,du$$

and in the limit as $K \to 0$,

$$\frac{d}{dm}(I(m)) \sim -\frac{1}{m} \quad \text{from (5.18)}$$

so that in this limit the planing

equation becomes

$$\frac{d\eta}{dx} = \frac{-1}{\rho U^2 \pi} \int_{-l}^{l} \frac{p(u)}{x-u}\, du \qquad (5.19)$$

This equation is identical to the airfoil equation, which gives the pressure on the underside of a thin wing. Therefore in the limit as $K \to 0$ the flow beneath the planing surface is identical to the flow beneath a thin wing of the same shape and at the same angle of attack. The airfoil equation has the solution

$$p(x) = C p_0(x) + p_1(x) \qquad (5.20)$$

where $p_0(x)$ is the solution of the homogeneous equation $d\eta/dx = 0$ on $(-l, l)$, and $p_1(x)$ is a particular solution. We can show that for the airfoil equation

$$p_0(x) = \frac{1}{\sqrt{l^2 - x^2}}$$

as follows:

(5.19) gives

$$-\rho U^2 \pi \frac{d\eta}{dx} = \int_{-l}^{l} \frac{1}{\sqrt{l^2-u^2}} \frac{1}{x-u}\, du$$

$$= \int_{\infty}^{0} \frac{(1+t^2)}{2t} \cdot \frac{(1+t^2)}{[(1+t^2)x - (1-t^2)l]} \cdot \frac{-4t}{(1+t^2)^2}\, dt$$

on changing variables to $\frac{u}{l} = \frac{1-t^2}{1+t^2}$

$$= 2\int_0^\infty \frac{1}{(1+x)t^2 - (1-x)}\,dt$$

$$= \frac{4}{1+x}\int_{-\infty}^{\infty} \frac{1}{\left(t+\sqrt{\frac{1-x}{1+x}}\right)\left(t-\sqrt{\frac{1-x}{1+x}}\right)}\,dt \qquad \text{if } x \in (-1,1)$$

This can be solved by considering

$$\frac{4}{1+x}\int_C \frac{1}{\left(z+\sqrt{\frac{1-x}{1+x}}\right)\left(z-\sqrt{\frac{1-x}{1+x}}\right)}\,dz$$

where C is the contour shown below:

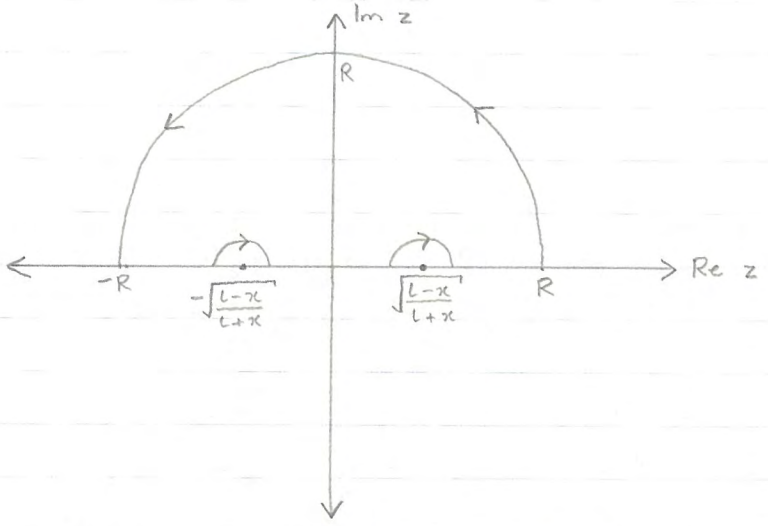

Since the integrand is $O\{R^{-2}\}$ as $R\to\infty$ the integral over the circular arc of radius R is

$$\int_0^{\pi} O\{R^{-2}\}.iRe^{i\theta}\,d\theta$$

which vanishes in the limit as $R\to\infty$.

Therefore

$$-\rho U^2 \pi \frac{d\eta}{dx} - \pi i \left[\frac{4}{L+x} \left(\frac{1}{2\sqrt{\frac{L-x}{L+x}}} \right) \right] - \pi i \left[\frac{4}{L+x} \left(\frac{1}{-2\sqrt{\frac{L-x}{L+x}}} \right) \right] = 0$$

using the residue theorem, which implies

$$\frac{d\eta}{dx} = 0 \quad \text{on} \quad (-L, L)$$

Thus $p_0(x)$ satisfies the homogeneous equation. We note that $p_0(x)$ is singular both at $x = -l$ and at $x = l$. For the Kutta condition to be satisfied therefore, $p_1(x)$ must also be singular at $x = l$ and the constant C in (5.20) must be chosen so that the singularities cancel; alternatively, the constant C in (5.20) may equal zero.

6. The Pressure Singularity

The general solution of the planing equation for $p(x)$ in the limit as $K \to 0$ can be seen to have an inverse square-root singularity at $x = -l$, i.e. at the leading edge. This singularity remains present at general values of K, as used by Maruo (1951) in his assumption of the form of the pressure distribution.

Since in the real case the pressure at the leading edge is not infinite, this means that there must be an error somewhere in our assumptions. This error lies in the assumption that variations in velocity and pressure are everywhere small.

It is an observed fact that at the leading edge the flow does not in general attach smoothly to the body, but instead bifurcates with a dividing streamline meeting the body at right angles and the fluid above this streamline being projected forward. Therefore the real situation is not as depicted in figure 1 (which follows our assumptions), but rather as shown below.

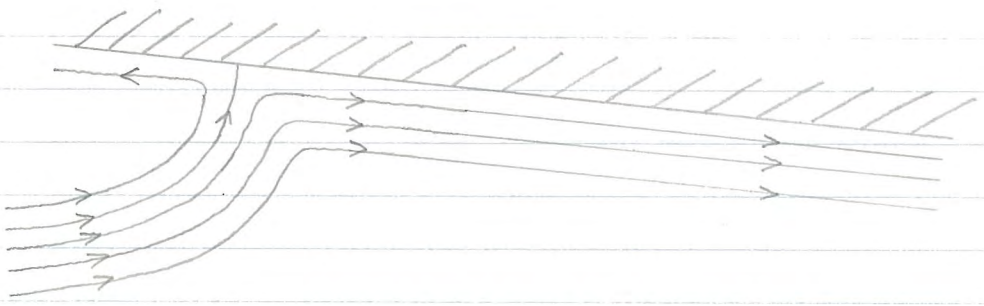

Fig. 2 Flow about the leading edge

The linearised equations of motion have been assumed to be asymptotically true in the limit as the small parameters (ε or β in (3.4)) tend towards zero; that is, all perturbations of the uniform stream should tend to zero as these variables tend to zero. However near the leading edge this is not true; the pressure and horizontal velocity perturbation at the stagnation point are asymptotically independent of ε and β. Therefore the ratio of the leading edge pressure to ε or β is asymptotically infinite, and this is the reason for the pressure singularity at the leading edge.

Everywhere other than in the vicinity of the leading edge the linearisation assumptions are quite good, but we might ask the question of how much the pressure aberration at the leading edge will affect net quantities like net lift, moment and drag. It is observed that for a real planing vessel the splash is small and one would expect it to have negligible effect on overall quantities. Wagner (1932) showed that the thickness of the splash jet is $O\{\beta^2\}$ and hence any contribution to net quantities caused by the splash will be of comparable magnitude to other terms already neglected in linearising the equations of motion. Therefore not including the splash will not change any net quantities to first order in β.

Similarly the effect of replacing it by a pressure singularity is at most of $O\{\beta^2\}$ since this will only affect the pressure very close to the leading edge, which will have negligible effect when integrating over $[-l, l]$. We can therefore modify our linearisation assumptions to require that variations in velocity and pressure are small everywhere except near the leading edge, with no loss of leading order accuracy.

The other issue that arises as a result of the splash is in the definition of the leading edge and hence of the wetted length. With the splash present there is no attachment point, since the flow divides and goes in both directions However as discussed, the pressure singularity in the linearised theory corresponds to the stagnation point in the real flow, so that if (as the solution demands) the singularity is at $x = -l$, the stagnation point in the real flow is, to leading order, at $x = -l$. Hence this must be the definition of the leading edge in the corresponding flow in which a splash is present - the location of the stagnation point.

7. Closing the Problem

7.1 Supplementary Equations

The planing equation (5.15) is an integral equation relating the pressure distribution $p(x)$ and the surface displacement $\eta(x)$ on $[-l, l]$. This can be solved for $p(x)$ if we know $\eta(x)$. However for the free-body problem, $\eta(x)$ (see equation (3.4)) contains two parameters that are not known in advance: the angle of attack β and the elevation h. As well as these, the wetted length $2l$ is also an unknown. Therefore we need three supplementary equations or constraints, as well as the planing equation, to be able to solve for the four unknowns $p(x)$, β, h and l.

The first of these constraints is the Kutta condition at the trailing edge, i.e.

$$p(l) = 0 \tag{7.1}$$

The second constraint is that for the body to be in equilibrium the net lift must equal the weight of the body, i.e.

$$\int_{-l}^{l} p(u)\, du = Mg \tag{7.2}$$

to leading order.

The third and final constraint is that the net moment on the body must be zero. Taking moments about $x=0$ requires

$$\int_{-l}^{l} u\, p(u)\, du = Mg(l-a) \qquad (7.3)$$

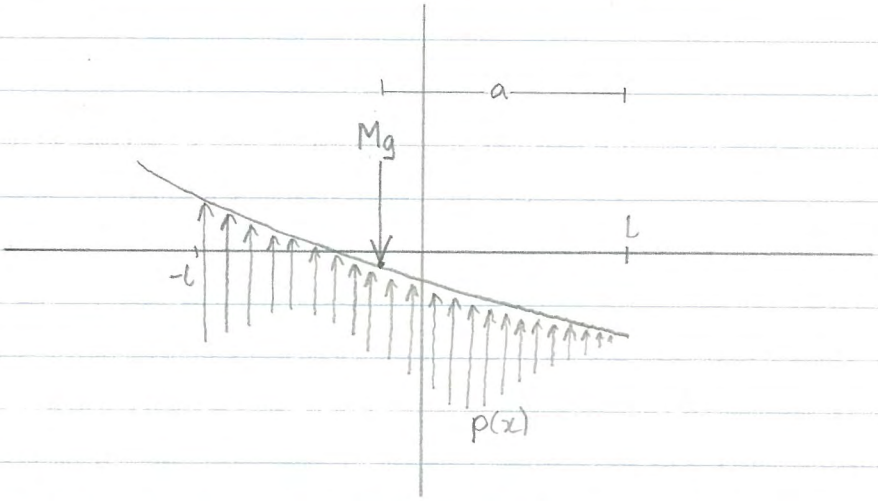

Fig. 3 Forces and Moments
(Net anticlockwise torque $= \int_{-l}^{l} u\, p(u)\, du + Mg(a-l)$.

We note that because of the linearisation (7.2) and (7.3) are independent of the shape of the body.

Thus the system of equations to be solved is

$$\varepsilon f(x) - \beta x + h = \frac{1}{pU^2\Pi} \int_{-l}^{l} p(u)\, I(x-u)\, du$$

$$p(l) = 0$$

$$\int_{-l}^{l} p(u)\, du = Mg$$

$$\int_{-l}^{l} u\, p(u)\, du = Mg(l-a)$$

7.2 Method of Solution

Since l is involved in the integration terminals it cannot be eliminated from the planing equation, so the process used to find l must be an inverse one. l is assumed known for the purposes of solving the planing equation and then solved for numerically later using (7.2) and (7.3). The unknown β in the planing equation is dealt with by dividing both sides by β. In the general case the quantity ε/β must then be given a value and β found later; the problem cannot be solved directly for a given ε. In the case of the flat plate, however $f(x) \equiv 0$ and this problem is avoided.

This leaves the quantity h/β as the last quantity to be dealt with in the planing equation. The simplest way to do this is to explicitly incorporate the Kutta condition into the numerical procedure, in which case h/β can be solved for explicitly. Once β is solved for this then determines h.

Therefore the free-body problem is a lot more complicated than the problem with l and β given because an inverse approach is required and cause and effect are harder to distinguish.

8. Flat Plate Numerical Solution

8.1 Non-Dimensionalisation

We define dimensionless variables

$$p' = \frac{p}{\rho U^2 \beta} \qquad x' = \frac{x}{l}$$

so that in terms of these, the planing equation for the flat plate (where $f(x) \equiv 0$) becomes

$$\frac{h}{l\beta} - x' = \frac{1}{\pi} \int_{-1}^{1} p'(lu')\, I'(x'-u')\, du' \qquad (8.1a)$$

where

$$I'(x'-u') = I(l(x'-u'))$$

$$= g(Kl(x'-u')) - 2\pi H(x'-u') \sin Kl(x'-u$$

$$= g\left(\frac{x'-u'}{F}\right) - 2\pi H(x'-u') \sin\left(\frac{x'-u'}{F}\right) \qquad (8.1b)$$

We note now that l has now been removed from the integration terminals and only appears in $F = U^2/gl$.

The lift and moment relations become, respectively,

$$\int_{-1}^{1} p'(lu')\, du' = \frac{Mg}{\rho U^2 \beta l} \qquad (8.2)$$

and

$$\int_{-1}^{1} u'\, p'(lu')\, du' = \frac{Mg(L-a)}{\rho U^2 \beta l^2} \qquad (8.3)$$

8.2 Change of Variables

As we will see, the accuracy of the numerical solution is aided by first making the change of variables

$$x' = -\cos\alpha$$
$$u' = -\cos\theta$$

whence the planing equation becomes

$$\frac{h}{l\beta} + \cos\alpha = \frac{1}{\pi}\int_0^\pi p'(-l\cos\theta)\sin\theta\, I'(\cos\theta - \cos\alpha)\, d\theta \qquad (8.4)$$

and the lift and moment equations become, respectively,

$$\int_0^\pi p'(-l\cos\theta)\sin\theta\, d\theta = \frac{Mg}{\rho U^2 \beta l} \qquad (8.5)$$

$$\int_0^\pi p'(-l\cos\theta)\sin\theta\cos\theta\, d\theta = -\frac{Mg(l-a)}{\rho U^2 \beta l^2} \qquad (8.6)$$

The integration range of the θ variable is $[0, \pi]$ as is the range of the α variable when x' is in $[-1, 1]$.

We now look at some of the properties of the integrand in (8.4). The kernel function $I'(\cos\theta - \cos\alpha)$ is still singular, since from (8.16) and (5.17)

$$I'(\cos\theta - \cos\alpha) \sim -\log_e\left|\frac{\cos\theta - \cos\alpha}{f}\right| \quad \text{as } \theta \to \alpha$$

so that

$$I'(\cos\theta - \cos\alpha) \to \infty \quad \text{as} \quad \theta \to \alpha$$

and the whole integrand tends to infinity as $\theta \to \alpha$. However the singularity in the integrand of the original planing equation (5.15) at the leading edge has effectively been removed by the change of variables. In the limit as $K \to 0$ considered in section 5.3, we saw that

$$p(x) = \frac{\text{constant}}{\sqrt{l^2 - x^2}} + p_1(x)$$

so that $p(x) \sim \dfrac{\text{constant}}{\sqrt{l+x}}$ as $x \to -l^+$

Hence

$$p(-l\cos\theta)\sin\theta \sim \frac{\text{constant}.\ \sin\theta}{\sqrt{1-\cos\theta}} \quad \text{as} \quad \theta \to 0^+$$

$$= \frac{\text{constant}.\ 2\sin\frac{\theta}{2}\cos\frac{\theta}{2}}{\sqrt{2\sin^2\frac{\theta}{2}}}$$

$$\sim \text{constant} \quad \text{as} \quad \theta \to 0^+$$

so the integrand in (8.4) tends to

$$\text{constant}.\ I'(1-\cos\alpha) \quad \text{as} \quad \theta \to 0^+$$

which is bounded $\forall\ \alpha \in (0, \pi]$. In the general case this is also true since $p(x)$ still has an inverse square root singularity at the leading edge. Hence with this change of variables the only

singularity in the integrand is at $\theta = \alpha$.

We will be explicitly applying the Kutta condition at the trailing edge, so the pressure and therefore the whole integrand will tend to zero as $\theta \to \pi^-$. The basic form of the integrand based on these conclusions is shown in figure 4 of the next section.

8.3 Discretisation

The numerical method involves discretising the integral on the right hand side of the planing equation (8.4) and discretising the sampling points (values of α) so that the planing equation is changed from an integral equation into a matrix equation.

The integral in (8.4) is in the main approximated by a simple rectangle rule using equal spacings in the θ-variable, where the height of each rectangle is equal to the value of the integrand at the chosen discretised values of θ. These will be denoted by θ_j, $j = 1..N$, where N is the number of subdivisions. Each value of θ_j will therefore lie in the j^{th} subinterval.

We note that using equal spacings in θ does not correspond to equal spacings in u'. If we sketch the graph of u' against θ,

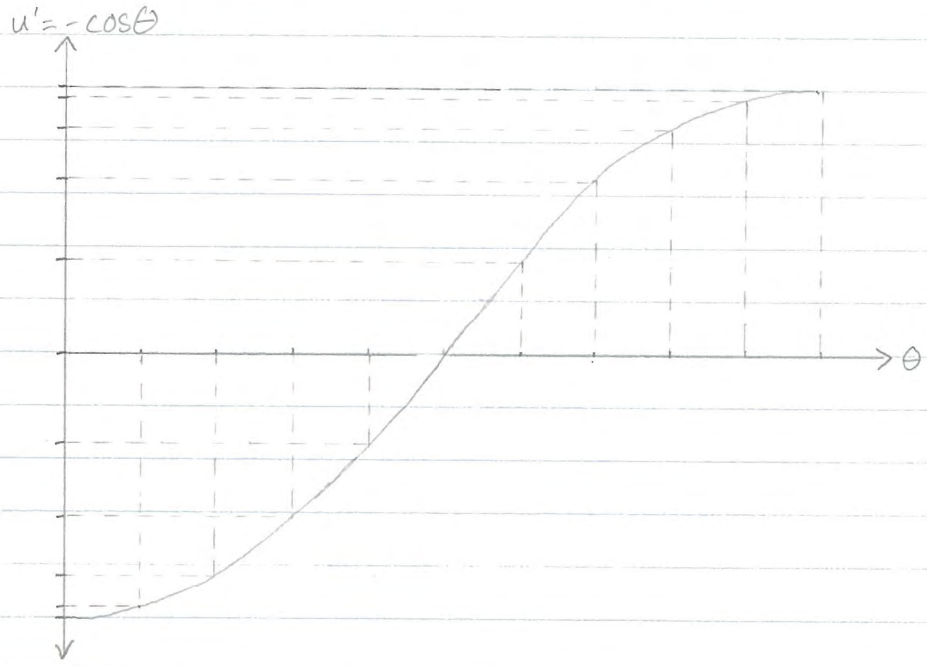

we see that a uniform grid in the θ variable means that gridpoints will be clustered towards the ends in the u' variable. In particular,

$$\Delta u = \sin\theta \, \Delta\theta \quad \text{as} \quad \Delta\theta \to 0$$

so Δu is smaller near the extremities.

This is an example of a Chebyshev grid in the u' variable, and it has clear advantages over a uniform grid. The pressure singularity at $u' = -1$ means that the pressure is changing very rapidly near here, so more gridpoints are needed near the leading edge than in the middle where the pressure is not changing as fast. Also, clustering the gridpoints towards the trailing edge at $u' = 1$ means that the Kutta condition can be better represented when the pressure is discretised.

The manner in which the integral in (8.4) is approximated by using the

rectangle rule is shown below in figure 4.

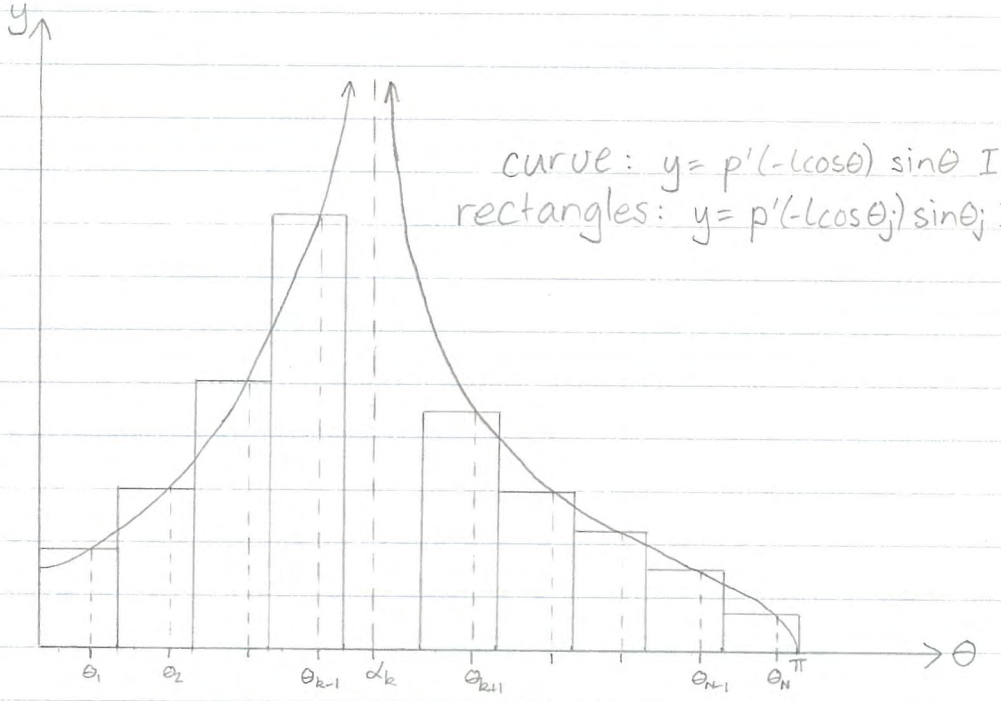

Fig. 4 Approximating the integral.

In the integral planing equation (8.4), α is a free variable such that $p'(-l\cos\theta)$ must satisfy this equation for all α in $[0,\pi]$. In the discretised case $p'(-l\cos\theta)$ is no longer continuous but has only $N-1$ degrees of freedom: the values of $p'(-l\cos\theta_j)$ for $j = 1..N-1$. These as well as the quantity h/μ are the N unknowns for which we have to solve, and to do this we need N equations. We therefore apply the discretised planing equation at N chosen values of α, i.e. at α_k, $k = 1..N$, where α_k lies in the k^{th} subinterval. This is called "collocation".

We see from figure 4 that the rectangle rule will provide a poor approximation to the integral over the

"diagonal" subinterval containing α_k, where $j=k$. We will therefore need to develop an alternative method for approximating the integral over this subinterval. The area thus calculated will be defined as $A(k,k)\, p'(-\cos\theta_k)\sin\theta_k\, \Delta\theta$, so that

$$A(k,k)\, p'(-\cos\theta_k)\sin\theta_k$$

is the effective height of the rectangle on the k^{th} subinterval.

The approximation to (8.4) is therefore

$$\frac{h}{\beta} + \cos\alpha_k = \frac{1}{\pi}\left\{ \sum_{\substack{j=1 \\ j\neq k}}^{N} p'(-\cos\theta_j)\sin\theta_j\; I'(\cos\theta_j - \cos\alpha_k) + A(k,k)\, p'(-\cos\theta_k)\sin\theta_k \right\} \cdot \Delta\theta$$

$$= \frac{1}{\pi} \sum_{j=1}^{N} A(k,j)\, p'(-\cos\theta_j)\sin\theta_j \cdot \Delta\theta \quad , k=1..N$$

where $A(k,j) \equiv I'(\cos\theta_j - \cos\alpha_k)$ for $j\neq k$ (8.7)

Since $\Delta\theta = \pi/N$, this becomes

$$\frac{Nh}{\beta} + N\cos\alpha_k = \sum_{j=1}^{N} A(k,j)\, p_j \sin\theta_j \quad , k=1..N \qquad (8.8)$$

where $p_j \equiv p'(-\cos\theta_j)$

This is not quite in the desired form yet since we still have an unknown on the left hand side, and the value of p_N on the right hand side is known to be zero from the Kutta condition. We therefore rearrange (8.8) into the form

$$N\cos\alpha_k = \sum_{j=1}^{N-1} A(k,j)\, p_j \sin\theta_j - \frac{Nh}{4\beta}\,, \quad k=1..N \qquad (8.9)$$

Note that we have made a further approximation by not applying the Kutta Condition actually at the trailing edge, but rather at $\theta = \theta_N$ which is somewhere in $[(\frac{N-1}{N})\pi, \pi]$. This will however be close to $\theta=\pi$ if N is large, and because of the clustering will be very close to $u'=1$.

In order to solve the system of equations (8.9), we write it in matrix form, with each row corresponding to a different value of k. We solve for $p_j \sin\theta_j$, $j=1..N-1$, instead of just p_j, as this will prove simpler in evaluating the lift and moment relations. The matrix equation is therefore

$$\underset{\sim}{A}\,\underset{\sim}{C} = \underset{\sim}{B}$$

where $\underset{\sim}{C} =$

$$\begin{bmatrix} p_1 \sin\theta_1 \\ p_2 \sin\theta_2 \\ \vdots \\ \vdots \\ \vdots \\ p_{N-1} \sin\theta_{N-1} \\ Nh/4\beta \end{bmatrix} \qquad (8.10a)$$

$$\underline{B} = \begin{bmatrix} N\cos\alpha_1 \\ N\cos\alpha_2 \\ \vdots \\ \vdots \\ \vdots \\ N\cos\alpha_N \end{bmatrix} \qquad (8.10b)$$

and

$$A = \begin{bmatrix} A(1,1) & A(1,2) & \cdots & A(1,N-1) & -1 \\ A(2,1) & A(2,2) & \cdots & A(2,N-1) & -1 \\ \vdots & \vdots & & \vdots & \vdots \\ A(N,1) & \cdots & & A(N,N-1) & -1 \end{bmatrix} \qquad (8.10c)$$

The solution of this matrix equation will give the pressures at the chosen values of θ_j, as well as the elevation h in terms of β.

The lift and moment relations (8.5) and (8.6) can be discretised in the same way as the planing equation to yield

$$\sum_{j=1}^{N-1} p_j \sin\theta_j = \frac{MgN}{\rho U^2 \pi \beta l} \qquad (8.11)$$

$$\sum_{j=1}^{N-1} p_j \sin\theta_j \cos\theta_j = \frac{MgN(a-l)}{\rho U^2 \pi \beta l^2} \qquad (8.12)$$

8.4 Error Considerations

Obviously we wish to set up the matrix equation so as to minimise the error in the solution vector $\underline{c}$. Up until now we have placed no restriction on the discretised values of θ and α other than that they lie in the appropriate subinterval. We now wish to choose these and the diagonal elements $A(k,k)$, $k=1..N-1$, so that the solution converges to the exact solution of the linearised planing equation as quickly as possible as N increases.

Errors in the values of p_j obtained will essentially come from two sources: the fact that we are only applying the planing equation at discrete values of α_k instead of over the entire range $[0,\pi]$, and the error that results from approximating the area under the curve by the rectangle rule.

The choosing of the points α_k, which are known as sensing or collocation points, is a complex mathematical process and is normally done by trial and error. The best positioning of the sensing points also depends in general on the discretised values of the integration variable (see e.g. James (1971) for the corresponding case of the airfoil equation). Therefore, for want of anything better, we will choose the sensing points to be a quarter of the

way along each subinterval, as in the vortex lattice method for airfoils (see e.g. James (1971)). One possible attribute of this is that the first few values of α_k will be quite close to the leading edge where the most pressure variation is. The values of α_k are thus given by

$$\alpha_k = (k - 3/4)\frac{\pi}{N} \qquad (8.13)$$

We will choose the values of θ_j so as to minimise the error of the rectangle rule as follows:

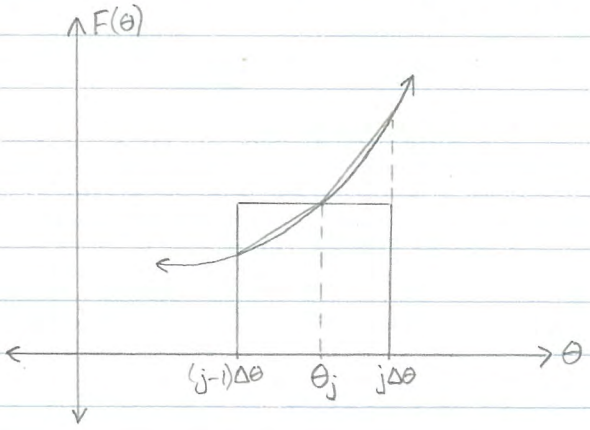

Fig. 5 The Rectangle Rule

Let $\theta_j = (j-r)\Delta\theta$, $0 \le r \le 1$
Then the error in approximating the section of the curve on $[(j-1)\Delta\theta, j\Delta\theta]$ by a rectangle with height θ_j is, to leading order in $\Delta\theta$, the difference in area of the two triangles shown in figure 5. That is,

$$e_j \equiv \int_{(j-1)\Delta\theta}^{j\Delta\theta} p'(-l\cos\theta)\sin\theta\, I'(\cos\theta-\cos\alpha_k)\,d\theta - A(k,j)\,p_j\sin\theta_j$$

$$= \{F(j\Delta\theta) - F(\theta_j)\}.\, r\frac{\Delta\theta}{2} + \{F((j-1)\Delta\theta) - F(\theta_j)\}(1-r)\frac{\Delta\theta}{2}$$

$$+ \text{higher order terms}$$

where $F(\theta) \equiv p'(-l\cos\theta)\sin\theta\, I'(\cos\theta-\cos\alpha_k)$

$$= \{F'(\theta_j).\, r\Delta\theta + O\{(\Delta\theta)^2\}\}.\, r\frac{\Delta\theta}{2}$$

$$+ \{F'(\theta_j).(r-1)\Delta\theta + O\{(\Delta\theta)^2\}\}.\,(1-r)\frac{\Delta\theta}{2} + \text{h.o.t.}$$

$$= F'(\theta_j).(2r-1)\frac{(\Delta\theta)^2}{2} + O\{(\Delta\theta)^3\}$$

Hence choosing $r=\frac{1}{2}$ will minimise the error over each subinterval as $\Delta\theta \to 0$, and since the $O\{(\Delta\theta)^3\}$ term is generally non-zero, this gives

$$e_j = O\{(\Delta\theta)^3\} \quad \text{as} \quad \Delta\theta \to 0 \qquad (8.14)$$

Therefore our values of θ_j will be given by

$$\theta_j = (j-\tfrac{1}{2})\frac{\pi}{N} \qquad (8.15)$$

We now need to find a way of computing the diagonal elements $A(k,k)$, $k=1..N-1$, so that their contribution to the error is of order the same as, or less than, the error due to using the rectangle rule on the other subintervals. Since from (8.14) the error on each of these subintervals is $O\{(\Delta\theta)^3\}$

the total error over the N-1 subintervals not containing α_k is $O\{(N-1).(\Delta\theta)^3\} = O\{(\Delta\theta)^2\}$ We therefore require

$$\int_{(k-1)\Delta\theta}^{k\Delta\theta} p'(-l\cos\theta)\sin\theta\, I'(\cos\theta - \cos\alpha_k)\, d\theta - A(k,k)\, p_k \sin\theta_k\, \Delta\theta = O\{(\Delta\theta)^2\} \qquad (8.16)$$

In order to approximate the integral in (8.16), which we shall denote by I_k, we note that by the mean value theorem

$$\int_{(k-1)\Delta\theta}^{k\Delta\theta} p'(-l\cos\theta)\sin\theta\, I'(\cos\theta - \cos\alpha_k)\, d\theta = p'(-l\cos\xi)\sin\xi \int_{(k-1)\Delta\theta}^{k\Delta\theta} I'(\cos\theta - \cos\alpha_k)\, d\theta$$

for some ξ in $[(k-1)\Delta\theta, k\Delta\theta]$

Also from Taylor's theorem:

$$p'(-l\cos\xi)\sin\xi = p'(-l\cos\theta_k)\sin\theta_k + O\{\xi - \theta_k\}$$

$$= p_k \sin\theta_k + O\{\Delta\theta\}$$

We see that I_k must be $O\{\Delta\theta\}$ for (8.16) to hold. Therefore

$$I_k = [\, p_k \sin\theta_k + O\{\Delta\theta\}\,] \int_{(k-1)\Delta\theta}^{k\Delta\theta} I'(\cos\theta - \cos\alpha_k)\, d\theta$$

$$= p_k \sin\theta_k \int_{(k-1)\Delta\theta}^{k\Delta\theta} I'(\cos\theta - \cos\alpha_k)\, d\theta + O\{(\Delta\theta)^2\}$$

to the desired order of accuracy.

In order to approximate this integral we use equation (5.18), i.e.

$$I(m) \to \text{constant} - \log_e Km + O(m) \quad \text{as } m \to 0$$

The constant comes from the cosine integral and can be found in, for example, Abramowitz and Stegun (1964) equation 5.2.16, to be the negative of Euler's constant $\gamma = 0.5772156649\ldots$
The dimensionless kernel is therefore

$$I'(m) = I(lm) = -\gamma - \log_e\left(\frac{m}{f}\right) + O(m) \qquad (8.18)$$

Now (8.17) becomes

$$I_k = p_k \sin\theta_k (\log_e f - \gamma)\Delta\theta - p_k \sin\theta_k \int_{(k-1)\Delta\theta}^{k\Delta\theta} \log_e |\cos\theta - \cos\alpha_k| \, d\theta + \int_{(k-1)\Delta\theta}^{k\Delta\theta} O\{\cos\theta - \cos\alpha_k\} \, d\theta + O\{(\Delta\theta)^2\} \qquad (8.19)$$

To find the order of the error we calculate

$$\int_{(k-1)\Delta\theta}^{k\Delta\theta} \cos\theta - \cos\alpha_k \, d\theta$$

$$= -\cos\alpha_k \Delta\theta + \sin k\Delta\theta - \sin(k-1)\Delta\theta$$

$$= -\Delta\theta\left[\cos\left((k-\tfrac{3}{4})\Delta\theta\right) - \cos\left((k-1)\Delta\theta\right) + O\{\Delta\theta\}\right]$$

$$= -\Delta\theta\left[-\sin\left((k-1)\Delta\theta\right) \cdot \frac{\Delta\theta}{4} + O\{\Delta\theta\}\right]$$

$$= O\{(\Delta\theta)^2\}$$

using repeatedly $f(x+h) - f(x) = f'(x) \cdot h + O\{h^2\}$

(8.19) therefore becomes

$$I_k = p_k \sin\theta_k \,(\log_e f - \gamma)\,\Delta\theta - p_k \sin\theta_k \int_{(k-1)\Delta\theta}^{k\Delta\theta} \log_e|\cos\theta - \cos\alpha_k|\,d\theta + O\{(\Delta\theta)^2\} \qquad (8.20)$$

$$= p_k \sin\theta_k \,(\log_e f - \gamma)\,\Delta\theta - p_k \sin\theta_k \int_{(k-1)\Delta\theta}^{k\Delta\theta} \log_e\left|-2\sin\left(\frac{\theta+\alpha_k}{2}\right)\sin\left(\frac{\theta-\alpha_k}{2}\right)\right| d\theta + O\{(\Delta\theta)^2\}$$

$$= p_k \sin\theta_k \left[\left(\log_e \frac{f}{2} - \gamma\right)\Delta\theta - \log_e\left|\sin\left(\frac{\theta_k+\alpha_k}{2}\right)\right|\Delta\theta + O\{(\Delta\theta)^3\} - \int_{(k-1)\Delta\theta}^{k\Delta\theta} \log_e\left|\sin\left(\frac{\theta-\alpha_k}{2}\right)\right| d\theta\right] + O\{(\Delta\theta)^2\} \qquad (8.21)$$

Letting $x = \dfrac{\theta-\alpha_k}{2} = \dfrac{\theta-(k-\frac{3}{4})\Delta\theta}{2}$ for the integral in (8.21) and integrating $\log_e|\sin x|$ by parts gives

$$\int_{(k-1)\Delta\theta}^{k\Delta\theta} \log_e\left|\sin\left(\frac{\theta-\alpha_k}{2}\right)\right| d\theta = 2\int_{-\frac{\Delta\theta}{8}}^{\frac{3\Delta\theta}{8}} \log_e|\sin x|\,dx$$

$$= 2\left[x\log_e|\sin x|\right]_{-\frac{\Delta\theta}{8}}^{\frac{3\Delta\theta}{8}} - 2\int_{-\frac{\Delta\theta}{8}}^{\frac{3\Delta\theta}{8}} \frac{x\cos x}{\sin x}\,dx$$

$$= 2\left[x\log_e|\sin x| - x + O\{x^2\}\right]_{-\frac{\Delta\theta}{8}}^{\frac{3\Delta\theta}{8}}$$

since $\dfrac{x\cos x}{\sin x} = 1 + O\{x\}$

$O(x^2)$, $\cos x < \dfrac{\sin x}{x} < 1$

Thus (8.21) becomes

$$I_k = p_k \sin\theta_k \Delta\theta \left[\log_e\left(\frac{f}{2}\right) - \gamma - \log_e \sin\left((k-3/8)\Delta\theta\right) - 2\left(\frac{3}{8}\log_e \sin\frac{3\Delta\theta}{8} - \frac{1}{2} + \frac{1}{8}\log_e \sin\frac{\Delta\theta}{8} \right)\right] + O\{(\Delta\theta)^2\}$$

$$\therefore I_k = p_k \sin\theta_k \Delta\theta \left[\log_e\left(\frac{f}{2}\right) + 1 - \gamma - \log_e \sin\left((k-3/8)\Delta\theta\right) - \frac{3}{4}\log_e \sin\frac{3\Delta\theta}{8} - \frac{1}{4}\log_e \sin\frac{\Delta\theta}{8} \right] + O\{(\Delta\theta)^2\} \quad (8.22)$$

Hence $A(k,k)$ is given by the term in square brackets in (8.22), which can otherwise be written

$$A(k,k) = \log_e\left(\frac{f}{2}\right) + 1 - \gamma - \frac{1}{4}\log_e\left(\sin^4\left((k-3/8)\Delta\theta\right)\sin^3\left(\frac{3\Delta\theta}{8}\right)\sin\left(\frac{\Delta\theta}{8}\right)\right) \quad (8.23)$$

$\frac{1}{2}$ in program?

8.5 The Final Matrix Equation

The off-diagonal elements of the matrix A are expressed in terms of sine and cosine integrals. These must be approximated in some way before the system can be solved numerically. These off-diagonal elements

$$A(k,j) = I'(\cos\theta_j - \cos\alpha_k)$$

are defined from (8.16) and (5.16) as

$$A(k,j) = -\cos y.\ ci(|y|) - \sin(|y|)\, si(|y|) - 2\pi H(y)\sin y$$

where $$y = \frac{\cos\theta_j - \cos\alpha_k}{f}$$

Since f can take any value greater than zero, y can also take any value so we will need both small and large y approximations for ci and si. The approximations used come from Abramowitz and Stegun (1964) section 5.2.

For $y < 2.5$ we use the convergent power series forms:

$$ci(y) = \gamma + \log_e y + \sum_{n=1}^{\infty} \frac{(-1)^n y^{2n}}{2n.(2n)!}$$

$$si(y) = -\frac{\pi}{2} + \sum_{n=0}^{\infty} \frac{(-1)^{n+1} y^{2n+1}}{(2n+1).(2n+1)!}$$

These are truncated at $n=6$ with

an error $< 10^{-6}$.

For $y > 2.5$ we use the rational approximations:

$$si(y) = -f(y)\cos y - g(y)\sin y$$

$$ci(y) = f(y)\sin y - g(y)\cos y$$

where

$$f(y) = \frac{1}{y}\left(\frac{y^8 + a_1 y^6 + a_2 y^4 + a_3 y^2 + a_4}{y^8 + b_1 y^6 + b_2 y^4 + b_3 y^2 + b_4}\right)$$

with

$a_1 = 38.027264$ $\quad b_1 = 40.021433$

$a_2 = 265.187033$ $\quad b_2 = 322.624911$

$a_3 = 335.677320$ $\quad b_3 = 570.236280$

$a_4 = 38.102495$ $\quad b_4 = 157.105423$,

$$g(y) = \frac{1}{y^2}\left(\frac{y^8 + a_1 y^6 + a_2 y^4 + a_3 y^2 + a_4}{y^8 + b_1 y^6 + b_2 y^4 + b_3 y^2 + b_4}\right)$$

with

$a_1 = 42.242855$ $\quad b_1 = 48.196927$

$a_2 = 302.757865$ $\quad b_2 = 482.485984$

$a_3 = 352.018498$ $\quad b_3 = 1114.978885$

$a_4 = 21.821899$ $\quad b_4 = 449.690326$

The error in each of these approximations is also $< 10^{-6}$.

This defines the off-diagonal elements of the matrix A. The diagonal elements A(k,k), k=1..N-1, are given by (8.23). We showed that the approximation to the integral equation is second order in $\Delta\theta$, so that net quantities like lift and drag which involve integrating

the pressure over the whole interval will also have an error which is $O\{(\Delta\theta)^2\}$ as $\Delta\theta \to 0$. One problem arises however with the diagonal elements $A(k,k)$ in that they are actually second order in $(\Delta\theta/f)$, so that if f is very small the error terms may not be negligible. Therefore we only use the expression given in (8.23) if $f > 0.1$, otherwise we use the same expression for $A(k,k)$ as for the off-diagonal elements. In this case the approximation is only first order accurate in $\Delta\theta$.

8.6 Computational Considerations

Programs were written in Fortran 77 to solve the matrix equation and compute the various output quantities. The NAG routine IFO4ATF was used, which utilises Crout's factorisation method to invert the matrix. One question that we might ask is whether the matrix A is diagonally dominant, which would ensure stability of the inversion process.

For diagonal dominance we require

$$|A(k,k)| \geq \sum_{\substack{j=1 \\ j \neq k}}^{N} |A(k,j)|$$

or from (8.7),

$$|A(k,k)\,\Delta\theta| \geq \sum_{\substack{j=1 \\ j\neq k}}^{N} |I'(\cos\theta_j - \cos\alpha_k).\,\Delta\theta| \quad \text{as } \Delta\theta\to 0 \qquad (8.24)$$

In order to evaluate $\lim_{\Delta\theta\to 0} A(k,k)\,\Delta\theta$ we note that

$$\lim_{\Delta\theta\to 0} \log_e(\sin^n \Delta\theta).\,\Delta\theta = \lim_{\Delta\theta\to 0} n\,\frac{\cos\Delta\theta.\,(\Delta\theta)^2}{\sin(\Delta\theta)}$$

$= 0$ by l'Hôpital's rule.

Therefore $\lim_{\Delta\theta\to 0} A(k,k)\,\Delta\theta = 0$ from (8.23).

However the quantity on the right in (8.24) is $O\{1\}$ as $\Delta\theta\to 0$, since it represents the rectangle rule approximation to the total area under the curve of $|I'(\cos\theta - \cos\alpha_k)|$ on $[0,\pi]$, not including the k^{th} interval. Hence (8.24) is false and the matrix is not diagonally dominant as $\Delta\theta\to 0$. We cannot therefore guarantee stability of the solution process.

A reasonably fine grid in which $N=200$ and $\Delta\theta = \pi/200$ was used for all final calculations. In order to see that the results were converging and get some idea of the error, tests were also run for $N=100$ and 150. The number of significant figures of which we were confident was the number that remained unchanged for these different values of N.

9. Flat Plate Results

9.1 The Pressure Distribution

We see from the matrix equation that the discretised pressures p_j, $j=1..N-1$, depend only on f. The shape of the pressure distribution for different values of f is shown in graph ①. The pressure is divided by $\rho U^2 \beta$ which is different for different values of f. The $f=\infty$ case is that discussed in section 5.3 and we see the inverse square-root singularity at $x'=-1$. As discussed earlier this pressure singularity is still present for the finite Froude number cases. Another feature we note is that the centre of pressure tends to move towards the leading edge $x'=-1$ as f increases This property will be witnessed in the graph of wetted length vs. Fa in the next section.

9.2 Other Outputs

We mentioned in section 7.1 that there are four unknowns for this problem: $p(x)$, l, β and h. We have so far solved for p_j, $j=1..N-1$, and h/β. In order to solve for l, β and h we will use the discretised lift and moment relations (8.11) and (8.12). To give an expression for l we divide (8.12) by (8.11) to give

$$\frac{a-l}{l} = \frac{\sum_{j=1}^{N-1} p_j \sin\theta_j \cos\theta_j}{\sum_{j=1}^{N-1} p_j \sin\theta_j}$$

or
$$\frac{l}{a} = \frac{s1}{s1+s2} \qquad (9.1)$$

where
$$s1 \equiv \sum_{j=1}^{N-1} p_j \sin\theta_j \qquad (9.2)$$

$$s2 \equiv \sum_{j=1}^{N-1} p_j \sin\theta_j \cos\theta_j \qquad (9.3)$$

Since p_j, $j = 1..N-1$ are only functions of $f = U^2/gl$, (9.1) is a relation between l/a and U^2/gl. By running the program for many different values of f we can build up a table of these data pairs. We can then multiply them together and take the square root to get a third column: $F_a = U/\sqrt{ga}$. Now l/a can be plotted against the true input quantity F_a. Graph ② shows the total wetted length $2l$ as a fraction of 'a' vs. F_a.

We see that if 'a' is held fixed and U increased the wetted length decreases sharply as F_a passes through 1, before staying approximately constant and tending to $4/3$ as $F_a \to \infty$. This is in agreement with the general observation that as the speed increases the vessel lifts out of the water and its wetted length decreases. However the graph is not quite monotonic; it has a shallow minimum at $F_a \simeq 1.5$ before

rising slowly towards 4/3. This is due to the fact that the angle of attack is changing as well, as we shall see.

Equation (8.11), i.e.

$$s1 = \frac{MgN}{\rho U^2 \pi \beta l} = \frac{MN}{\rho f \pi \beta l^2}$$

can be used with (9.1) to eliminate l, giving

$$\frac{\rho a^2 \beta}{M} = \frac{(s1+s2)^2}{s1^3} \cdot \frac{N}{f\pi} \qquad (9.4)$$

The right hand side in (9.4) again depends only on f, so if we include $\rho a^2\beta/M$ as another column in our table we can plot $\rho a^2\beta/M$ vs. F_a in the same way as for the wetted length. The result is shown in graph ③, which shows the variation in angle of attack with velocity if 'a' is constant.

In this graph we see another feature of the transition to planing: the rapid variations in angle of attack that occur. As F_a passes through 1, β reaches a sharp maximum before tending monotonically to zero as $F_a \to \infty$. Here we see the reason behind the wetted length increasing slightly as F_a gets large: the angle of attack is decreasing, causing the leading edge to be lowered relative to the trailing edge and the flow to attach earlier.

At this point we might ask

what the implications of this graph are with regard to the linearisation. We have assumed that β is small so that terms of order β^2 can be neglected. From the graph we can see that when F_a is reasonably small, $\rho a^2\beta/M$ is of order 1. For β to be small we therefore need a small mass and/or a large value of 'a'. Thus in the transition region where $F_a \simeq 1$ the results obtained will apply better to larger, lighter vessels. However when F_a is large, $\rho a^2\beta/M$ is small so having a larger mass and/or smaller value of 'a' will still mean that β is small. Therefore provided that they are moving sufficiently fast, linearisation is still justified for small and/or heavy vessels.

Graph ③ effectively gives the angle of attack vs. speed when 'a' is constant. For some vessels, however, 'a' can be changed substantially by the rider moving forwards or backwards. Good examples include surfboards, windsurfers and skiff dinghies. For these craft we may want to find the effect changing 'a' has on the angle of attack. If we multiply (9.4) by F_a^4 we obtain

$$\frac{\rho U^4 \beta}{Mg^2} = \frac{Nf}{\pi s l} \qquad (9.5)$$

which is used in the same way as (9.1) and (9.4) to give the angle of attack

vs. F_a at constant velocity. This is shown in graph ④.

From this graph we see that as 'a' decreases and F_a increases, the angle of attack increases monotonically as would be expected. We note a sharp increase in the transition region around $F_a = 1$. The graph is of course skewed since the x axis is proportional to $a^{-1/2}$.

The other output quantity that was solved for was the elevation 'h' of the plate above $x=0$. The last element of the solution vector $\underline{c}$ was

$$C(N) = \frac{Nh}{L\beta} \qquad (9.6)$$

Since we now have tables of L and β in terms of input quantities we can solve for h. Multiplying (9.6) by (9.1) and (9.4) gives

$$\frac{\rho a h}{M} = \frac{C(N)}{f\pi} \cdot \frac{(s1+s2)}{s1^2} \qquad (9.7)$$

This is used as before to give a plot of $\rho ah/M$ vs. F_a which shows the height of the plate above the origin when 'a' is fixed. This is shown in graph ⑤.

As we would expect, at very small velocities the plate sinks down below the water. We must remember that one of our assumptions was that

of smooth detachment, which does not hold in the limit as the velocity tends to zero. We should therefore think of the low F_a limit as corresponding to large values of 'a'. If we now keep 'a' fixed and increase the velocity, the centre height initially decreases. This phenomenon also occurs for displacement vessels and is known as "squat". However in the transition region $F_a = 1$ the elevation rises sharply before reaching a positive maximum and then tending monotonically down towards zero.

This graph shows another important feature of the transition to planing: the fact that the vessel lifts up out of the water, so that its centre is actually above the undisturbed surface height for large F_a. The decrease in h with F_a for large F_a is related to the changing angle of attack; as β tends towards zero the disturbance of the water becomes less and less and the plate lowers until at $F_a = \infty$ it is sitting flat on $y=0$.

We now know that the centre of the plate rises above $y=0$, but what about the trailing edge? The trailing edge height H is given to first order in β by

$$H = h - l\beta$$

so that from (9.7), (9.1) and (9.4),

$$\frac{path}{M} = \frac{(C(N) - N)}{f\pi} \cdot \frac{(s1 + s2)}{s1^2} \qquad (9.8)$$

Thus $path/M$ can be plotted against F_a in the same way as for the other graphs and the result is shown in graph ⑥. This graph is similar to the centre height graph apart from the effects of the changing angle of attack and wetted length. Where the centre height falls to a minimum at $F_a \simeq 0.85$ the trailing edge height drops further to a sharper minimum because the angle of attack is just here reaching a maximum. As the centre height subsequently increases the trailing edge height increases faster. This is because β and l are both decreasing, so $h - l\beta$ is increasing faster than h. We see that the trailing edge height does rise above $y=0$ for $F_a \geq 2.15$ and reach a maximum before tending towards zero. Therefore for large values of F_a, not just the centre but the whole plate is actually above the undisturbed water surface height.

9.3 General Comments

The stability and convergence of the computations was good everywhere except for very small values of f. Since $F_a \sim (f/2)^{1/2}$ this corresponded to a not-so-small range of values of F_a. For $f \leq 0.05$ or $F_a \leq 0.2$ the results became oscillatory, quite possibly due to the instability of the matrix inversion process. Trying different values of N as discussed earlier indicated that the results were generally three-figure accurate except for very small f. Since this is the region where the assumption of smooth detachment is likely to be false, and the main region of interest is at and beyond the transition to planing region $F_a \geq 0.5$, this does not overly concern us.

9.4 The Planing Sequence

Now that we know ℓ, β and h in terms of F_a we can look at the overall positioning of the plate as F_a increases. This can be thought of as the orientation of the vessel as it starts from rest and slowly accelerates through different values of U, so the motion can be considered steady. A diagrammatic representation for different values of F_a can be sketched as follows.

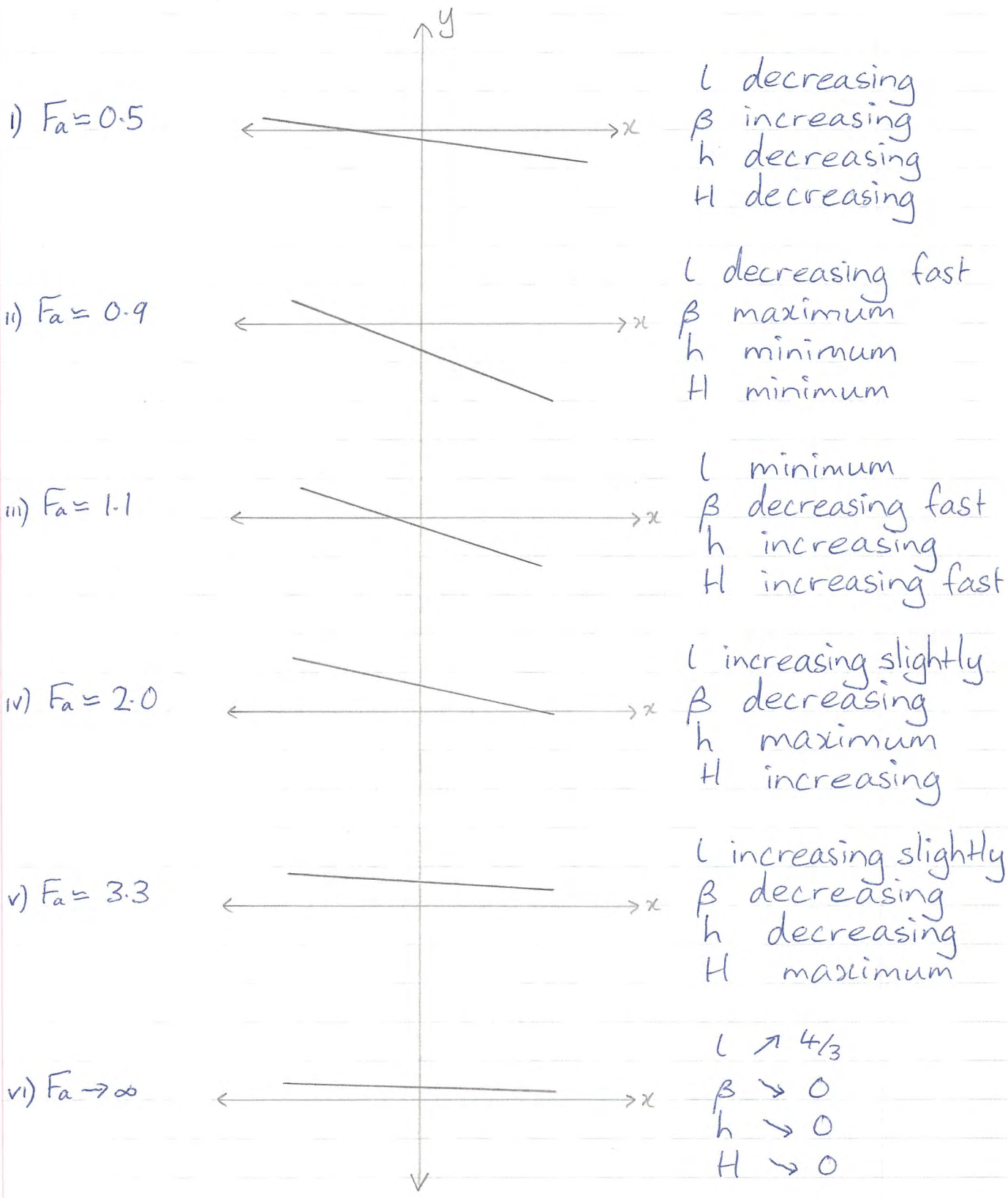

Fig. 6 The Planing Sequence

9.5 Drag

Probably the most important quantity that we are interested in is the total drag on the vessel. This is made up of inviscid and viscous drag, both of which are obtainable from quantities already computed.

The inviscid drag per unit breadth can be found simply by the component of the pressure force tangential to the motion, i.e.

$$D_{inv} = \beta \int_{-l}^{l} p(u)\, du \qquad \text{to first order}$$

$$\therefore \quad D_{inv} = Mg\beta \qquad (9.9)$$

from (7.2). Therefore for given M, D_{inv} is proportional to the angle of attack. From graph ③ it has a maximum at $F_a \simeq 0.9$ before decreasing as F_a increases.

Energy is taken from the vessel in the form of inviscid drag by two mechanisms: the waves downstream and the splash. It can be shown (see e.g. Newman (1977) pp. 267-268) that the wave drag is given by $\frac{1}{4}\rho g A^2$, where A is the wave amplitude. The wave amplitude can be found from the planing equation once we have solved for the pressure distribution as follows:

As $x \to \infty$, $g(Km) \to 0$

so $I(m) \to 2\pi \sin Km$

$$\therefore \eta(x) \to \frac{2\pi}{\rho U^2 \pi} \int_{-l}^{l} p(u) \sin K(x-u)\, du$$

$$= 2l\beta \int_{-1}^{1} p'(lu') \sin\left(\frac{x'-u'}{f}\right) du'$$

$$= 2l\beta \left\{ \sin\left(\frac{x'}{f}\right) \int_{-1}^{1} p'(lu') \cos\frac{u'}{f}\, du' - \cos\left(\frac{x'}{f}\right) \int_{-1}^{1} p'(lu') \sin\left(\frac{u'}{f}\right) du' \right\}$$

$$= A \sin\left(\frac{x'}{f} - \delta\right)$$

where $$A = 2l\beta \left[\left(\int_{-1}^{1} p'(lu') \cos\left(\frac{u'}{f}\right) du' \right)^2 + \left(\int_{-1}^{1} p'(lu') \sin\left(\frac{u'}{f}\right) du' \right)^2 \right]^{\frac{1}{2}}$$

The splash drag, which is the difference between the total drag and the wave drag, can be found explicitly by solving the nonlinear problem at the leading edge, and this provides a check of the method used to find it.

For the viscous drag we use the concept of the drag coefficient:

$$C_D = \frac{D_{vis}}{\frac{1}{2}\rho U^2 L} \qquad (9.10)$$

Empirical observations suggest that the flow past a flat plate becomes turbulent when the Reynolds number Re defined

by

$$Re = \frac{UL}{\nu} = \frac{2UL}{\nu} \qquad \text{in our case,}$$

is greater than 5×10^5 (Newman (1977) p.17). We will be using $\nu = 1.2 \times 10^{-6}$, the value for salt water at 15°C (Newman (1977) p.388). For the flow to be turbulent would therefore require $2UL > 0.6\ m^2 s^{-1}$. For all the planing vessels mentioned in the introduction this will practically always be true, so we can use the turbulent drag coefficient relation given by Schoenherr (see Newman (1977) p.17):

$$Re = \frac{10^{0.242/\sqrt{C_D}}}{C_D}$$

$$\text{or} \quad UL = \frac{6.0 \times 10^{-7} \times 10^{0.242/\sqrt{C_D}}}{C_D} \qquad (9.11)$$

This is the drag coefficient for one side of a submerged flat plate moving in the longitudinal direction. This should still be reasonably accurate for a flat plate gliding along the surface since both have a similar stagnation point at the leading edge. Also the effect of the angle of attack will be of higher order in β and can be neglected.

Thus the viscous drag per unit breadth is given by

$$D_{vis} = \tfrac{1}{2} \rho U^2 L C_D = \rho U^2 l C_D \qquad (9.12)$$

with C_D defined as in (9.11). The total drag

is the sum of (9.9) and (9.12), i.e.

$$D_{tot} = Mg\beta + \rho U^2 l C_D$$

$$= \frac{M^2 g N (s1+s2)^2}{\rho a^2 f \pi s1^3} + \rho g f l^2 C_D$$

using (9.4). Since l is not known in advance and is related to 'a', l and 'a' cannot be specified simultaneously. Also since f and C_D both involve l we shall eliminate 'a' and solve for it later - again an inverse approach. Hence

$$D_{tot} = \frac{M^2 g N}{\rho l^2 f \pi s1} + \rho g f l^2 C_D \qquad (9.13)$$

using (9.1). Unlike the other output quantities, the drag cannot be made a function only of f, so we must specify both f and l, or alternatively both U and l. There is also another problem: the mass per unit breadth M is not present in the second term of (9.13) so we cannot eliminate it from the right hand side. We must therefore specify M in some way.

If we divide (9.13) by ρg we obtain

$$\frac{D_{tot}}{\rho g} = \frac{\mu^2 N}{f l^2 \pi s1} + f l^2 C_D \qquad (9.14)$$

where $$\mu \equiv \frac{M}{\rho} \qquad (9.15)$$

We shall use SI units so that the units of μ are m^2. Hence the units of (Drag/ρg) are also m^2. μ must be specified at the beginning, so we choose a value that is typical of the planing vessels mentioned in the introduction: $\mu = 0.3 m^2$. We shall use this for all drag calculations, but the results can easily be modified for different values of μ.

Equation (9.11) cannot be rearranged to get C_D in terms of L, so we decide to make C_D the independent variable. We can now solve (9.14) for a given value of U by putting in a value of C_D, which implies a value of L and then a value of f. The planing equation is then solved as before to output the value of L/a from (9.1); since L is known 'a' can be found uniquely. At the same time the drag is calculated from (9.14). Building up a set of data pairs of (Drag/ρg) vs. 'a' in this way we can then plot the results, as shown in graphs ⑦ and ⑧ for $U = 6 m/s$ and $U = 20 m/s$ respectively.

We see that both these graphs have minima. This is to be expected since from observation all planing vessels operate most efficiently at finite non-zero values of 'a'. We can see that the viscous drag is a monotonically increasing function of 'a'; since C_D is only very weakly dependent on L, D_{vis} is approximately proportional to L from (9.12).

Also, from graph ②, L/a increases or is approximately constant with 'a', so L increases monotonically with 'a'. Therefore D_{vis} increases monotonically with 'a'.

From graph ④ the inviscid drag decreases monotonically as 'a' increases. Therefore the total drag is the sum of a monotonically increasing and a monotonically decreasing function of 'a'. With $U = 6$ m/s the scaled total drag has a shallow minimum of about $0.029\ m^2$ at $a = 1.5$ m. With $U = 20$ m/s the scaled total drag has a minimum of about $0.021\ m^2$ at $a = 0.1$ m. This illustrates the property of planing vessels with variable weight positioning that minimum drag is obtained by positioning the weight forward at low speeds and back at high speeds.

We shall now consider the above-mentioned type of vessel and try to find the minimum possible total drag for a given speed without having to plot the whole graph. This can be done by using Newton's method to find the point at which the derivative of total drag with respect to 'a' vanishes. This will be the same as finding when the derivative with respect to L or C_D vanishes, since the relationship between 'a' and L, and between L and C_D, is one-one. Since we are using C_D as the input quantity we shall consider

$$\frac{D_{tot}}{\rho g} = f(C_D)$$

for given U, and use Newton's iterative formula for finding C_D such that $f'(C_D)=0$, i.e.

$$C_D^{(n+1)} = C_D^{(n)} - \frac{f'(C_D^{(n)})}{f''(C_D^{(n)})} \qquad (9.16)$$

where the superscript denotes iteration number. The derivatives are approximated using three-point centred-difference forms to give

$$C_D^{(n+1)} = C_D^{(n)} - \frac{\varepsilon_0}{2}\left[\frac{f(C_D^{(n)}+\varepsilon_0) - f(C_D^{(n)}-\varepsilon_0)}{f(C_D^{(n)}+\varepsilon_0) - 2f(C_D^{(n)}) + f(C_D^{(n)}-\varepsilon_0)}\right] \qquad (9.17)$$

as our iterative method. The computer program uses three element arrays for C_D and $(D_{tot}/\rho g)$, where $C_D(1) = C_D^{(n)} - \varepsilon_0$, $C_D(2) = C_D^{(n)}$, $C_D(3) = C_D^{(n)} + \varepsilon_0$ and $D_{tot}(i) = f(C_D(i))$, $i=1,2,3$. The program overwrites $C_D(2)$ by $C_D^{(n+1)}$ as computed in (9.17) until the difference in the values of $D_{tot}(i)$, $i=1,2,3$ is negligible. Careful choosing of $C_D^{(0)}$ was necessary for fast convergence and ε_0 was decreased at each successive iteration.

The minimum scaled total drag is shown in graph ⑨ as a function of U. Here we see one of the major attributes of planing vessels – the ability to operate at high speeds with low drag. If L was kept constant the total drag would rise very quickly because the viscous drag is proportional to U^2. However, L can be made to decrease dramatically by decreasing 'a'; not only L but the ratio L/a decreases

from graph ②. This is in addition to the shortening of the wetted length that results from increasing U at constant 'a' (see graph ②). Therefore for velocities between 10 and 25 m/s the minimum possible drag is approximately constant before thereafter rising very slowly and monotonically.

The peak at U = 5·5 m/s corresponds to a region where there is large inviscid drag over most values of 'a', so 'a' must be quite large to overcome this, thus increasing the viscous drag. For small values of U the viscous drag is very small so large values of 'a' can be used, producing very small inviscid drag (see graph ④).

Graph ⑩ shows the corresponding values of 'a' that should be chosen for minimising drag at a given speed. Here we see the tendency for 'a' to decrease with increasing velocity as discussed. For large values of U 'a' is very small indeed; for example when U = 20m/s the centre of mass should be only 0·18m from the trailing edge for minimum possible drag. On the other hand when U = 2 m/s the centre of mass should be 3·5m from the trailing edge for minimum possible drag – a huge variation. The sharp change around U = 5·5 m/s can be attributed to the very shallow minima of total drag as a function of 'a' for velocities in this region. Graph

⑦, where U=6m/s, is at the end of this sharp decrease in 'a'; we see from this graph that if U and hence Dis is decreased just slightly, the minimum will move quickly to a much higher value of 'a'.

10. A Modified Shape

10.1 Setting up the equations

The flat plate is known to have low drag over a large speed range. One contribution to this is the splash drag which is always present. This prompts us to ask whether the splash can be removed by changing the shape of the plate at the leading edge, whilst leaving the rest the same to preserve the low wave drag that makes flat vessels so efficient.

In order for there to be no splash the flow must attach tangentially to the plate, instead of at right angles as happens when there is a dividing streamline. When there is a splash we know that the flow rises upwards to meet the leading edge. Therefore in order for the flow to attach tangentially we should bend the front of the plate downwards. We shall therefore try a shape function of the form

$$f(x) = \begin{cases} -(x+m)^2/L & -l < x < -m \\ 0 & -m < x < l \end{cases} \qquad (10.1)$$

which is flat for $x > -m$ and parabolic for $x < -m$ such that the first derivative is continuous as shown below:

(3.4) now becomes

$$\eta(x) = h - \beta x + \begin{cases} -\varepsilon(x+m)^2/l & -l < x < -m \\ 0 & -m < x < l \end{cases} \qquad (10.2)$$

where ε will henceforth be referred to as the curvature, although it is different to the normal concept of curvature. The planing equation (5.15) for this shape is

$$h - \beta x + \begin{cases} -\varepsilon(x+m)^2/l & -l < x < -m \\ 0 & -m < x < l \end{cases} = \frac{1}{\rho U^2 \pi} \int_{-l}^{l} p(u)\, I(x-u)\, du \qquad (10.3)$$

The non-dimensionalised form analogous to (8.1) becomes

$$\frac{h}{l\beta} - x' - \begin{cases} \frac{\varepsilon}{\beta}(x'+m')^2 & -1 < x' < -m' \\ 0 & -m' < x' < 1 \end{cases} = \frac{1}{\pi} \int_{-1}^{1} p'(lu')\, I'(x'-u')\, du' \qquad (10.4)$$

where $m' \equiv m/l$. Changing variables and discretising as in sections 8.2 and 8.3 gives

$$\frac{Nh}{l\beta} + N\cos\alpha_k - \begin{cases} N\frac{\varepsilon}{\beta}(\cos\alpha_k - m')^2 & \cos\alpha_k > m' \\ 0 & \cos\alpha_k < m' \end{cases}$$

$$= \sum_{j=1}^{N-1} p_j \sin\theta_j\, A(k,j) \quad , \quad k = 1..N \qquad (10.5)$$

where $A(k,j)$, $j = 1..N-1$, $k = 1..N$ are the same as for the flat plate.

The criterion for zero splash is the same as that for smooth detachment at the trailing edge; for the flow to meet the plate tangentially the pressure

must be continuous at the leading edge. A major feature of splash-free flows is that linearisation is still valid at the leading edge because there is no pressure singularity. This does away with the need to use a different method of solution to describe the flow near the leading edge and makes outputs given by the linearised theory more accurate.

We can enforce the smooth attachment condition in (10.5) in the same way as we did for the trailing edge: by setting $p_1 = 0$. This will actually be just inside the leading edge, the same as for the Kutta condition at the trailing edge. Rearranging and setting $p_1 = 0$ gives

$$N\cos\alpha_k = \begin{cases} N\frac{\varepsilon}{\beta}(\cos\alpha_k - m')^2 & \cos\alpha_k > m' \\ 0 & \cos\alpha_k < m' \end{cases} + \sum_{j=2}^{N-1} p_j \sin\theta_j A(k,j) - \frac{Nh}{4\beta}, \quad k = 1..N \qquad (10.6)$$

which can be written in matrix form

$$A\underline{C} = \underline{B}$$

where

$$\underline{B} = \begin{bmatrix} N\cos\alpha_1 \\ N\cos\alpha_2 \\ \vdots \\ N\cos\alpha_N \end{bmatrix} \qquad (10.7)$$

$$\underline{C} = \begin{bmatrix} \varepsilon/\beta \\ p_2 \sin\theta_2 \\ p_3 \sin\theta_3 \\ \vdots \\ p_{N-1} \sin\theta_{N-1} \\ Nh/L\beta \end{bmatrix} \qquad (10.8)$$

$$A = \begin{bmatrix} N(\cos\alpha_1 - m')^2 H(\cos\alpha_1 - m') & A(1,2) & A(,) & \cdots & A(1,N-1) & -1 \\ N(\cos\alpha_2 - m')^2 H(\cos\alpha_2 - m') & A(2,2) & & & & -1 \\ \vdots & & & & & \vdots \\ N(\cos\alpha_N - m')^2 H(\cos\alpha_N - m') & A(N,2) & \cdots & \cdots & A(N,N-1) & -1 \end{bmatrix} \qquad (10.9)$$

where $H(x)$ is the Heaviside unit step function.

We see that in this form A and $\underline{B}$ depend only on f and m', so if we specify these we can solve explicitly for ε/β and then use the lift and moment relations to eliminate β. This will give us the value of ε needed for zero splash drag for a given f and m'.

This situation is different to that of the flat plate in that the wetted length need not, and indeed should not, be an unknown quantity. In order for the flow to attach tangentially to the plate, the plate must be cut off sharply at the leading edge as shown below:

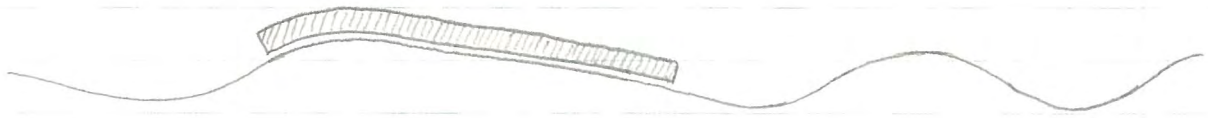

Fig. 7 Idealised Case

If this were not so and the plate was continued out, the flow would either attach earlier and cause a splash, or not have a solution at all (i.e. wash over the vessel). We must therefore consider L to be an input quantity. The angle of attack and elevation are still unknowns so we now have one less degree of freedom in the weight distribution. If we still consider M to be given, as we shall, this implies that 'a' cannot be chosen arbitrarily but rather is determined by the solution. Therefore for a given value of ϵ and m', there will only be a splash-free solution for a certain value of the curvature ε and for a certain value of 'a'.

The value of m' will be chosen to be close to 1 so that the plate is only curved very near the leading edge. We decide to choose $m' = 0.8$ and keep it fixed for all the calculations; hence our vessel is flat for 90% of its total length and parabolic only on the front 10%.

10.2 Curvature and Angle of Attack

In order to solve for ε we rearrange (8.11) to make β the subject:

$$\beta = \frac{MN}{\rho f \pi l^2 s1} \tag{10.10}$$

Since ε/β is given by the first element of the solution vector $\underline{c}$, we have

$$\varepsilon = \frac{MN\,C(1)}{\rho f \pi l^2 s1}$$

or

$$\frac{\rho l^2 \varepsilon}{M} = \frac{N\,C(1)}{f \pi s1} = \frac{N\,C(1)}{4\pi F_i^2 s1} \tag{10.11}$$

This gives the required curvature ε, scaled using ρ, l and M which are all assumed fixed, in terms of the velocity which is incorporated in F_i. The results are plotted in graph (11).

We see that the required curvature has a sharp peak at $F_i = 0.6$ before tending monotonically towards zero as $F_i \to \infty$ (results are only plotted on $[0, 2.25]$ to show the peak clearly). This is a discouraging result in that the required value of ε is constantly changing, so that for every different speed we need a different curvature in order to eliminate the splash. The stationary point at $F_i \simeq 0.65$ is quite sharp, so ε is not constant over any appreciable range of F_i around $F_i = 0.65$.

This is an obvious drawback to designing a splash-free vessel with this shape – it will only work at one, or perhaps two, particular speeds.

The angle of attack of the vessel can also be plotted as a function of F_l when l is constant from (10.10). The result of this is shown in graph (12), which we see has approximately the same shape as the curvature graph. This graph has the same characteristics as the angle of attack for the flat plate (graph (3)), in that it rises to a maximum before tending monotonically towards zero. The maximum here is at $F_l = 0.55$, whereas for the flat plate it is at $F_a = 0.95$ which corresponds to $F_l = 0.8$. Also the maximum value of $pl^2\beta/m$ for this shape is approximately 1.1, while for the flat plate it is approximately 0.8. Therefore if we keep l fixed this shape rises to a higher maximum angle of attack at a lower speed. This is deceptive because we would expect that eliminating the pressure singularity would decrease the clockwise torque and hence the angle of attack. The problem with comparing these two shapes lies in the fact that they each have different independent length scales. We cannot justly scale the flat plate angle of attack using 'l' nor this shape's angle of attack using 'a', and hence we are unable to properly compare their angles of attack.

10.3 Drag

We can now calculate the viscous and inviscid drag for this shape. The inviscid drag per unit breadth is given by

$$D_{inv} = -\int_{-l}^{l} p(x)\,\frac{d\eta}{dx}\,dx \qquad (10.12)$$

which becomes, using (10.2)

$$D_{inv} = \beta\int_{-l}^{l} p(x)\,dx + \frac{2\varepsilon}{l}\int_{-l}^{-m} p(x).\,(x+m)\,dx$$

$$= Mg\beta + 2\varepsilon l\rho U^2\beta\int_{-1}^{-m'} p'(lx')\,(x'+m')\,dx'$$

$$= Mg\beta + 2\varepsilon l\rho U^2\beta\int_{0}^{\cos^{-1}m'} p'(-l\cos\theta).(m'-\cos\theta).\sin\theta\,d\theta$$

$$= Mg\beta + 2\varepsilon l\rho U^2\beta\frac{\pi}{N}\left(m'\sum_{D_1} p_j\sin\theta_j - \sum_{D_1} p_j\sin\theta_j\cos\theta_j\right)$$

where D_1 is the set of integers j such that $j \geq 1$ and $\cos\theta_j > m'$. Hence

$$\frac{D_{inv}}{\rho g} = \frac{\mu^2 N}{f\pi l^2 s1}\left[1 + 2\,\frac{C(1)}{s1}\left(m'\sum_{D_1} p_j\sin\theta_j - \sum_{D_1} p_j\sin\theta_j\cos\theta_j\right)\right] \qquad (10.13)$$

The viscous drag is again given by (9.12) and we will assume that the viscous drag coefficient is the same as that for the flat plate; also the wetted arc length is still $2l$ to first order in β.

Therefore the total drag is

$$\frac{D_{tot}}{\rho g} = fl^2 C_0 + \frac{\mu^2 N}{f\pi l^2 s1}\left[1 + \frac{2C(1)}{s1}\left(m' \sum_{D_1} p_j \sin\theta_j - \sum_{D_1} p_j \sin\theta_j \cos\theta_j\right)\right] \quad (10.14)$$

with l given in terms of C_0 by (9.11). This can be plotted as a function of the wetted length $2l$ for a given value of U by using C_0 as the input quantity as for the flat plate. The results are shown in graphs (13) and (14) for $U = 6$ m/s and $U = 20$ m/s respectively. This modified flat plate is labelled "Vent plate", and the other results are for the parabola that we will consider in the next chapter.

We see that this shape has very low inviscid drag except when $2l$ is very small, so that viscous drag is dominant for most values of the wetted length. For $U = 6$ m/s, the modified flat plate has a minimum scaled drag of $0.0086\ m^2$, compared to $0.029\ m^2$ for the flat plate - a 70% reduction. As with the angle of attack it is pointless comparing the two shapes at the same value of l or 'a'; we should only compare their minimum drags in order to conclude which is more efficient.

For $U = 20$ m/s the minimum drag for the modified flat plate is $0.0023\ m^2$, while for the flat plate it is $0.021\ m^2$ - an 89% reduction. Therefore for both these speeds this modified flat plate has a much smaller minimum drag than the flat

plate.

Because the inviscid drag is so small, the minimum drag for the modified flat plate occurs at very small values of the wetted length (0.1 m for $U = 6$ m/s and 0.01 m for $U = 20$ m/s). The total drag still rises dramatically however as the wetted length tends to zero, as it does for the flat plate as 'a' tends to zero. In the next chapter we shall consider a shape for which this is not the case, so that the total drag need not have a minimum.

11. The Splash-free Parabola

11.1 Setting up the Equations

We shall now consider another shape that is capable of producing a splash-free flow: the vertex-up parabola. This has the shape function

$$f(x) = -\frac{x^2}{l}$$

so that $\eta(x)$ is given by (3.4) to be

$$\eta(x) = -\frac{\varepsilon x^2}{l} - \beta x + h \qquad (11.1)$$

We note that this is the most general equation for a vertex-up parabola, since to first order rotating the parabola is the same as shifting its vertex. Hence if we had set

$$f(x) = -\frac{(x+m)^2}{l} + \frac{m^2}{l}$$

then $\eta(x)$ could still be written in the form

$$\eta(x) = -\frac{\varepsilon x^2}{l} - \beta' x + h$$

where $\beta' = \beta + 2m\varepsilon/l$, and we would just use β' instead of β as our unknown. We note also that the parabola is a special case of the modified flat plate considered in the previous chapter with $m \equiv -l$, so that the whole body is parabolic instead of just the leading edge.

The non-dimensionalised planing

equation analogous to (8.1) becomes

$$\frac{h}{4\beta} - x' - \frac{\varepsilon}{\beta} x'^2 = \frac{1}{\pi} \int_{-1}^{1} p'(4u')\, I'(x'-u')\, du' \qquad (11.2)$$

which on changing variables and discretising as before gives

$$N\cos\alpha_k = N\frac{\varepsilon}{\beta}\cos^2\alpha_k + \sum_{j=2}^{N-1} p_j \sin\theta_j A(k,j) - \frac{Nh}{4\beta} \qquad (11.3)$$

where we have enforced $p_1 = 0$ as in Chapter 10. The matrix equation is

$$A\underline{C} = \underline{B}$$

where $\underline{B}$ and $\underline{C}$ are as in (10.7) and (10.8), and A is given by

$$A = \begin{bmatrix} N\cos^2\alpha_1 & A(1,2) & A(1,3) & \cdots & A(1,N-1) & -1 \\ N\cos^2\alpha_2 & A(2,2) & & & & \\ \vdots & \vdots & & & & \\ N\cos^2\alpha_N & A(N,2) & \cdots & \cdots & A(N,N-1) & -1 \end{bmatrix} \qquad (11.4)$$

$A(k,j)$, $j = 2..N-1$, $k = 1..N$ are again the same as for the flat plate. As for the flat plate and modified flat plate the matrix equation depends only on ε.

11.2 Curvature and Angle of Attack

Since the first element of the solution vector is ε/β, the same as for the modified flat plate, and the lift and moment relations are the same, equations (10.11) and (10.10) still hold for the splash-free parabola. We can therefore plot $\rho l^2 \varepsilon/M$ using (10.11) and $\rho l^2 \beta/M$ using (10.10), both as functions of F_l. The results are shown in graphs (15) and (16) respectively.

We see that the graph of the required parabola curvature for splash-free flow is similar to that of the modified flat plate: a maximum at a reasonably low value of F_l before tending monotonically towards zero. There are however two important differences. Firstly the required curvature is much greater for the modified flat plate (about eight times the peak height). Since however the modified flat plate is only curved over one tenth of its total length, the leading edge of the parabola is at a greater distance below $y=0$ when unrotated as sketched below:

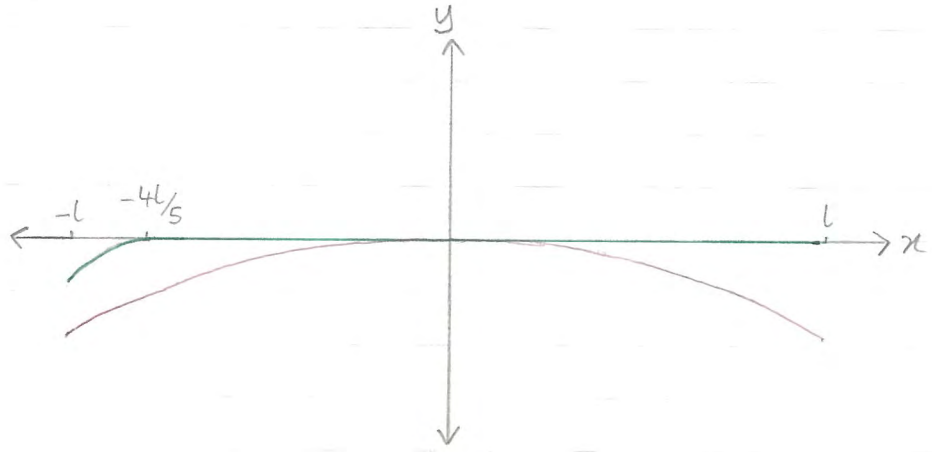

Fig. 8 Comparing curvatures for splash-free parabola and modified flat plate

Secondly the maximum occurs at a lower value of F_l, namely $F_l \simeq 0.45$ compared with $F_l = 0.65$ for the modified flat plate. This is also true for the angle of attack (graph ⑯); the parabola reaches its maximum angle of attack at a lower speed, and hence moves into the true planing region of small angle of attack earlier.

The maximum angle of attack for these shapes is quite similar, with the parabola's being slightly higher. However for larger values of F_l the angle of attack is seen to drop much more sharply for the parabola, so that for values of F_l greater than about 2 the angle of attack is very small indeed. We might therefore expect that for large values of F_l, not only will the splash drag be zero, but the wave drag will be very small.

11.3 Drag

As before the inviscid drag per unit breadth is given by

$$D_{inv} = -\int_{-l}^{l} p(x)\,\frac{d\eta}{dx}\,dx$$

which becomes, with $\eta(x)$ given by (11.1),

$$D_{inv} = \frac{2\varepsilon}{l}\int_{-l}^{l} x\,p(x)\,dx + \beta\int_{-l}^{l} p(x)\,dx$$

$$= 2\varepsilon l\int_{-1}^{1} u'\,p(lu')\,du' + Mg\beta$$

$$= 2\varepsilon l\rho U^2\beta\,.\,-\int_{0}^{\pi} p'(-l\cos\theta)\sin\theta\cos\theta\,d\theta + Mg\beta$$

$$= -2\varepsilon l\rho U^2\beta\,\frac{\pi}{N}\,s2 + Mg\beta$$

Therefore

$$\frac{D_{inv}}{\rho g} = \frac{\mu^2 N}{f l^2 \pi s1}\left[1 - 2C(1)\frac{s2}{s1}\right] \qquad (11.5)$$

This can be plotted along with the viscous drag (which is again given by (9.12)) as a function of the wetted length for a given value of U, by again using C_0 as the input quantity. The results are shown in graphs (13) and (14) for $U = 6$ m/s and $U = 20$ m/s respectively.

For $U = 6$ m/s, we see that the inviscid drag for the parabola is very

similar to that of the modified flat plate for values of the wetted length greater than about 1 metre. However for very small values of l the inviscid drag still stays approximately constant instead of rising dramatically like that for the flat plate and modified flat plate. The same thing occurs in graph (14) for $U = 20\,m/s$, with the inviscid drag being extremely small even for very small values of $2l$.

Therefore since the viscous drag is approximately proportional to the wetted length, and the inviscid drag is approximately independent of the wetted length, minimum drag occurs at extremely small values of the wetted length, if a minimum exists at all. This must prompt us to ask whether it is valid to take the limit as $l \to 0$ subject to our assumptions, and what happens in this limit.

11.4 The Small Wetted Length Limit

The four equations that we are solving in the general case are:

$$\eta(x) = \mathcal{E} f(x) - \beta x + h = \frac{1}{\rho U^2 \pi} \int_{-l}^{l} p(u)\, I(x-u)\, du \qquad (11.6)$$

$$Mg = \int_{-l}^{l} p(u)\, du \qquad (11.7)$$

$$Mg(l-a) = \int_{-l}^{l} u\, p(u)\, du \qquad (11.8)$$

$$p(l) = 0 \qquad (11.9)$$

We note first that l is asymptotically independent of β since the wetted length tends to a constant as $\beta \to 0$ if 'a' is fixed. Also, as stated in Chapter 3, $p(x)$ is of order β from Bernoulli's equation. (11.7) then implies that the mass supported must tend to zero as $l \to 0$ if $p(x)$ is to remain small; if M is kept constant as $l \to 0$ $p(x)$ will tend to infinity and the linearisation will no longer hold. It is not evident from (11.6) that $\eta(x)$ should tend to infinity as $l \to 0$ and $p(x) \to \infty$; this can only be seen from the Bernoulli equation. The linearised Bernoulli equation being used is equation (3.9), i.e.

$$\frac{p(x)}{\rho} + g\eta + U \frac{\partial \phi}{\partial x} = 0 \quad \text{on} \quad y = 0$$

so that if $p(x) \to \infty$ we expect that $\partial\phi/\partial x \to -\infty$ since the horizontal velocity is no longer negligibly less than U. If these two quantities are unbounded we might also expect that $\eta(x)$ will be unbounded, and this will be seen to be the case.

As yet we have no way of knowing through which of the parameters (ε, β or h) $\eta(x)$ will tend to infinity as $l \to 0$; this will depend on the shape function $f(x)$. For the flat plate $f(x) \equiv 0$ and we see from graph ④ that β increases seemingly boundlessly as 'a' decreases. Also from graph ②, l/a decreases or is approximately constant as 'a' decreases so β must also increase without bound as l decreases. Although it cannot be seen from graph ⑤ since the vertical axis depends on 'a', the centre height h tends to a constant as $l \to 0$ with U fixed.

In order to see how $\eta(x) \to \infty$ as $l \to 0$ for the splash-free parabola we can plot graphs of ε, β and h scaled using U instead of l, and see which of these tends to infinity as $l \to 0$. The results are shown in graphs ⑰, ⑱ and ⑲.

For the parabola the angle of attack does not tend to infinity as $l \to 0$; instead the curvature ε increases without bound as l decreases. The centre height h increases slowly and monotonically but it is not obvious from the graph whether

it tends to a constant or increases without bound.

Therefore if we have a planing vessel of fixed mass we cannot justifiably take the limit as the wetted length tends to zero without violating the assumption of small disturbances; hence the graphs of drag vs. wetted length are of little value for very small values of $2l$. The value of $2l$ below which $\eta(x)$ is too large to be linearised will depend on the mass of the vessel.

12. About Splash-free Flows

12.1 General Comments

We have seen that the two splash-free shapes considered are capable of operating with very low inviscid drag. In order to achieve this for a real planing vessel there are certain practical considerations that must be dealt with. The shapes considered were idealised cases in which the leading edge was cut away sharply, and parameters were found for which the flow would attach smoothly to it as shown:

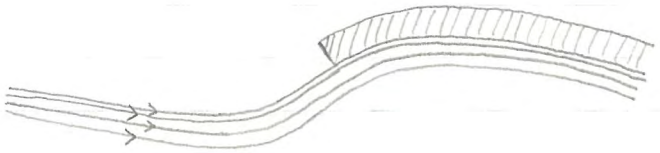

The first problem is that we have only found the steady-state solution. If a vessel is starting from rest it cannot be taken for granted that this flow is actually attainable for a given curvature and final speed if 'a' is fixed. The danger is that at lower speeds the flow will attach before the sharp leading edge, either hitting the blunt bow of the vessel or washing over it, both of which are undesirable. If 'a' is variable it can always be decreased for lower speeds so that the flow attaches later, but this will be accompanied by large inviscid drag.

The next question that must be

addressed is that of stability with respect to small changes in either 'a' or U. If 'a' is decreased or U increased slightly we would expect that the flow will simply attach later with an increase in inviscid drag. However if 'a' is increased or U decreased slightly it is quite possible that the flow could wash completely over the vessel, depending on its bow shape.

Stability is the foremost criterion that the flow must satisfy; given this, the next issue to be addressed is that of robustness. We know that these shapes can produce very low drag if U and 'a' are exactly right for a given shape, but this is pointless if a slight deviation in either of these causes a large increase in drag. The ideal case, where the leading edge is cut off at 90°, is likely to have large inviscid drag if the flow attaches prematurely due to the resulting splash as shown below:

The splash drag here will be asymptotically independent of ε since to leading order the leading edge is perpendicular to the oncoming stream. This is of course assuming that the flow is stable in the first place.

This ideal shape therefore has major inherent problems and is unlikely to work in a practical situation. If it is indeed unstable we should look to see if there are ways to achieve stability at the possible expense of a small splash drag. One solution might be to make the leading edge less sharply cut off as shown below:

This will increase the stability but may cause the flow to attach earlier. If the ideal shape was indeed stable a more robust flow, if it turned out to be stable, might be obtained with a pointed leading edge as shown below:

so that if the flow attached slightly prematurely it could just wash over the vessel.

12.2 Conclusions

Although eliminating the splash of a planing surface causes a large decrease in inviscid drag, it has serious limitations from the practical point of view. If the flow can be made stable then the next step is to find a shape that produces little splash over a reasonable speed range. Neither of the two shapes considered here satisfied this criterion, both of them only working at the exactly-right speed. Nevertheless they showed that the flat plate is by no means the most efficient possible planing shape at a given speed.

13. Bibliography

Abramowitz, M and Stegun, I.A., "Handbook of Mathematical Functions", Dover republication, N.B.S., 1964.

Bessho, M., "On a consistent linearised theory of the wave-making resistance of ships", Journal of Ship Research, Vol. 38 No. 2, June 1994.

Cumberbatch, E., "Two-dimensional planing at high Froude number", Journal of Fluid Mechanics, Vol. 4 (1958) pp. 466-478.

Green, A.E., "The gliding of a plate on a stream of finite depth", Proceedings of the Cambridge Philosophical Society, Vol. 31 (1936) pp. 589-603.

James, R.M., "On the remarkable accuracy of the vortex lattice method", Computer Methods in Applied Mechanics and Engineering 1 (1972) pp. 59-79

Lamb, H. "Hydrodynamics", sixth ed., Dover Publications (1945), first published 1932

Maruo, H., "Two-dimensional theory of the hydroplane", Proc. 1st Japan Nat. Congr. for Appl. Mech., Tokyo 1951.

Newman, J.N., "Marine Hydrodynamics", MIT Press, 1977

Oertel, R.P., "The steady motion of a flat ship, including an investigation of the local flow near the bow", Ph.D. thesis, The University of Adelaide, 1975

Squire, H.B., "The motion of a simple wedge along the water surface", Proc. Roy. Soc. Lond. Ser. A, Vol 243 (1957), pp. 48-64

Wagner, H., Zeit. Angew. Math. Mech., Vol. 12 (1932), p. 193

Wang, D.P. and Rispin, P., "Three dimensional planing at high Froude number", Journal of Ship Research, Vol. 15, 1971

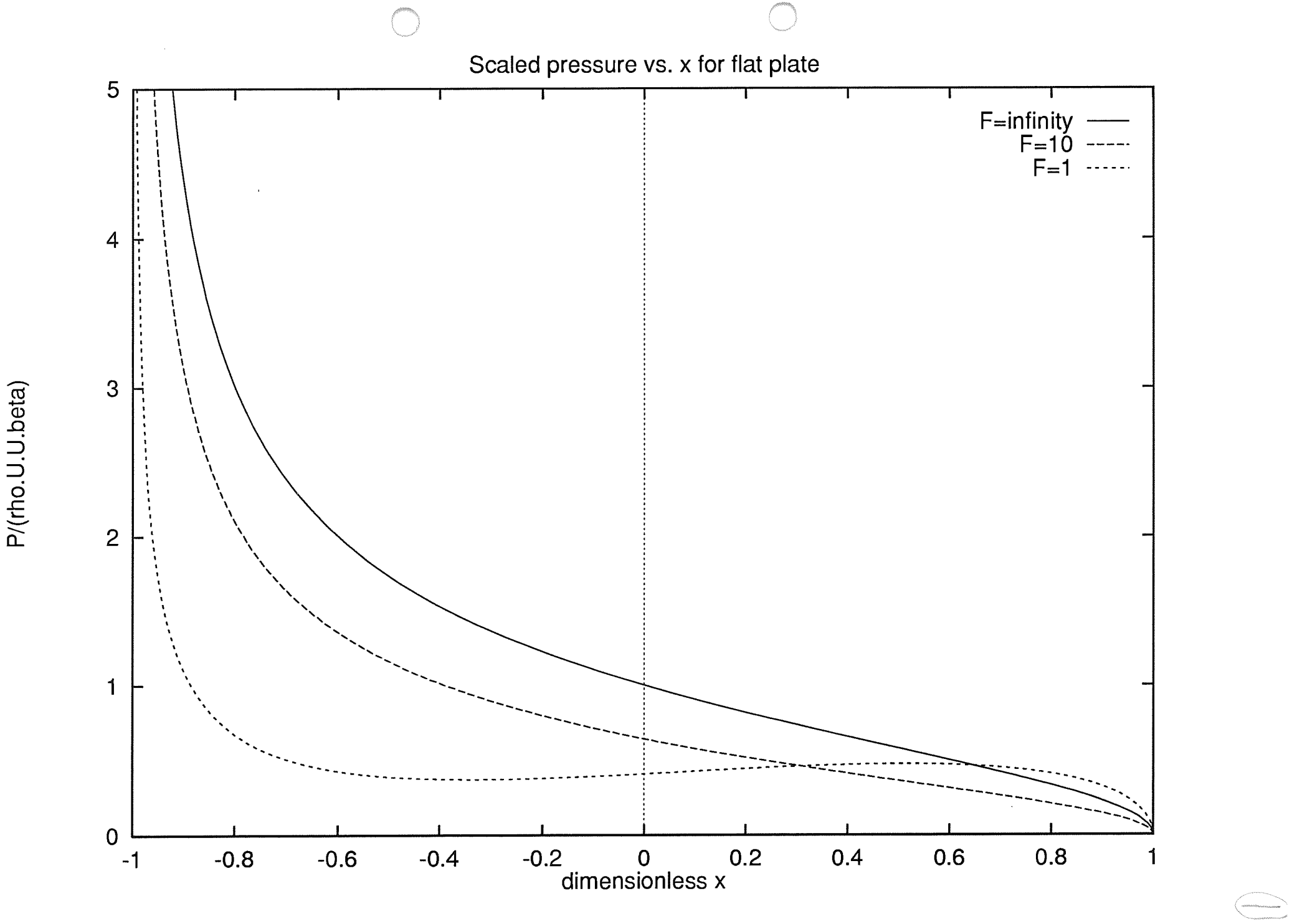
Scaled pressure vs. x for flat plate
F=infinity
F=10
F=1
P/(rho.U.U.beta)
dimensionless x
5
4
3
2
1
0
-1
-0.8
-0.6
-0.4
-0.2
0
0.2
0.4
0.6
0.8
1

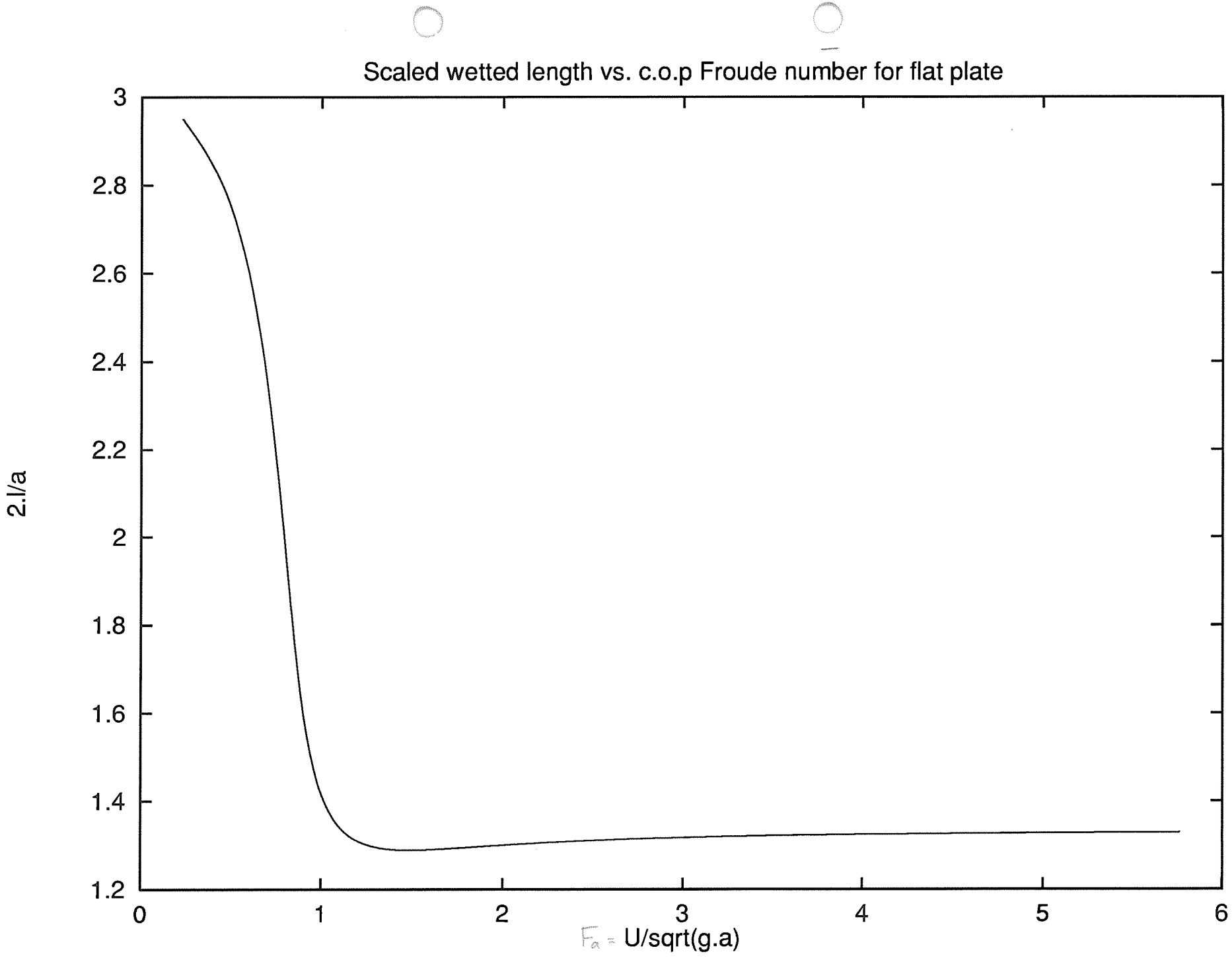
Scaled wetted length vs. c.o.p Froude number for flat plate
2.l/a
3
2.8
2.6
2.4
2.2
2
1.8
1.6
1.4
1.2
0
1
2
3
4
5
6
Fa = U/sqrt(g.a)

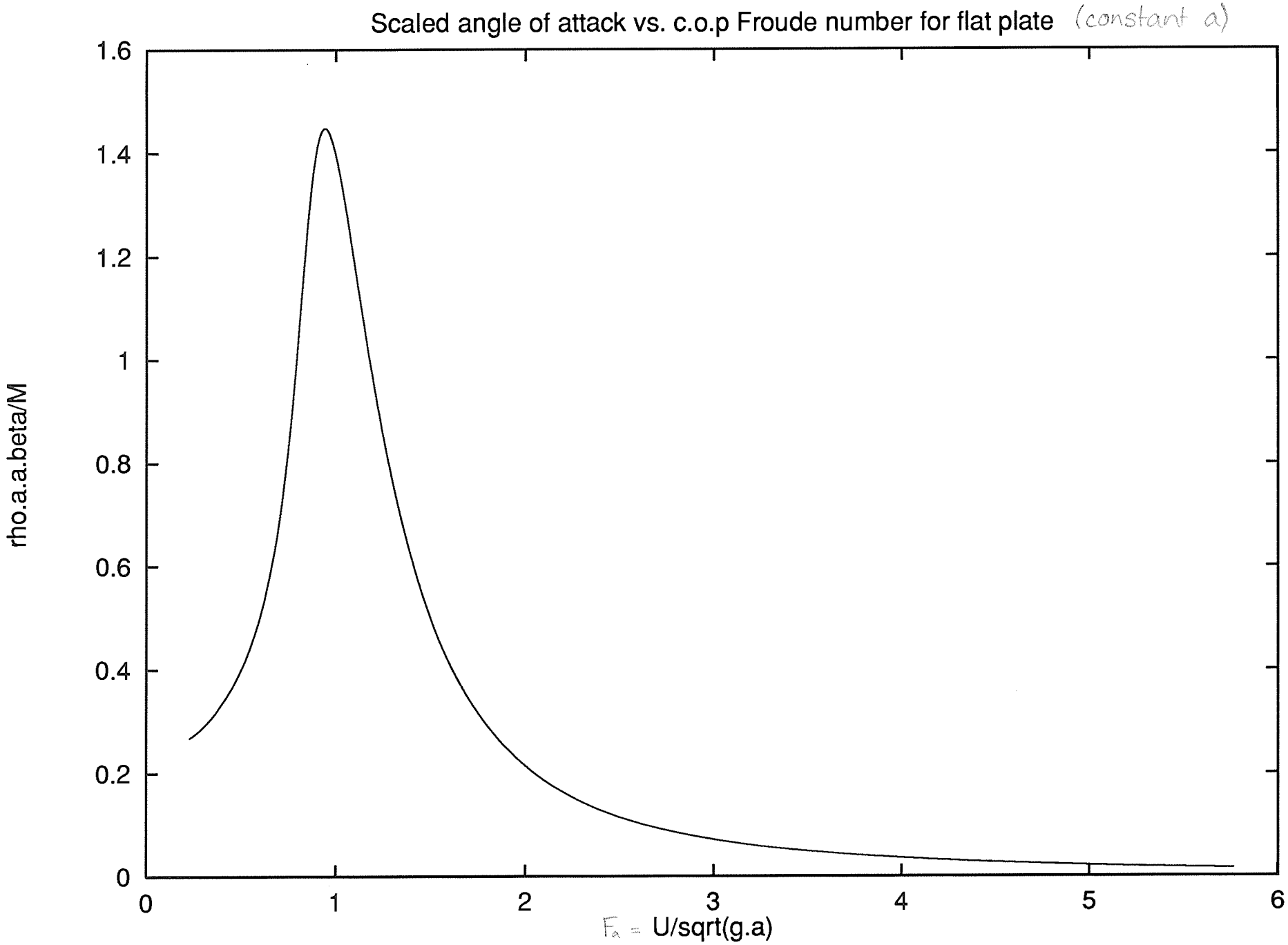
Scaled angle of attack vs. c.o.p Froude number for flat plate (constant a)
rho.a.a.beta/M
1.6
1.4
1.2
1
0.8
0.6
0.4
0.2
0
0
1
2
3
4
5
6
Fa = U/sqrt(g.a)

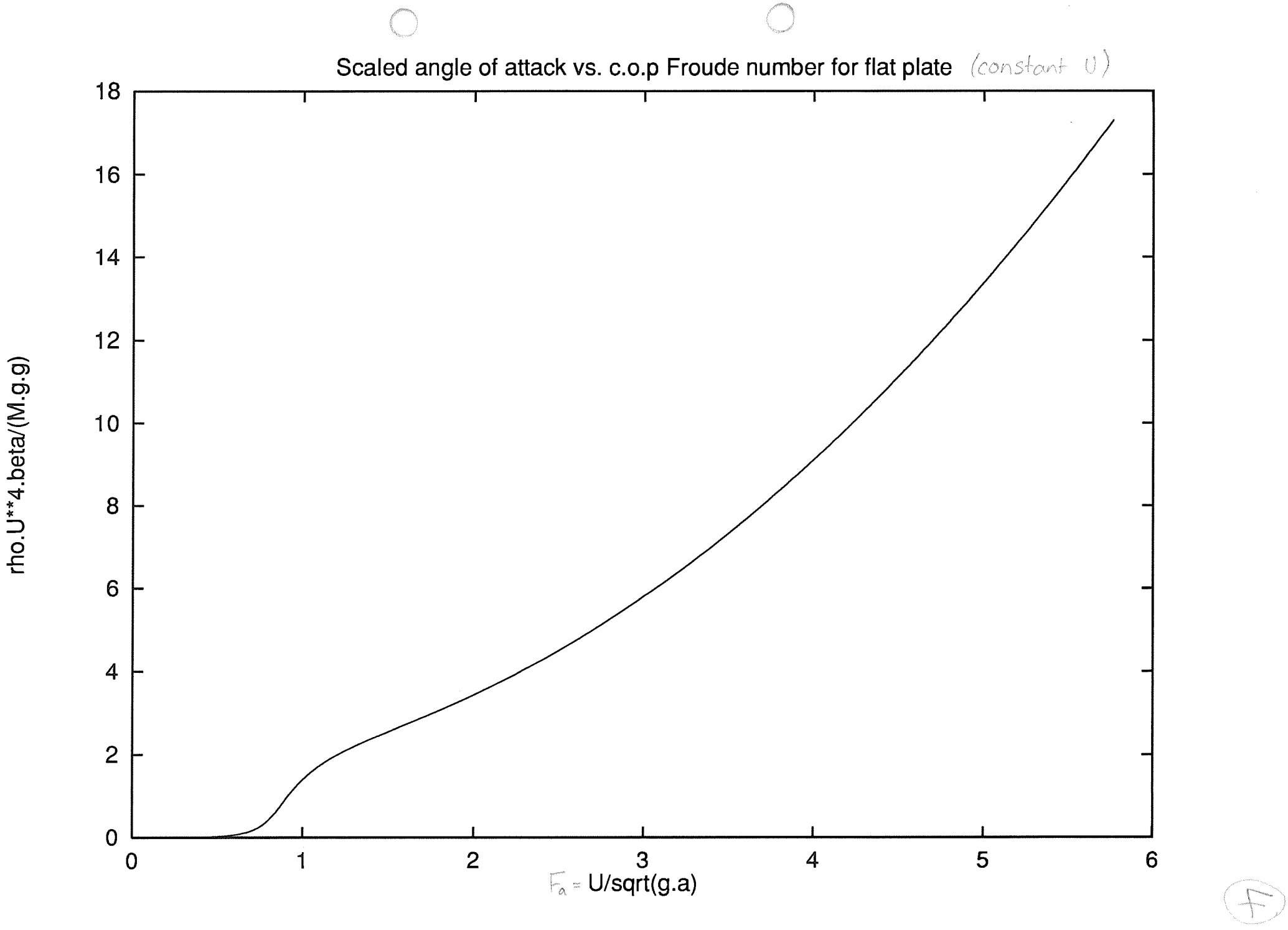
Scaled angle of attack vs. c.o.p Froude number for flat plate (constant U)
rho.U**4.beta/(M.g.g)
0
2
4
6
8
10
12
14
16
18
0
1
2
3
4
5
6
Fa = U/sqrt(g.a)

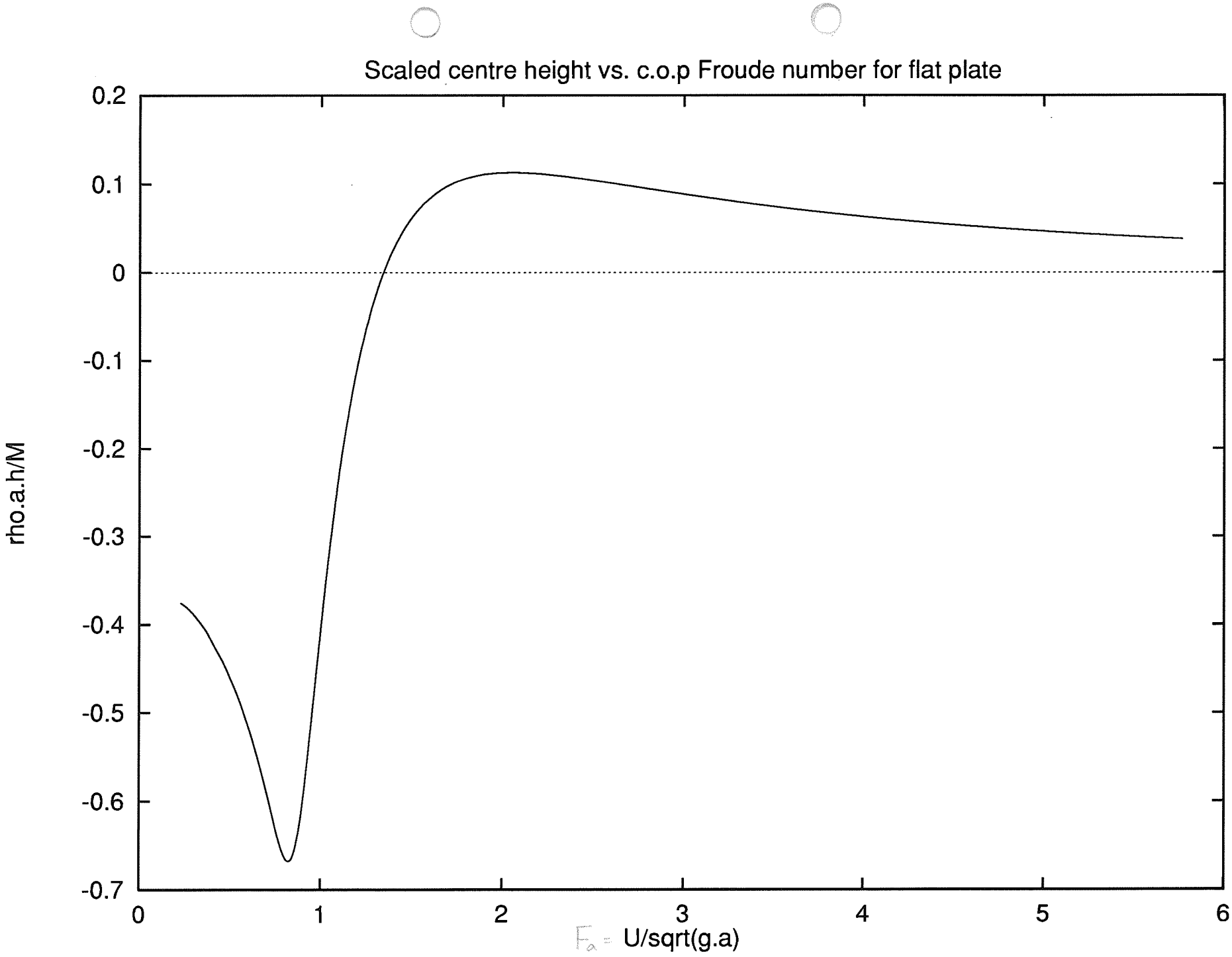
Scaled centre height vs. c.o.p Froude number for flat plate
rho.a.h/M
0.2
0.1
0
-0.1
-0.2
-0.3
-0.4
-0.5
-0.6
-0.7
0
1
2
3
4
5
6
F_a = U/sqrt(g.a)

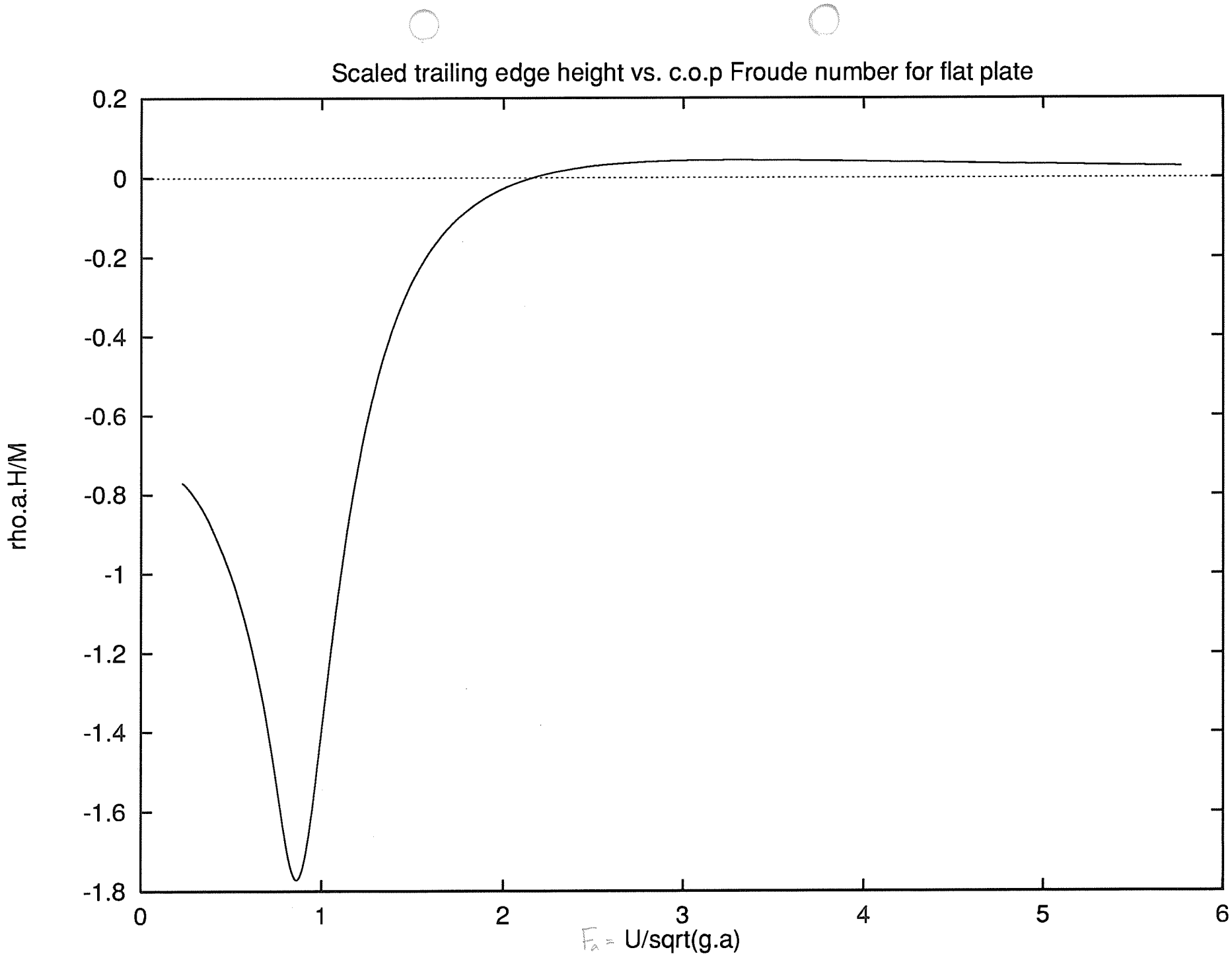
Scaled trailing edge height vs. c.o.p Froude number for flat plate
rho.a.H/M
0.2
0
-0.2
-0.4
-0.6
-0.8
-1
-1.2
-1.4
-1.6
-1.8
0
1
2
3
4
5
6
F_a = U/sqrt(g.a)

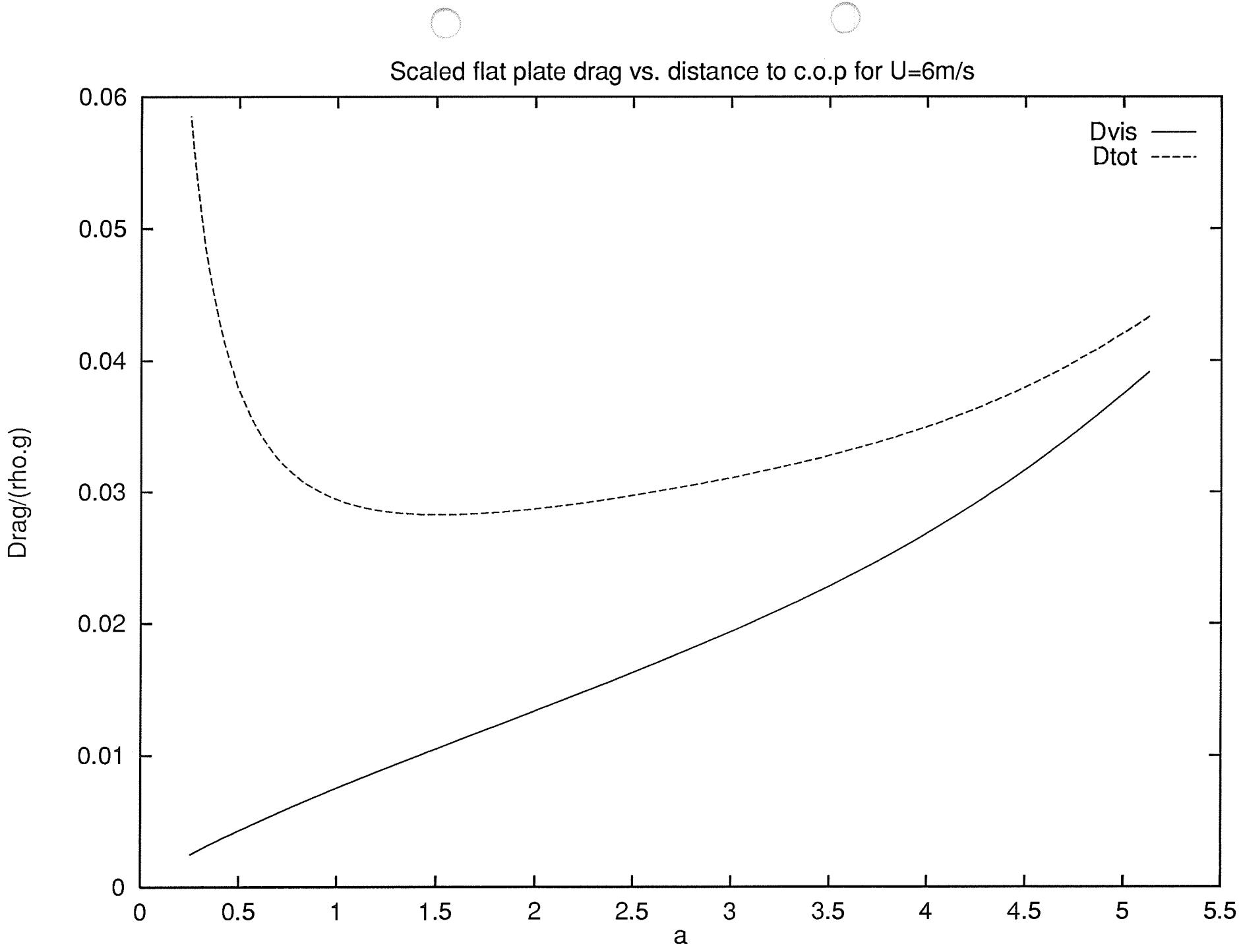
Scaled flat plate drag vs. distance to c.o.p for U=6m/s
Dvis
Dtot
Drag/(rho.g)
a
0.06
0.05
0.04
0.03
0.02
0.01
0
0
0.5
1
1.5
2
2.5
3
3.5
4
4.5
5
5.5

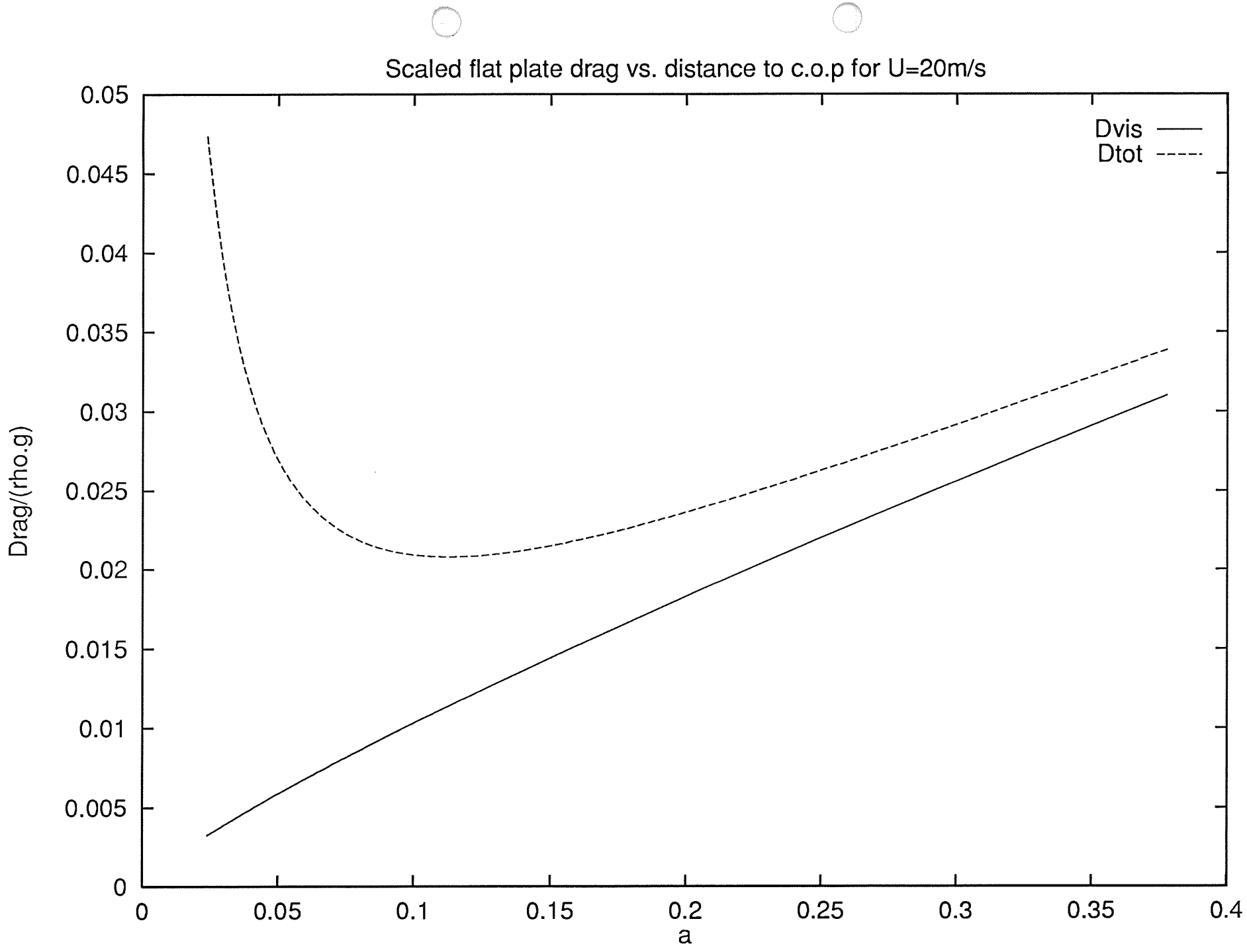
Scaled flat plate drag vs. distance to c.o.p for U=20m/s
Dvis
Dtot
Drag/(rho.g)
a
0.05
0.045
0.04
0.035
0.03
0.025
0.02
0.015
0.01
0.005
0
0
0.05
0.1
0.15
0.2
0.25
0.3
0.35
0.4

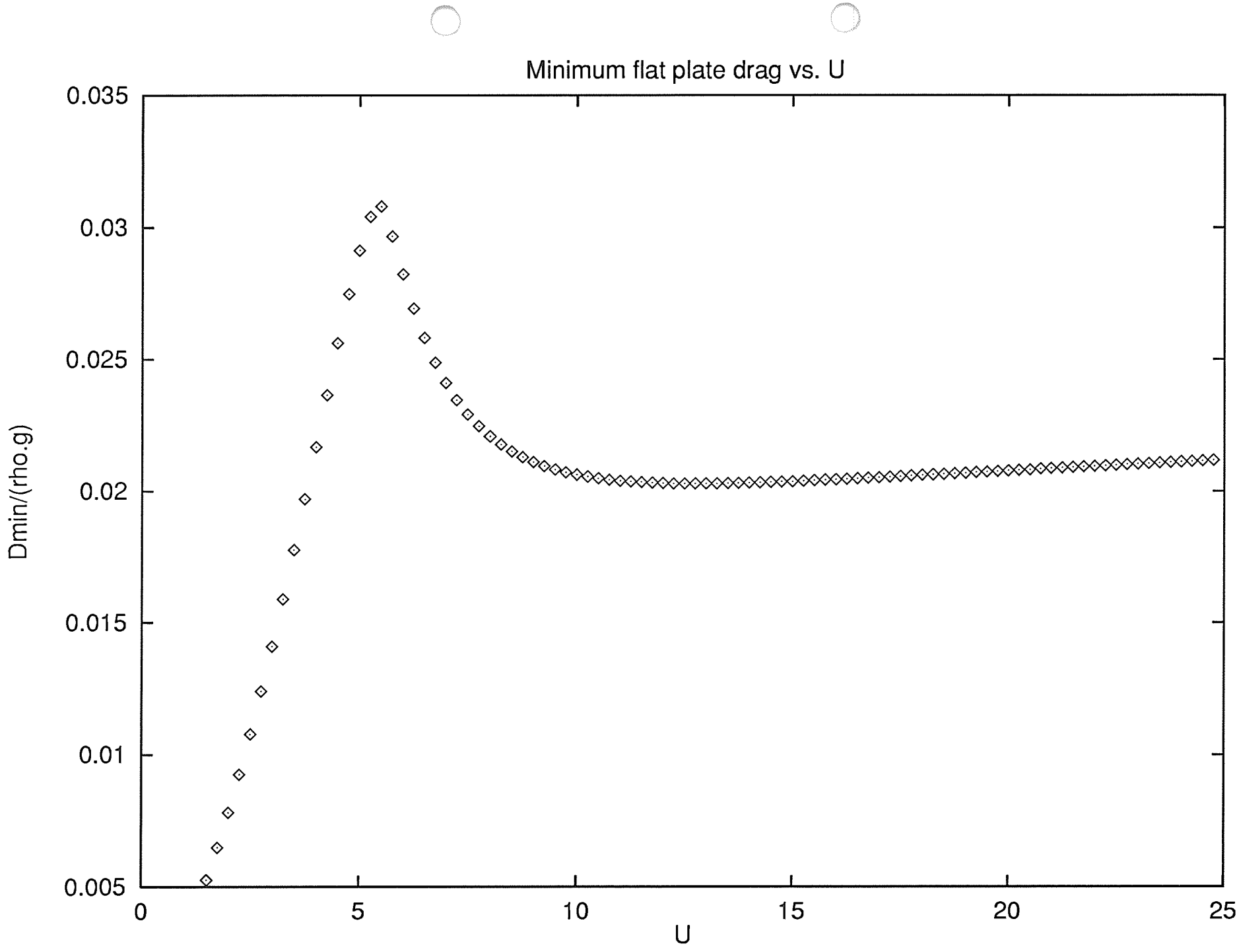
Minimum flat plate drag vs. U
Dmin/(rho.g)
U
0.035
0.03
0.025
0.02
0.015
0.01
0.005
0
5
10
15
20
25

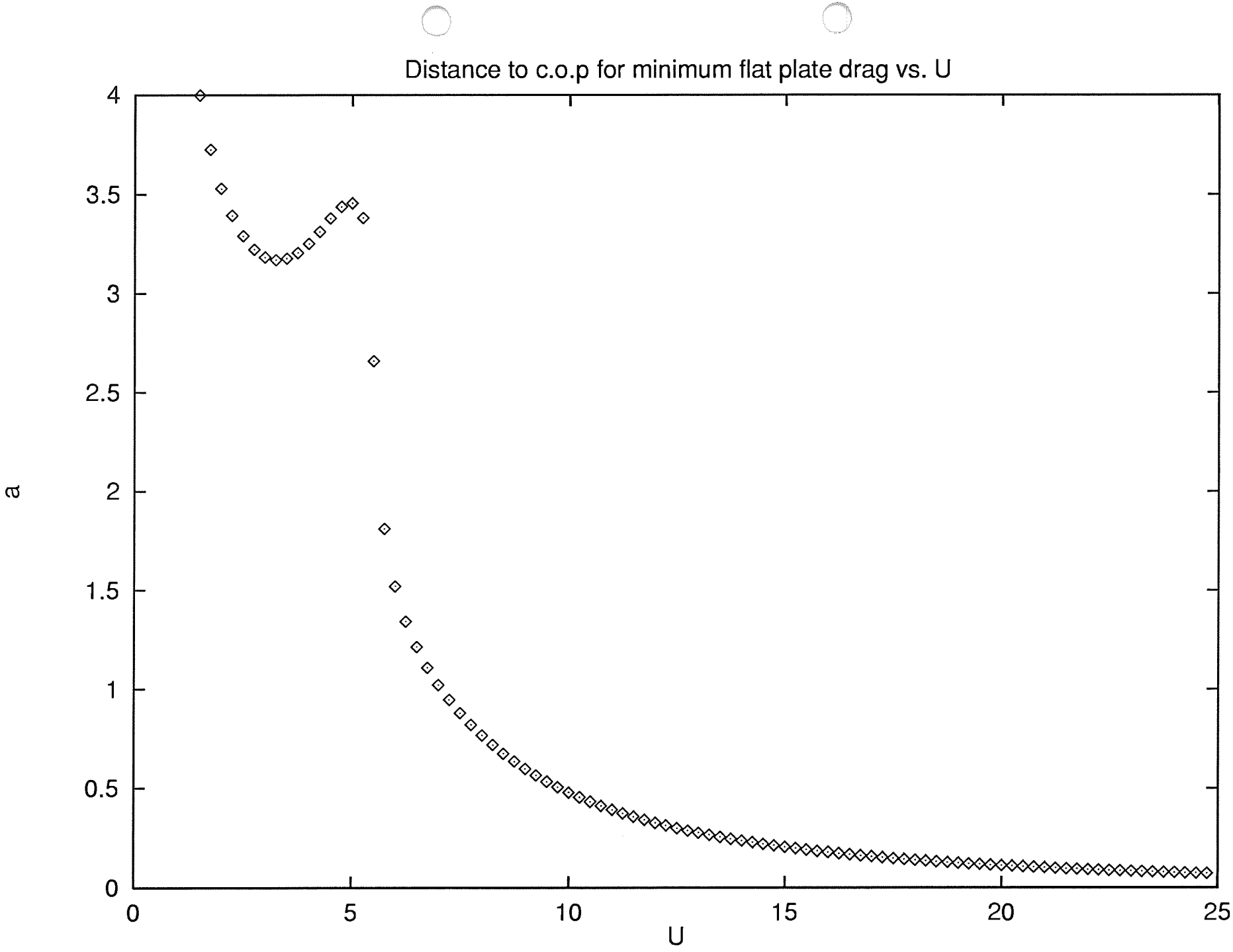
Distance to c.o.p for minimum flat plate drag vs. U
a
U
0
0.5
1
1.5
2
2.5
3
3.5
4
0
5
10
15
20
25

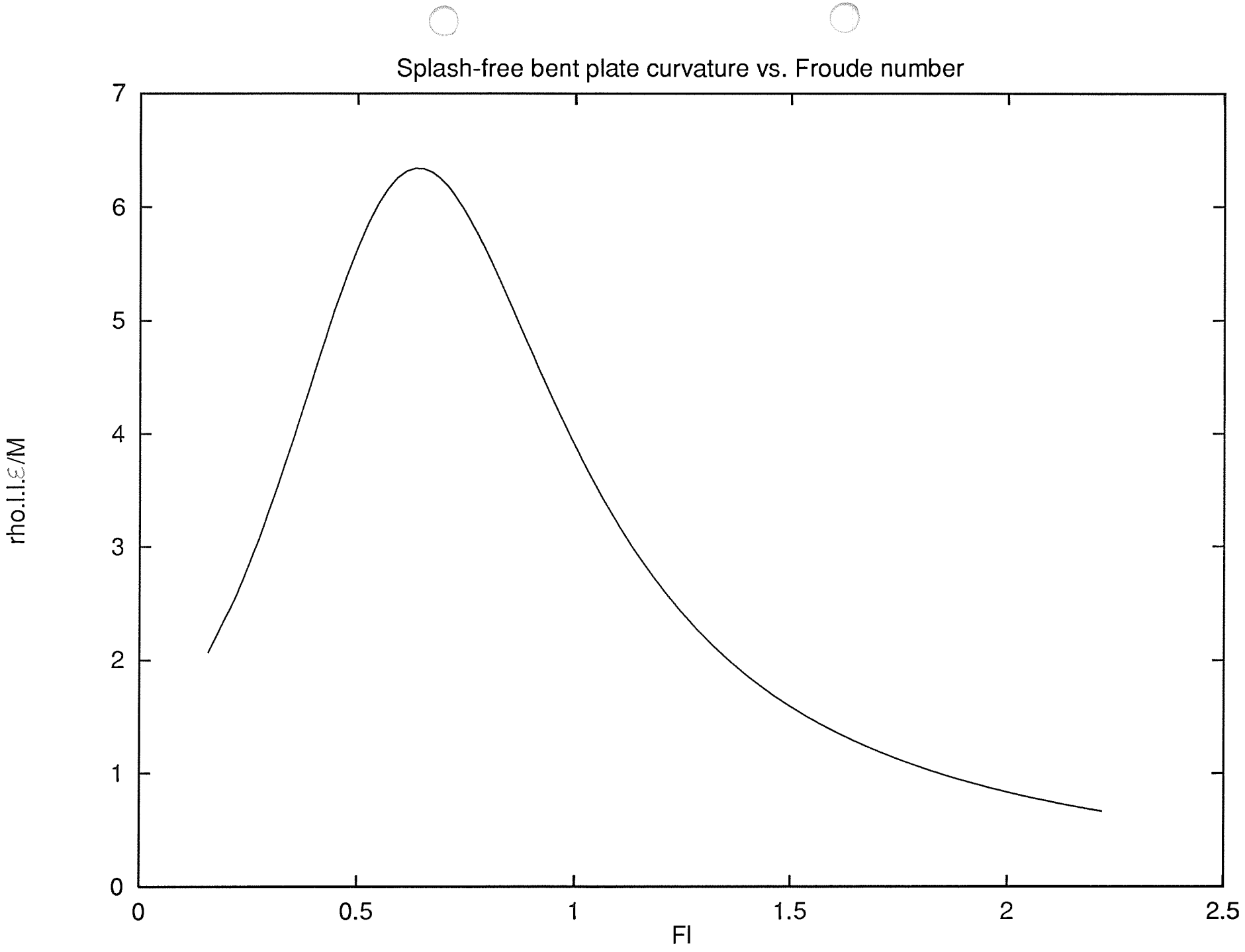
Splash-free bent plate curvature vs. Froude number
rho.l.l.ε/M
Fl
0
1
2
3
4
5
6
7
0
0.5
1
1.5
2
2.5

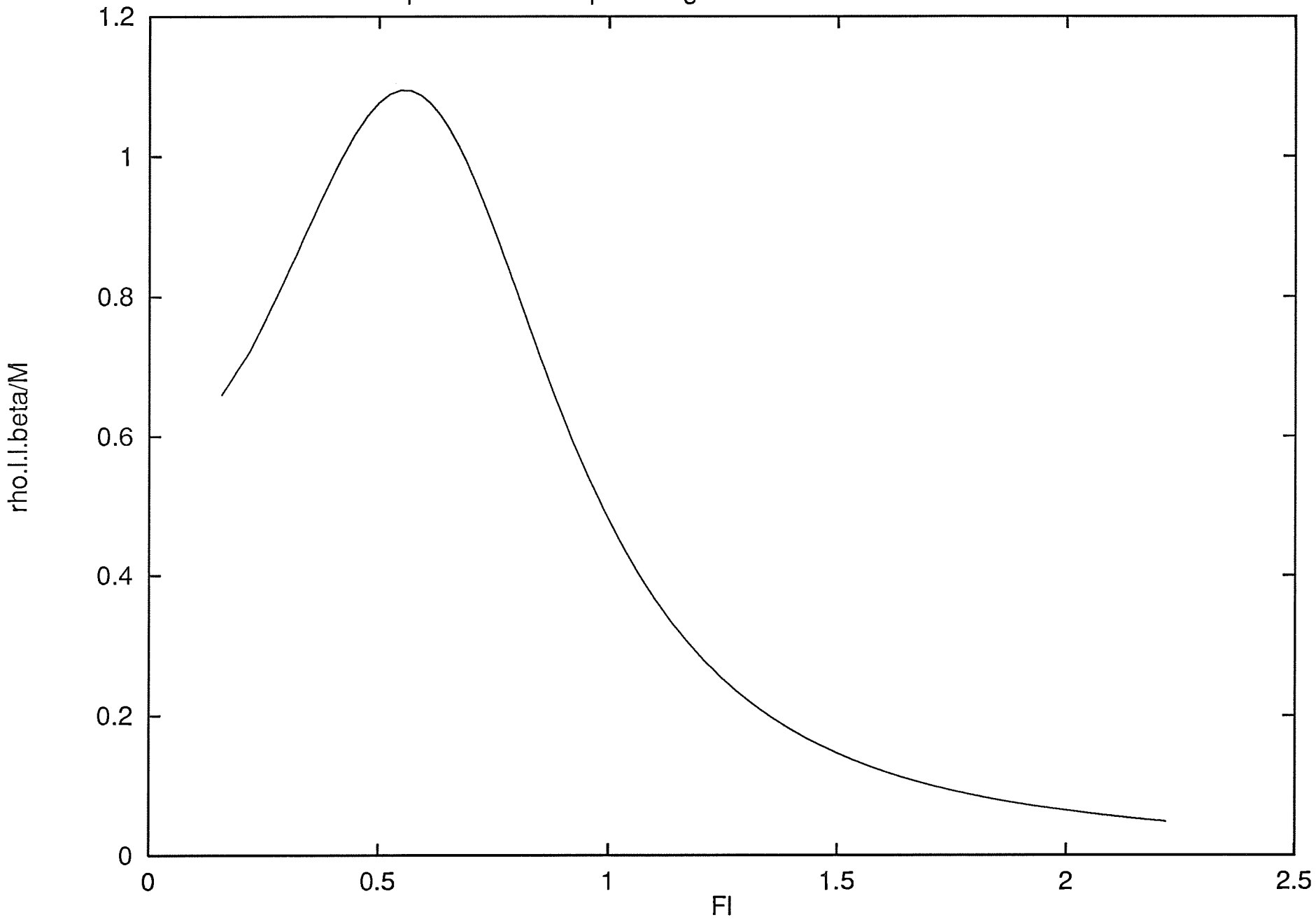
Splash-free bent plate angle of attack vs. Froude number
rho.l.l.beta/M
Fl
1.2
1
0.8
0.6
0.4
0.2
0
0
0.5
1
1.5
2
2.5

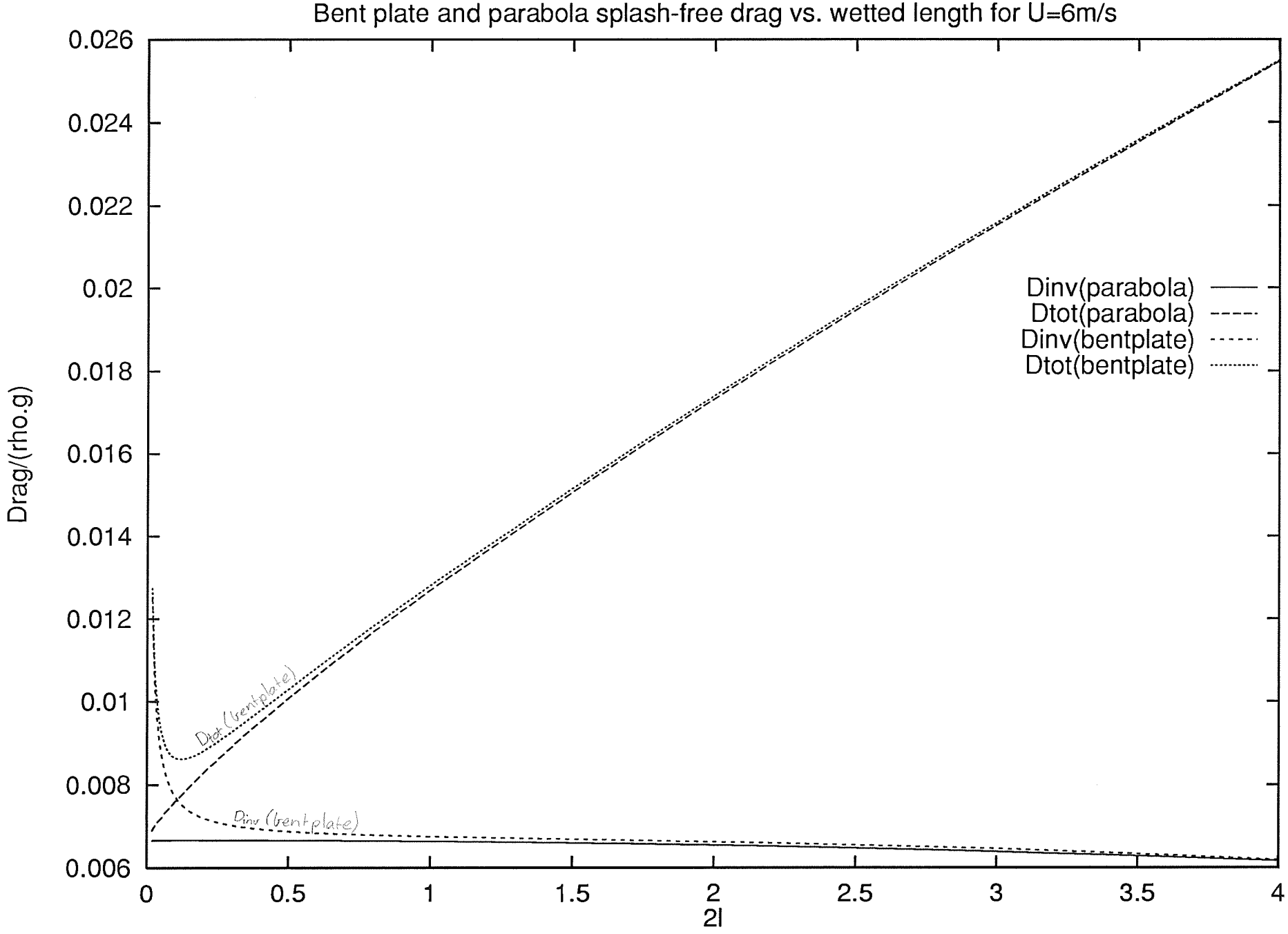
Bent plate and parabola splash-free drag vs. wetted length for U=6m/s
Drag/(rho.g)
2l
0.026
0.024
0.022
0.02
0.018
0.016
0.014
0.012
0.01
0.008
0.006
0
0.5
1
1.5
2
2.5
3
3.5
4
Dinv(parabola)
Dtot(parabola)
Dinv(bentplate)
Dtot(bentplate)
Dtot (bentplate)
Dinv (bentplate)

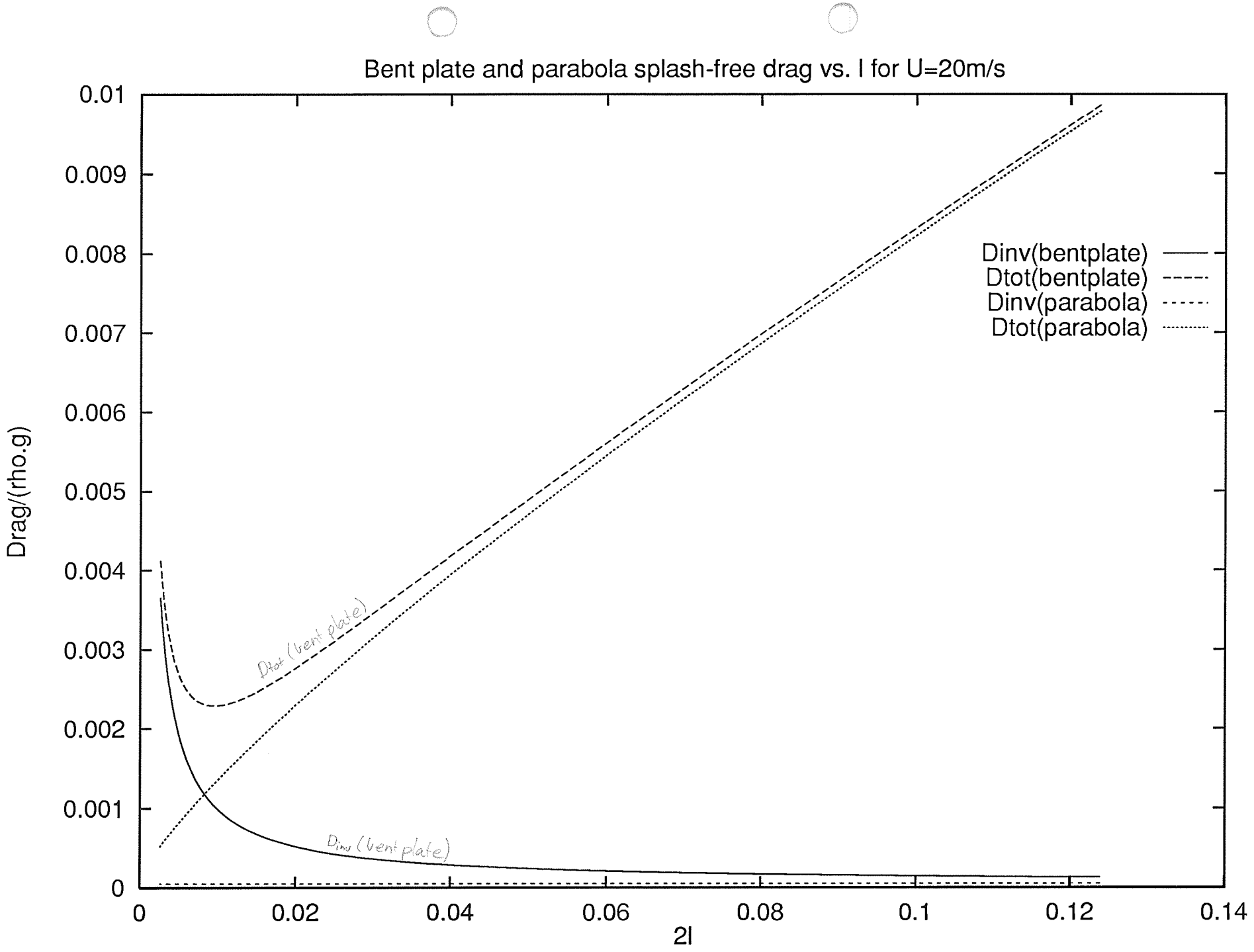
Bent plate and parabola splash-free drag vs. l for U=20m/s
Drag/(rho.g)
2l
0.01
0.009
0.008
0.007
0.006
0.005
0.004
0.003
0.002
0.001
0
0
0.02
0.04
0.06
0.08
0.1
0.12
0.14
Dinv(bentplate)
Dtot(bentplate)
Dinv(parabola)
Dtot(parabola)
Dtot (bent plate)
Dinv (bent plate)

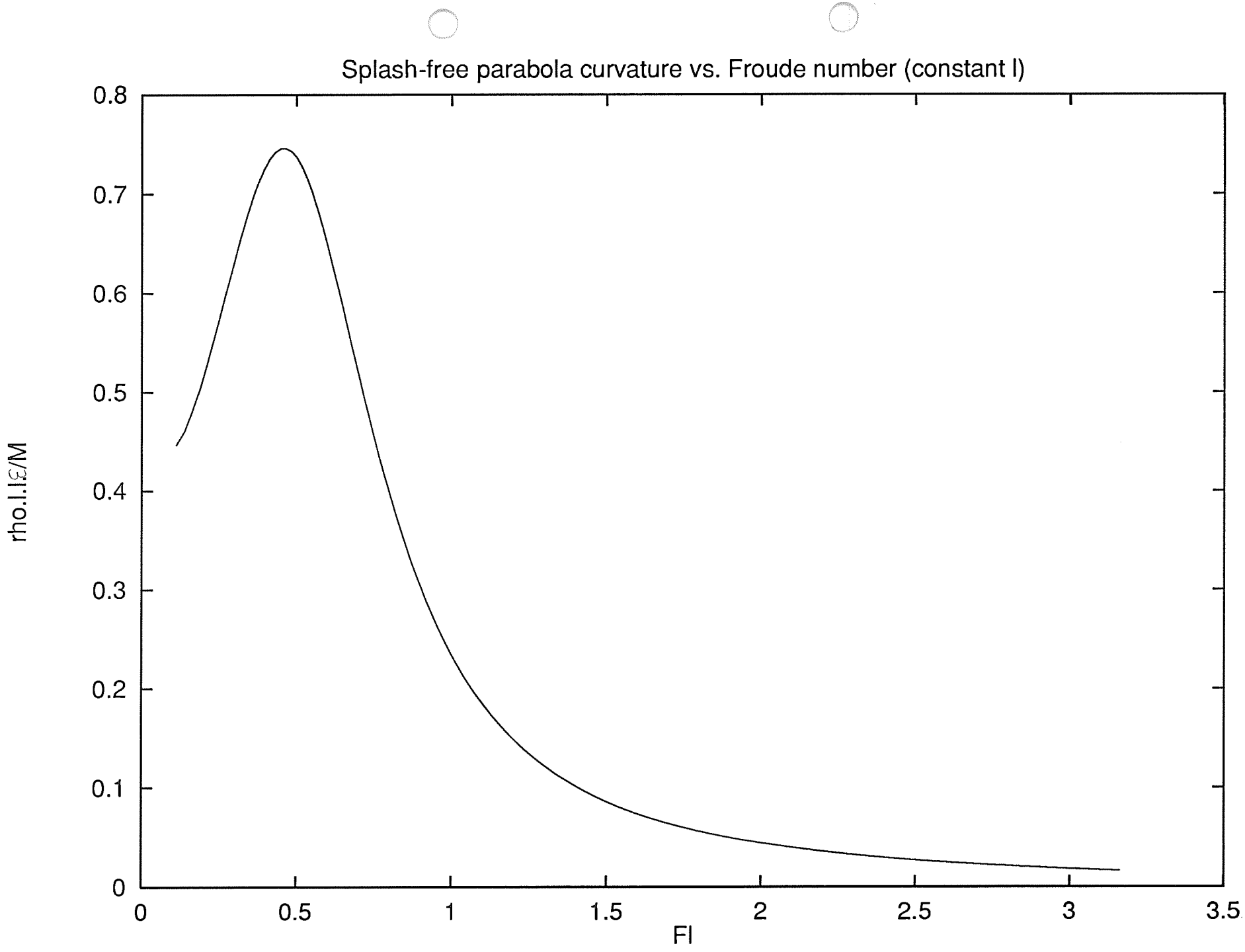
Splash-free parabola curvature vs. Froude number (constant l)
rho.l.l∃/M
Fl
0.8
0.7
0.6
0.5
0.4
0.3
0.2
0.1
0
0
0.5
1
1.5
2
2.5
3
3.5

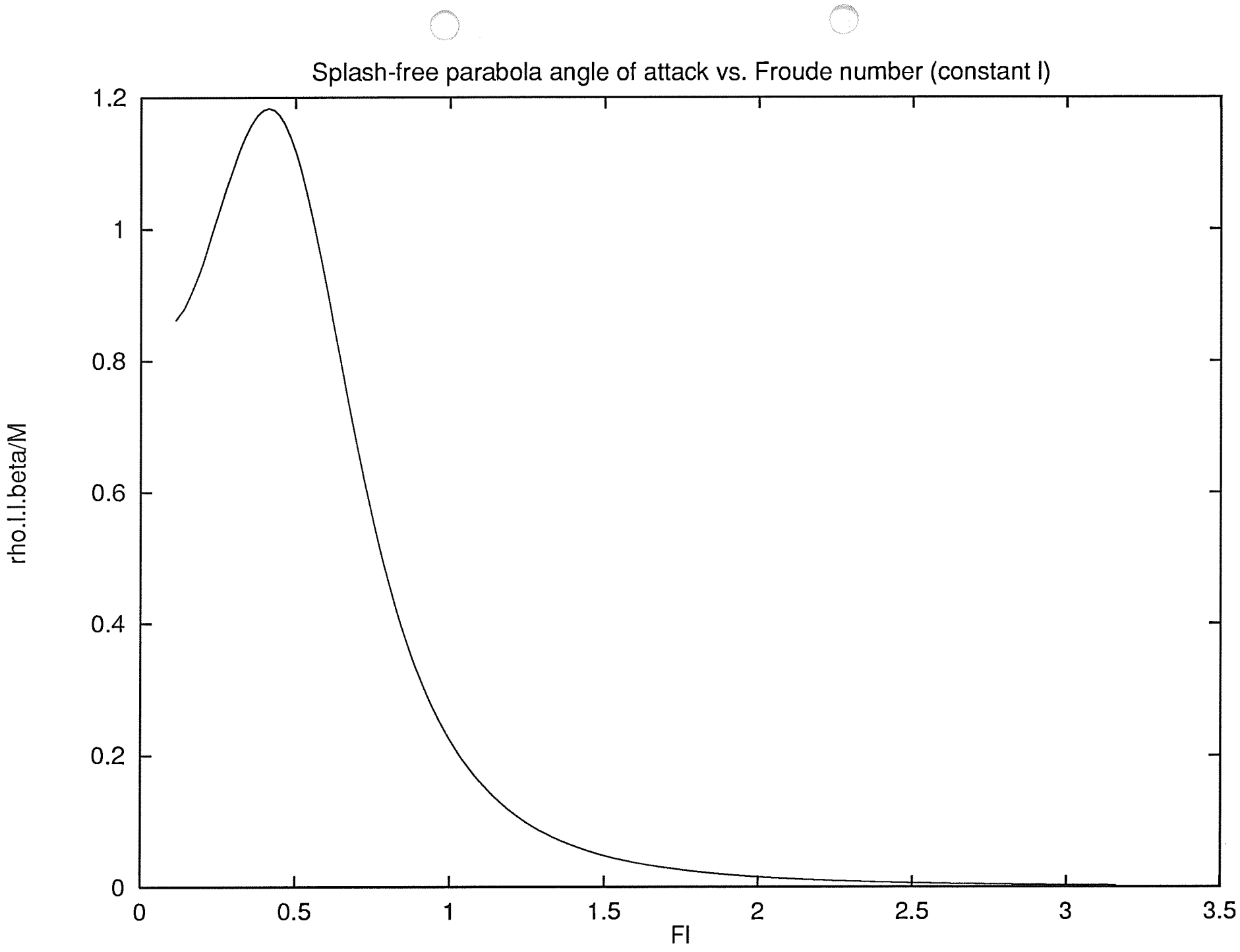
Splash-free parabola angle of attack vs. Froude number (constant l)
rho.l.l.beta/M
Fl
1.2
1
0.8
0.6
0.4
0.2
0
0
0.5
1
1.5
2
2.5
3
3.5

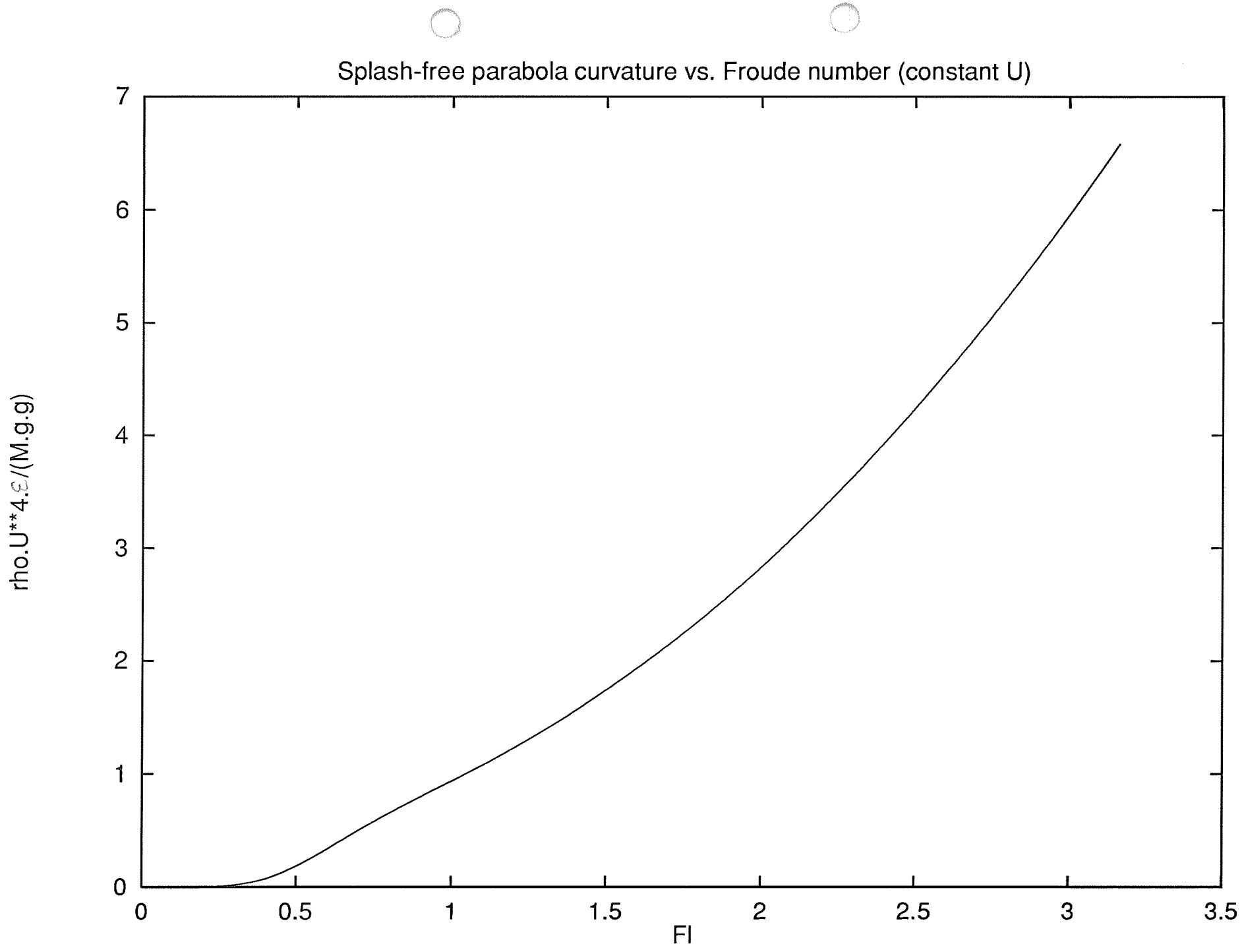
Splash-free parabola curvature vs. Froude number (constant U)
rho.U**4.ℓ/(M.g.g)
Fl
0
1
2
3
4
5
6
7
0
0.5
1
1.5
2
2.5
3
3.5

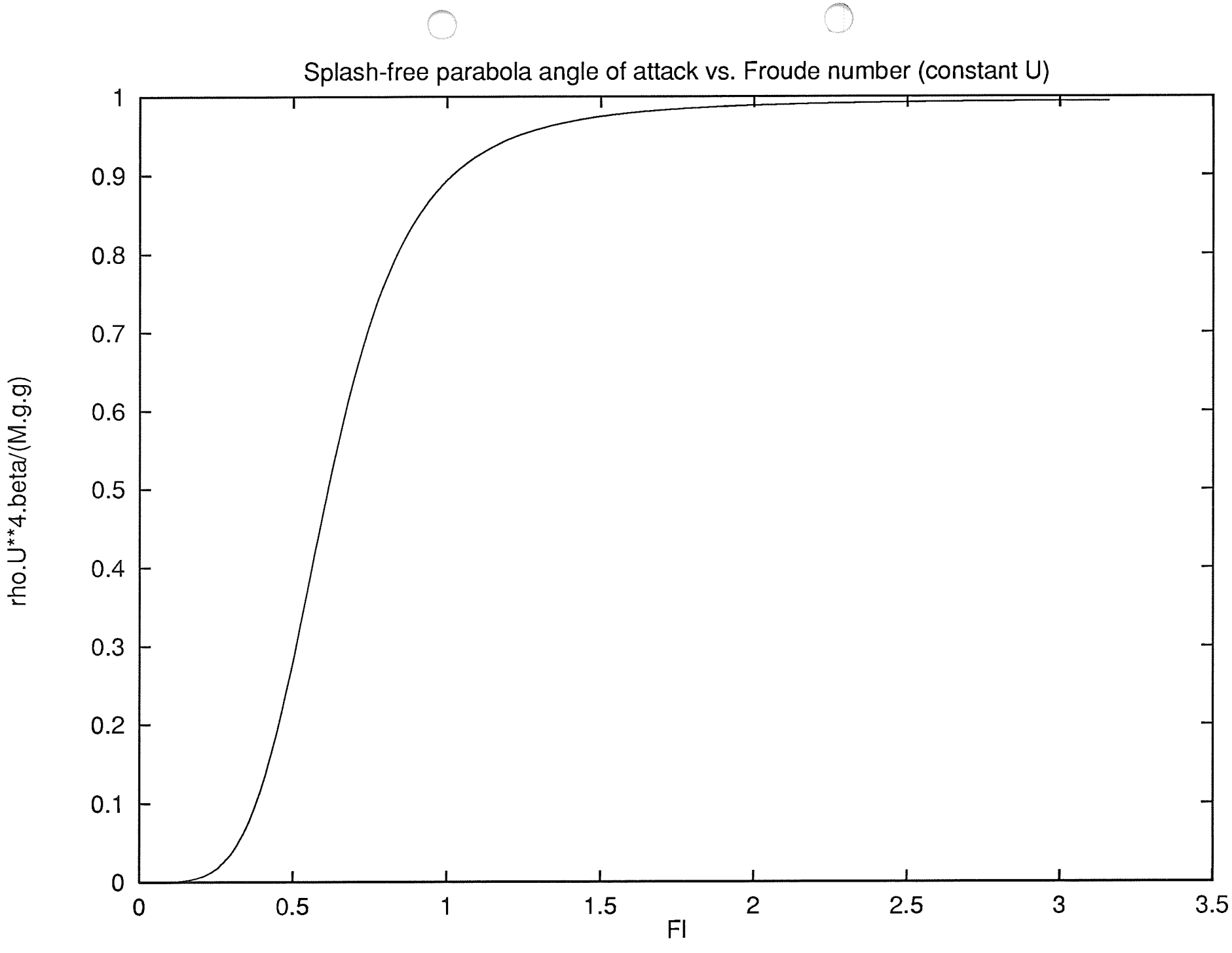
Splash-free parabola angle of attack vs. Froude number (constant U)
rho.U**4.beta/(M.g.g)
Fl
0
0.1
0.2
0.3
0.4
0.5
0.6
0.7
0.8
0.9
1
0
0.5
1
1.5
2
2.5
3
3.5

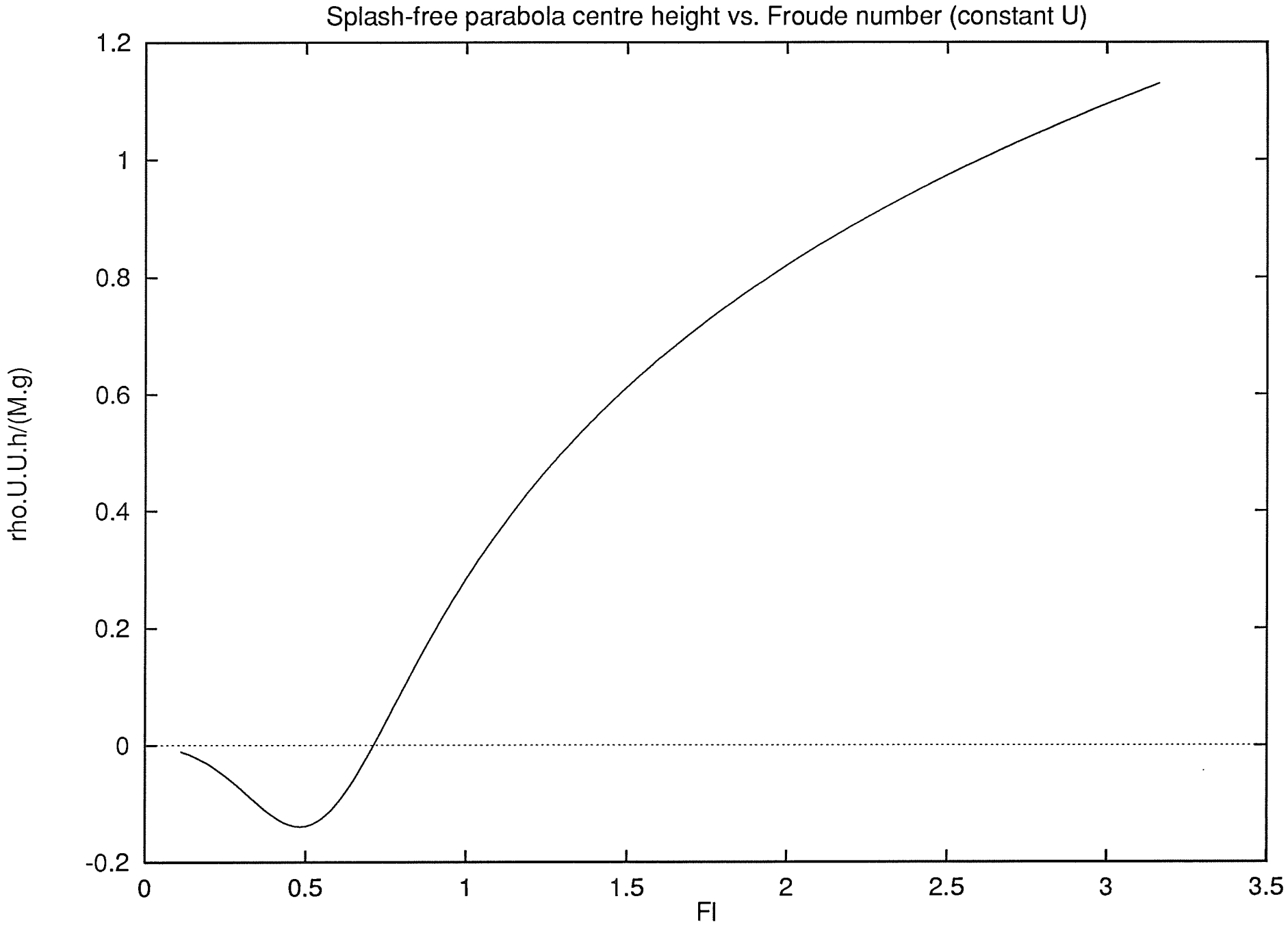
Splash-free parabola centre height vs. Froude number (constant U)
rho.U.U.h/(M.g)
Fl
1.2
1
0.8
0.6
0.4
0.2
0
-0.2
0
0.5
1
1.5
2
2.5
3
3.5